FINAL REPORT FOR THE DOE/ARM PROJECT TITLED
Parameterizing Size Distributions in Ice Clouds

David L. Mitchell[1] and Daniel DeSlover[2]

1. Atmospheric Sciences Center, Desert Research Institute
University of Nevada System, Reno, Nevada

2. Cooperative Institute for Meteorological Satellite Studies (CIMSS)
University of Wisconsin, Madison, Wisconsin

1. Introduction

This is the final report for the Department of Energy's Atmospheric and Radiation Measurement (ARM) Program for the grant DE-FG02-06ER64201 covering the period 15 March 2006-14 March 2008. The objectives of this project were to (1) develop, test and refine ice particle size distribution (PSD) parameterizations based on ice water content (IWC) and temperature appropriate for the three ARM sites: SGP, TWP and NSA, and (2) develop and implement a method for retrieving the LWP and the ice water path (IWP) in Arctic mixed phase clouds when the total condensate is less than 130 g m^{-2}. These objectives were mostly accomplished as described below. In addition, the following tasks were fulfilled that were not part of the science plan:

1. Comparison of the modified anomalous diffraction approximation (MADA) ice optics scheme with other ice optics schemes and subsequent implementation of the MADA scheme in the Community Atmosphere Model (CAM4), along with related CAM research.
2. Development of new MADA code for analysis of aircraft PSD measurements using the new 2D-S probe. Ice cloud optical properties are calculated directly from measurements of ice particle projected area, mass and number concentration.
3. Ice cloud PSD retrievals from this project were used to test the PSD predicted by the new CAM4 microphysics package.

The main results from this project will first be briefly described, and papers addressing the details of these results are included as appendices. Then the other three results (listed above) that were not addressed in the science plan will be briefly discussed.

2. Ice cloud size distributions

a. Climatological PSD analysis

The central idea of this project was to use radiation measurements to estimate the relative concentrations of small ice crystals in cirrus cloud PSDs. PSD schemes in the literature would be compared with the PSD predicted using infrared radiances. The original idea was to use AERI (Atmospheric Emitted Radiance Interferometer) channels at 8.5 μm and 11 μm to evaluate the small ice crystal concentrations. At 8.5 μm,

absorption efficiencies (Q_{abs}) are ~1.0 for ice particles > 60 μm in length and that Q_{abs} < 1.0 for smaller ice crystals. For the 11 μm channel, Q_{abs} ~1.0 for both small and larger ice particles. Therefore the 8.5/11.0 μm absorption optical depth ratio can be used as a measure of small ice crystal concentration.

While this remains true, a more elegant method for evaluating small ice crystal concentrations was developed as described in the paper submitted to J. Atmos. Sci., featured in Appendix A. This method uses the principle of photon tunneling to assess small ice crystal concentrations since tunneling is sensitive only to small (D < 60 μm) ice crystals. Tunneling contributes significantly to absorption at 12 μm but not at 11 μm, making the 12/11 μm absorption optical depth ratio ideal for assessing small ice crystal contributions to cirrus PSD. This method was used for this project. Henceforth, the 12/11 μm absorption optical depth ratio will be referred to as β.

While we originally intended to use AERI data from the tropics, the water vapor concentration in the tropical atmosphere is too high to interpret the cirrus cloud signal in the AERI data. Therefore we used satellite data instead, since relatively little water vapor exists between cirrus and satellites, making it easy to retrieve β. β was retrieved for both anvil cirrus and in situ cirrus during the TWP-ICE and TC4 field campaigns, as described in Appendix A.

Six temperature-dependent PSD schemes, four of which are published in the journal literature, were modified in regards to their small ice crystal concentrations based on the above radiance method. Based on three case studies sampling 117,768 km^2 of cirrus from satellite, β was found to be independent of temperature with a value of 1.065 on average using the MODIS instrument. These PSD schemes had their small ice crystal concentrations modified so that the predicted PSD β values were consistent with the mean observed β of 1.065. These modified PSDs were compared with their corresponding PSDs from the original PSD scheme as shown in Appendix A. It was found that small ice crystal concentrations were generally higher in the original PSD schemes than in the radiance "corrected" PSD schemes. A possible reason for this is the phenomena known as shattering, where ice particles sampled by PSD-measuring instruments may shatter if they impact the rim of the inlet tube. This produces a swarm of small, shattered ice artifacts that are counted as real ice crystals, thus artificially inflating the concentration of small ice crystals.

Since satellite retrievals of β can sample vast areas of cirrus cloud coverage, the retrieved temperature-dependent PSDs were used to calculate *climatological* estimates of cirrus cloud effective diameter D_e and mass-flux weighted fall velocity V_f in relation to cirrus cloud temperature. These two properties are very important in determining cirrus optical properties, with V_f being more important than D_e perhaps due to its strong affect on climate feedback and climate sensitivity (Mitchell et al. 2008; Sanderson et al. 2008).

b. TWP-ICE case study analysis

Prior to applying this retrieval algorithm to evaluate PSD, D_e and V_f on a climatological basis, it was tested against in situ data using an ARM TWP-ICE case study. This is described in the peer reviewed paper in Appendix B. In addition to retrieving the relative concentration of small ice crystals, the retrieval algorithm can be used to retrieve the cirrus ice water path (IWP), PSD slope and mean size (assuming

monomodal spectra), D_e and V_f. This assumes $\beta > 1.035$ ($\beta < 1.035$ indicates broad PSD associated with relatively large ice particles with small ice crystals contributing little to PSD projected area). To test the physics of this retrieval algorithm, MODIS radiances from the TERRA satellite overpass on 2 February 2006, corresponding to cirrus in situ sampling during the TWP-ICE experiment, were converted to β values. Retrieved cirrus pixels were matched with in situ measurements spatially and within 4 minutes temporally. These in situ PSD measurements were unique in that the probes were designed to minimize the problem of shattering. Thus a comparison between retrieved and measured PSD should be meaningful. The comparison of the retrieved PSD from MODIS with PSD measurements from the Proteus aircraft are shown in Appendix B, Fig. 3, left panel. It is seen that using the monomodal PSD assumption results in a retrieved PSD slope very similar to the observed slope. Naturally the retrieved and observed D_e and mean size agreed as well. Comparisons between satellite retrievals and in situ measurements are hard to come by and this ARM case study has been very useful in validating this retrieval algorithm.

c. Arctic cirrus

Provided that β for tropical anvil and in situ cirrus is essentially the same for midlatitude in situ cirrus (as the journal literature indicates), the above work characterizes the cirrus PSD for both tropical anvil and midlatitude synoptic (in situ) cirrus. Note that some of the PSD schemes considered in Section 2a were derived from midlatitude synoptic cirrus while others were derived from tropical anvil cirrus measurements.

Cirrus PSD for the Arctic were characterized by (1) developing a PSD parameterization based on cirrus in situ PSD measurements from the ARM M-PACE project and (2) using AERI radiance measurements during M-PACE to estimate the concentrations of small ice crystals. This work was undertaken primarily by the PhD student on this project and is described in Appendix C. The methodology for developing the Arctic PSD parameterization is described in the Appendix of Mitchell et al. (2009; see Appendix A). Prior to the completion of the Arctic PSD scheme, the Ivanova PSD scheme for midlatitude cirrus was used as a surrogate for Arctic PSD so that the M-PACE AERI measurements could be used to do a preliminary evaluation of the concentrations of small ice crystals in Arctic cirrus. The results of that study are described in Appendix C. No evidence was found that Arctic PSDs are bimodal or that elevated or anomalously high concentrations of small ice crystals exist. For typical cirrus IWC of 10 mg liter^{-1}, total ice particle concentrations were ~3-8 per liter.

3. Retrieval of the ice fraction in Arctic mixed phase clouds

a. AERI and radar retrievals

An interesting finding from this research shared by other published studies is that the mean value of β is roughly constant for all temperatures corresponding to all-ice conditions ($T < -36\ ^oC$). For thin to moderately thick cirrus, $\beta \approx 1.06 \pm 0.04$. For warmer

temperatures, recent reliable in situ PSD measurements (when converted to optical properties) indicate the mean β should not exceed this value for the ice PSDs (Jensen et al. 2009). But when liquid water is present, β is predicted to exceed this value due to the relatively small droplet sizes and the difference in the imaginary part of the refractive index for water between 11 and 12 um wavelengths. Therefore, when β retrieved by ground- or space-based remote sensing significantly exceeds this value for cirrus clouds, it indicates the presence of cloud liquid water.

An algorithm has been designed to exploit this principle for AERI (Atmospheric Emitted Radiance Interferometer) retrievals and is described in the peer reviewed paper in Appendix D. Appendix D illustrates the retrieval for a cirrus cloud sampled during M-PACE, showing how the AERI retrieval interprets the cloud to be mostly ice but with a few patches of liquid water (Fig. 3). Radar depolarization ratios confirmed that the cloud is mostly all ice. The AERI instrument measures the total water path (TWP) regardless of phase. But using the above β principle, the liquid water fraction can also be retrieved from AERI as shown in Fig. 3.

Also shown in Fig. 3 of Appendix D is the retrieved ice water path (IWP) in the same cloud based on the MMCR radar. This was done by employing the radar-IWC equation described in Mitchell et al. (2006). It is seen that for this Arctic cirrus case study, the IWP from the MMCR radar generally matches the TWP retrieved from the AERI in most cases. This partially validates the TWP retrieval from the AERI since we know the cloud is almost all ice.

In spite of these encouraging results, there is a drawback to this technique. The AERI retrieval for β depends on Dr. Dave Turner's radiation transfer model which includes multiple scattering for greater accuracy. This RT model combines with a retrieval algorithm developed by Dr. Turner's group that estimates β for our microphysics algorithm. Unfortunately some of the assumptions made in the β retrieval (such as an assumed effective diameter) may add a relatively high level of uncertainty to our microphysical mixed phase cloud retrievals. For this reason, we turned to a satellite method that appears to be free of these complicating factors.

b. Satellite retrievals of mixed phase cloud composition

The AERI mixed phase cloud retrieval described above can be easily adapted to satellite remote sensing. While not part of the work plan of our new ARM project, it would be a missed opportunity not to apply our mixed phase microphysics retrieval algorithm from the last ARM project to satellite remote sensing. To date we know of no technique that retrieves the ice and liquid water fraction of mixed phase clouds from space. Thus the work described in this section was completed during our current ARM project (start date 15 March 2009) and exploits advances made during the last project (the subject of this report).

Accurate prediction of the feedback from clouds in global climate models (GCMs) requires the partitioning of ice and liquid water in clouds. Whether this is done by parameterizing measurements or physical processes, accurate measurements of the ice/liquid fraction will be needed. Since this fraction may differ based on many factors including cloud type and latitude, global measurements from satellites may be necessary.

A new method for retrieving the ice/liquid fraction in mixed phase clouds has been developed that is based on (1) a new satellite retrieval for cloud temperature T and emissivity in two infrared window channels and (2) a new microphysics retrieval algorithm that interprets β for mixed phase cloud conditions. The satellite retrieval was developed by Dr. Robert d'Entremont (a collaborator on this project) and the PI. This method solves for T independently of emissivity, using MODIS carbon dioxide channels. In brief, T is estimated using radiances measured in two CO_2 channels centered at 13.3 and 14.2 μm. The real refractive index here is 1.52 and 1.58 respectively, indicating the absorption contribution from tunneling (i.e. wave resonance) is almost the same in these channels. The imaginary index n_i is 0.355 and 0.246, respectively, yielding a PSD absorption efficiency of ~1.0 for each wavelength when tunneling is neglected. For these reasons the emissivity in each channel is essentially the same ($\varepsilon_{13.3} = \varepsilon_{14.2}$), allowing us to solve for T using radiance observations from these two channels. Knowing T, cloud emissivity in two window channels (i.e. 11 & 12 μm) can be calculated from standard theory. From these emissivities the 12/11 μm absorption optical depth ratio, or β, can be calculated. Note that solving for T using ground-based remote sensing might not be possible using CO_2 channels since radiances in those channels might be exclusively from CO_2 between the sensor and the cirrus and not the cirrus clouds themselves.

Application of this retrieval to several case studies, as well as findings from other studies, reveal that the mean β is roughly constant with temperature for all-ice conditions. This makes it possible to discriminate between glaciated and mixed phase conditions, since mean β increases once liquid water is present. The amount of increase reveals the mean ice/liquid fraction of the cloud field. The retrieved standard deviations (SD) for β (at a given T) provide an estimate of the variance in the ice/liquid fraction under mixed-phase conditions, which may also be useful for parameterizing mixed-phase clouds.

The particle size distribution (PSD) of the microphysics retrieval algorithm is formulated as bimodal with the small mode corresponding to cloud droplets. A mean droplet diameter of 11 μm was assumed based on measurements in mixed phase clouds during M-PACE. As observed β increases above its threshold value for ice, liquid water is added to the small mode until a match is achieved between predicted and observed β. Using other plausible values of the mean droplet diameter can change the mean ice/liquid fraction by a factor of ~2.

This retrieval methodology was applied to a case study during the TC4 field campaign in 2007 near Costa Rica since that data was available from the last ARM project. The cloud field consisted of mostly anvil and in situ cirrus, and deep convective clouds. It was found that clouds having mid-level temperatures < 235 K were glaciated while warmer clouds were mixed phase. For cloud temperatures ~250 K, the mean percent liquid water was 15% while the positive SD corresponded to 79% liquid water. These results are shown in Figure 1 and 2 below. We expect to test this retrieval by applying it to mixed phase clouds sampled during the ARM ISDAC field campaign.

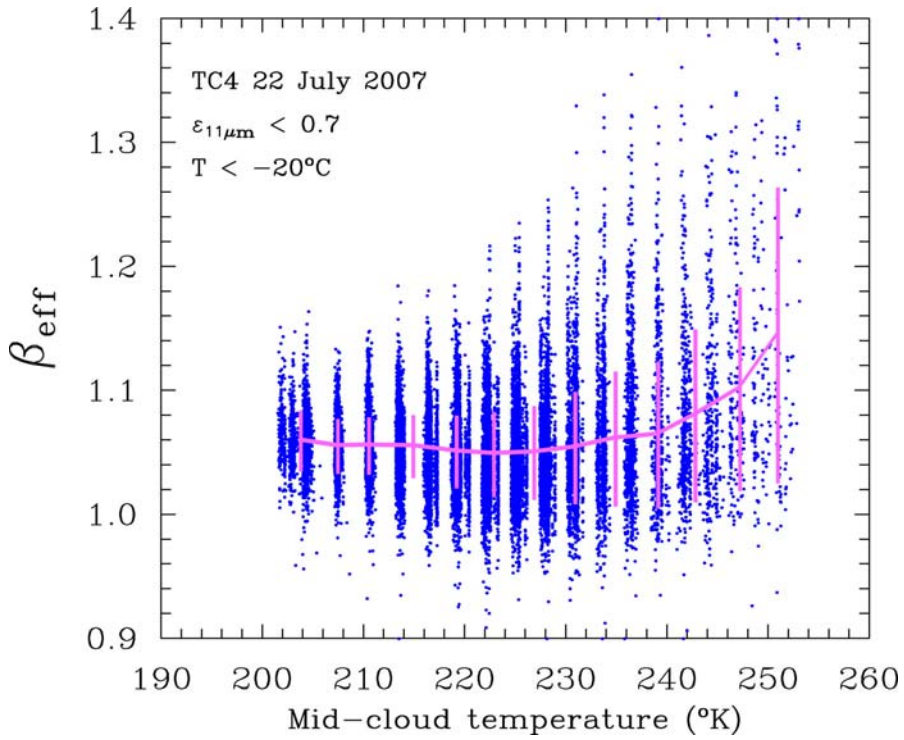

Figure 1. Temperature dependence of the retrieved β for a cloud field sampled by MODIS during the TC4 field campaign. Mean values and standard deviations are in pink.

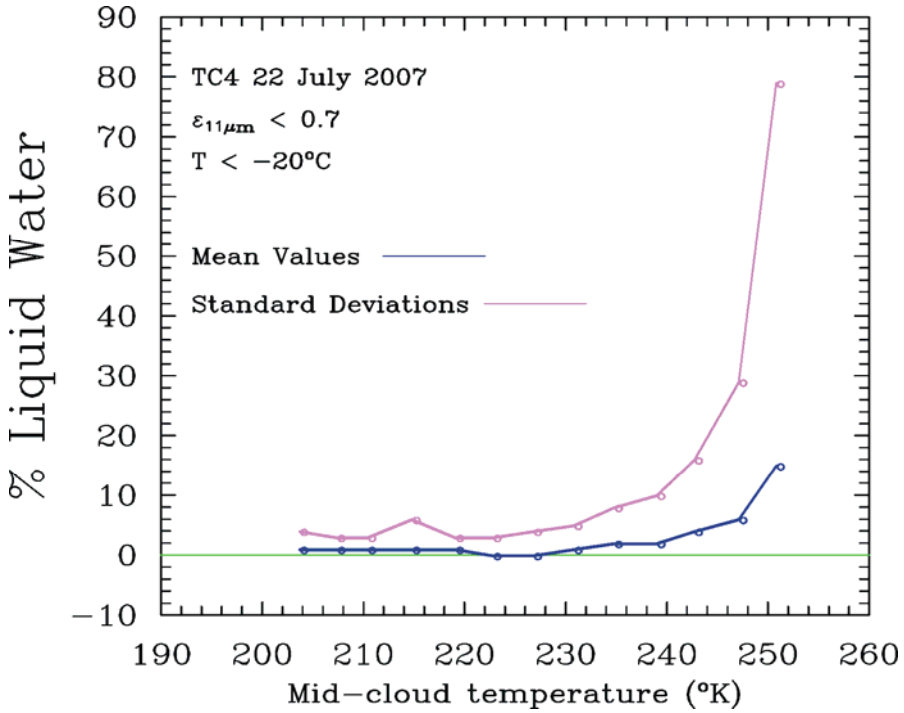

Figure 2. Satellite retrieval of liquid fraction from a MODIS scene of cirrus (T < 235 °K) and mixed phase clouds. Positive standard deviations in β were used to predict the positive SDs in percent liquid water.

4. Other accomplishments not listed in the project work plan

a. Implementation of the MADA scheme in the Community Atmosphere Model (CAM4) and related CAM research

During this project the Modified Anomalous Diffraction Approximation or MADA, which was developed under ARM funding, was implemented in the new Community Atmosphere Model, CAM4, to treat the optical properties of ice clouds. CAM4 is part of the new Community Climate System Model, CCSM4. CAM4 should be available to the public by the end of this year. This implementation process involved a rigorous comparison between MADA and the optics scheme used in CAM3 (the Ebert and Curry 1994 ice optics scheme), as well as the ice optics treatment developed by Qiang Fu (1996, 1998). These optics schemes were compared at all solar and terrestrial wavelengths. The MADA and Fu schemes were in close agreement, but the MADA scheme had the advantage of adapting to any wavelength resolution desired, whereas the resolution in the Fu scheme is fixed and could introduce errors if adapted to CAM4 wavelength bands. The Ebert and Curry ice optics scheme overestimated absorption in the near- and thermal infrared regions. The standard ice optics treatment in CAM4 consists of a look-up table of MADA output.

During 2004 and 2005, the PI took sabbatical time working with Dr. Philip Rasch in the Climate and Global Dynamics group at NCAR. During this ARM project, the PI published results from that research in Geophysical Research Letters (GRL). Temperature-dependent ice PSD schemes developed under ARM funding, as well as the MADA and ice particle fall velocity schemes developed under ARM funding, were implemented in CAM3. The MADA and ice sedimentation schemes are formulated in terms of the PSD and ice particle mass- and area-dimension relationships. Two CAM3 simulations were performed; one using PSD having moderate concentrations of small ($D < 60$ μm) ice crystals and one using PSD having relatively high concentrations of small ice crystals. These differences produced substantial differences in PSD weighted ice sedimentation rates. This in turn resulted in large differences in cirrus IWP and coverage and consequently large differences in cirrus radiation feedback and heating rates. Temperatures in the tropical upper troposphere differed by more than 3 ^{o}C between simulations. These results illustrate the importance of small ice crystals and the cirrus ice sedimentation rate in determining cloud feedbacks and climate sensitivity.

b. Collaboration with SPEC, Inc.

The company SPEC, Inc. that develops and manufactures cloud microphysics instruments asked us if we could develop software for calculating cirrus cloud optical properties from their in situ measurements. The new 2D-S probe from SPEC provides not only size distributions with respect to number and projected area (which are directly measured), but also estimates the mass-size distribution. Integrating over this mass-size distribution yields the IWC, and these IWCs are in good agreement with IWCs directly measured by the CVI probe mounted on the same aircraft. The MADA scheme is formulated to take advantage of these new measurements and new code was written

to calculate optical properties by numerically integrating over a measured PSD. This removes the restriction of expressing the PSD as a gamma function. The 2D-S probe measures the ice particle mass and area concentration in each bin of a PSD, and MADA calculates the optical properties in each bin from this mass-to-area concentration ratio. No information about ice particle shape is needed except for calculating the scattering phase function at solar wavelengths (shape information is provided by the Cloud Particle Imager or CPI probe). In this way the cloud optical properties are calculated directly from the 2D-S measurements.

The heating rates of cirrus clouds sampled by the 2D-S probe during the TC4 field campaign have been calculated using this new MADA code, and a paper containing these results has been submitted to J. Geophysical Research. This new MADA code was given to SPEC, Inc. and will be used in their future research.

c. Testing of the new CAM4 microphysics package

The new cloud microphysics scheme for CAM4 was tested using PSD retrievals from this ARM project, and these results were reported last spring at the Atmosphere Model Working Group at NCAR. CAM4 ice mixing ratios q and ice particle number concentrations N were obtained for a fixed latitude, longitude and pressure level corresponding to frequent cirrus cloud occurance. Using formulas in the CAM4 ice microphysics code, q and N were converted to PSD. There PSD were compared with climatological cirrus PSD obtained using our retrieval method described in Section 2a. In addition, the PSD weighted fall speed V_f and effective diameter D_e were calculated from the CAM4 PSD in the same way these properties were calculated from the climatological PSD. It was found that the concentration of small ice crystals was much higher in the CAM4 PSD than in the climatological PSD, resulting in much smaller D_e in CAM4 relative to the climatological D_e values. The CAM4 V_f values were similar to the climatological V_f values, but the CAM4 V_f was not based on the PSDs; rather it was based on empirical fallspeed power laws from the literature that are not based on the ice particle mass/area ratio. For realistic estimates of climate sensitivity, CAM4 will need to have physically based V_f estimates since V_f has a strong impact on climate sensitivity (Mitchell et al. 2008; Sanderson et al. 2008).

5. Publications from this project

a. Peer reviewed publications

Mitchell, D.L., P.J. Rasch, D. Ivanova, G.M. McFarquhar, T. Nousiainen, 2008: Impact of small ice crystal assumptions on ice sedimentation rates in cirrus clouds and GCM simulations. *Geophys. Res. Lett*., **35**, doi:10.1029/2008GL033552.

Mitchell, D.L., R.P. d'Entremont and R.P. Lawson, 2009: Inferring cirrus size distributions through satellite remote sensing and microphysical databases. Under 2nd review for publication in *J. Atmos. Sci*.

Mishra, S., D.L. Mitchell, and D. DeSlover, 2009: Ground based retrievals of small ice crystals and water phase in Arctic cirrus. AIP Conference Proceedings 1100, *Current Problems in Atmospheric Radiation (IRS 2008)*, Proceedings of the International Radiation Symposium (IRC/IAMAS), Eds. Teruyuki Nakajima and Marcia Akemi Yamasoe, Foz de Iguassu, Brazil, 3-8 August 2008, 482-485.

Mitchell, D.L., and R.P. d'Entremont, 2009: Satellite remote sensing of small ice crystal concentrations in cirrus clouds. AIP Conference Proceedings 1100, *Current Problems in Atmospheric Radiation (IRS 2008)*, Proceedings of the International Radiation Symposium (IRC/IAMAS), Eds. Teruyuki Nakajima and Marcia Akemi Yamasoe, Foz de Iguassu, Brazil, 3-8 August 2008, 185-188.

Lawson, R.P., E. Jensen, D.L. Mitchell, B. Baker, Q. Mo and B. Pilson, 2009: Microphysical and Radiative Properties of Tropical Clouds Investigated in TC4 and NAMMA. Submitted to *J. Geophys. Res*.

b. Conference papers

Mitchell, D.L., P.J. Rasch, D. Ivanova, G. McFarquhar and T. Nousiainen, 2006: The impact of controversial small ice crystals on GCM simulations. 12th AMS Conference on Cloud Physics, 10-14 July 2006, Madison, Wisconsin, paper J2.9 (available on CD).

Mitchell, D.L., R.P. d'Entremont and R.P. Lawson, 2006: Passive thermal retrievals of ice and liquid water path, effective size and optical depth and their dependence on particle and size distribution shape. 12th AMS Conference on Atmospheric Radiation, 10-14 July 2006, Madison, Wisconsin, paper 12.5 (on CD)

Mitchell, D.L., R.P. d'Entremont and R.P. Lawson, 2007: Ice cloud microphysical properties and their application to satellite remote sensing. Hyperspectral Imaging and Sounding of the Environment (HISE), Optical Society of America (OSA), 12-15 February 2007, Santa Fe, New Mexico, on CD.

Mishra, S., D.L. Mitchell, D. DeSlover and G. McFarquhar, 2008: Ground based remote sensing of small ice crystal concentrations in Arctic cirrus clouds. International Conference on Clouds and Precipitation, Cancun, Mexico, 7-11 July 2008. Available on CD.

Mitchell, D.L., and R.P. d'Entremont, 2008: Satellite remote sensing of small ice crystal concentrations in cirrus clouds. International Conference on Clouds and Precipitation, Cancun, Mexico, 7-11 July 2008. Available on CD.

Mitchell, D.L., 2009: New understanding of split-window emissions provides insight on small ice crystal concentrations. Hyperspectral Imaging and Sensing of the Environment (HISE), *Technical Digest*, Optical Society of America.

d'Entremont, R.P., and D.L. Mitchell, 2009: A causational argument for the influence of contrail ice particle shape on thermal infrared radiance observations. AMS Annual Meeting, Phoenix, Arizona, January 2009.

6. References cited in this report

Ebert, E. and J.A. Curry 1992: A parameterization of ice cloud optical properties for climate models. *J. Geophys. Res*., **97**, 3831-3836.

Fu, Q., 1996: An accurate parameterization of the solar radiative properties of cirrus clouds for climate models. *J. Climate*, **9**, 2058-2082.

Fu, Q., P. Yang and W.B. Sun, 1998: An accurate parameterization of the infrared radiative properties of cirrus clouds for climate models. *J. Climate*, **11**, 2223-2237.

Jensen, E. J., P. Lawson, B. Pilson, B. Baker, Q. Mo, A. J. Heymsfield, A. Bansemer, T.P. Bui, M. McGill, D. Hlavka, G. Heymsfield, S. Platnick, G. T. Arnold, and S. Tanelli, 2008: On the importance of small ice crystals in tropical cirrus. *Atmos. Chem. Phys. Discuss.*, **9**, 5321-5370.

Mitchell, D.L., A. Huggins, V. Grubisic, 2006: A new snow growth model with application to radar precipitation estimates. *Atmos. Research*., **82**, 2-18.

Mitchell, D.L., P.J. Rasch, D. Ivanova, G.M. McFarquhar, T. Nousiainen, 2008: Impact of small ice crystal assumptions on ice sedimentation rates in cirrus clouds and GCM simulations. *Geophys. Res. Lett*., **35**, doi:10.1029/2008GL033552.

Mitchell, D.L., R.P. d'Entremont and R.P. Lawson, 2009: Inferring cirrus size distributions through satellite remote sensing and microphysical databases. Under 2nd review for publication in *J. Atmos. Sci*.

Sanderson, B.M., C. Piani, W.J. Ingram, D.A. Stone, M.R. Allen, 2008: Towards constraining climate sensitivity by linear analysis of feedback patterns in thousands of perturbed physics GCM simulations. Clim. Dyn., 30, 175-190.

Appendix A

Inferring Cirrus Size Distributions Through Satellite Remote Sensing and Microphysical Databases

David L. Mitchell[1], Robert P. d'Entremont[2] and R. Paul Lawson[3]

1. Desert Research Institute, Reno, Nevada
2. Atmospheric and Environmental Research, Inc., Lexington, Massachusetts
3. SPEC, Inc., Boulder, Colorado

Revised for the Journal of the Atmospheric Sciences
August 2009

Corresponding author address: Dr. David L. Mitchell, Desert Research Institute, Division of Atmospheric Sciences, Reno, NV 89512-1095. E-mail: mitch@dri.edu

ABSTRACT

Since cirrus clouds have a substantial influence on the global energy balance that depends on their microphysical properties, climate models should strive to realistically characterize the cirrus ice particle size distribution (PSD), at least in a climatological sense. To date, the airborne in situ measurements of the cirrus PSD have contained large uncertainties due to errors in measuring small ice crystals ($D < \sim 60$ μm). In this paper we present a method to remotely estimate the concentration of the small ice crystals relative to the larger ones using the 11 and 12 μm channels aboard several satellites. By understanding the underlying physics producing the emissivity difference between these channels, this emissivity difference can be used to infer the relative concentration of small ice crystals. This is facilitated by enlisting temperature-dependent characterizations of the PSD (i.e. PSD schemes) based on in situ measurements.

An average cirrus emissivity relationship between 12 and 11 μm is developed here using the MODIS satellite instrument and is used to "retrieve" the PSD based on six different PSD schemes. The PSDs from the measurement-based PSD schemes are compared with corresponding retrieved PSDs to evaluate differences in small ice crystal concentrations. The retrieved PSDs generally had lower concentrations of small ice particles, with total number concentration independent of temperature. In addition, the temperature dependence of the PSD effective diameter D_e and fallspeed V_f for these retrieved PSD schemes exhibited less variability relative to the unmodified PSD schemes. The reduced variability in the retrieved D_e and V_f was attributed to the lower concentrations of small ice crystals in their retrieved PSD.

1. Introduction

The measurement of small ice crystals (D < 60 μm) has been a controversial issue in the atmospheric sciences community largely because their concentrations may be partially due to the shattering of larger ice particles at the inlet of the probes that measure them, resulting in artifact ice crystals. Depending on the in situ measurements one uses, these small ice crystals may affect cirrus cloud optical depth by a factor of two (McFarquhar et al. 2007). The concentration of these small crystals relative to larger ice particles is critical to climate prediction (Mitchell et al. 2008) since this affects the overall ice sedimentation rate of the ice particle size distribution (PSD). Through their impact on ice fallspeeds, their relative concentration affects the cirrus cloud feedback and climate sensitivity (the equilibrium change in global mean surface temperature) in global climate models (GCMs). Sanderson et al. (2008) show that next to the entrainment coefficient, the ice fallspeed has the greatest impact on climate sensitivity in thousands of perturbed physics GCM experiments.

The measured concentrations of small ice crystals are often orders of magnitude greater than that of the larger particles (McFarquhar and Heymsfield 1998; Ivanova et al. 2001; Lawson et al. 2006a; Garrett et al. 2005). The instruments used to measure the concentrations of small ice crystals include, but are not limited to, the ice particle replicator (Hallett 1976), the Video Ice Particle Sampler or VIPS (McFarquhar and Heymsfield 1996), the Forward Scattering Spectrometer Probe or FSSP (Knollenberg 1981) and the Cloud Aerosol Spectrometer or CAS (Baumgardner et al. 2001). The FSSP and the CAS have an inlet tube where ice particle shattering could easily occur. The replicator and VIPS do not have an inlet tube but their collection efficiency varies as a function of particle size.

Recent progress in instrument design and signal processing has resulted in new probes for measuring cloud PSDs (Baumgardner et al. 2001; Lawson et al. 2006b). Evidence of ice artifact production resulting from shattering is given in Field et al. (2003), McFarquhar et al. (2007), Heymsfield (2007a) and Jensen et al. (2009). Evidence that the FSSP can measure realistic number concentrations is given in Ivanova et al. (2001) and Gayet et al. (2006).

In view of these types of conflicting results regarding the measurements of small ice crystal concentrations, this study addresses this issue using results derived from in situ measurements and from satellite remote sensing. A new satellite remote sensing technique has been developed that uses parameterized results from aircraft measurements to help characterize the larger ice particles ($D > 60$ μm). That is, in situ measurements of ice particle size distributions (PSD) are parameterized by temperature and ice water content (IWC), henceforth referred to as PSD schemes. To characterize the smaller ice crystals of the PSD, the effective cirrus cloud absorption optical depth ratio obtained from satellite measured radiances at 12 and 11 μm is used. Based on several satellite remote sensing studies of midlatitude and tropical cirrus, the ratio appears to have climatological significance and so also the relative concentration of small ice crystals estimated from this ratio. Combining the satellite inferred information with the PSD estimate for the larger ice particles yields the entire parameterized PSD for a given IWC. While satellite measurements have their own uncertainties, the problem of artifact small ice particles from shattering is avoided using this approach.

Theory concerning ice particle-radiation interactions is described in Section 2. Section 3 describes two retrieval methods for the cirrus absorption optical depth ratio and microphysics. The results are presented and discussed in Section 4, and a summary is given in Section 5.

2. Radiation theory for cloud particles

The modified anomalous diffraction approximation (Mitchell et al. 1996, 2006a; Mitchell 2000, 2002), or MADA, is used to treat the ice cloud optical properties in the retrieval algorithm. With MADA, extinction and absorption are expressed in terms of the parameters of a gamma function PSD and the representative measured mass- and projected area-dimension power law relationships. This dependence allows us to estimate PSD information from satellite radiances.

To evaluate the relative concentration of small ice crystals in cirrus clouds, we use the cloud emissivity difference retrieved in the 12- and 11-μm bands that are a common component of many environmental satellite sensors. To understand how this is possible, the absorption processes involved and how they differ between liquid water and ice particles needs to be understood. These fundamental insights are illustrated in Fig. 1, where the real and imaginary refractive index (n_r and n_i) for bulk ice and water are plotted against wavelength (refractive indexes from Warren and Brandt 2008; Downing and Williams 1975). Also plotted is the cloud particle absorption efficiency, Q_{abs}, which is given by the simple anomalous diffraction theory (ADT) described in Mitchell and Arnott (1994):

$$Q_{abs,ADT} = 1 - \exp(-4 \pi n_i d_e / \lambda) , \quad (1)$$

where λ is wavelength and particle effective size d_e is defined as $d_e = m/\rho A_p$ where m = particle mass, ρ = bulk density of water or ice, and A_p = particle cross-section or projected area. The $Q_{abs,ADT}$ values correspond to a cloud droplet and ice particle d_e of 10 and 25 μm, respectively, with 10 μm being typical for water clouds. In the absence of very high concentrations of small ice crystals, an ice particle d_e of 25 μm is considered small with more than about 90% of the PSD projected area residing with larger particles (Jensen et al. 2009). Thus for most cirrus ice particles, for wavelengths greater than 10.5 μm, $Q_{abs,ADT} \approx 1.0$, meaning that all radiation

incident upon the particle's cross-section is absorbed. Under such conditions we can apply the zero-scattering approximation for cloud emissivity ε:

$$\varepsilon = 1 - \exp(-\tau_{abs} / \cos\theta) = 1 - \exp(-\ \overline{Q}_{abs}\ P_t\ \Delta z / \cos\theta) \qquad (2)$$

where τ_{abs} = absorption optical depth, θ = satellite viewing angle, $\overline{Q}_{abs} = \beta_{abs}/P_t$, β_{abs} = absorption coefficient, P_t = PSD projected area, and Δz = cloud depth. If $\overline{Q}_{abs}$ in (2) is approximated as $\overline{Q}_{abs,ADT}$ using (1), then ε(11 μm) ≈ ε(12 μm). Thus there must be an additional process other than the Beer's Law absorption represented in ADT that is responsible for the observed differences between ε(11 μm) and ε(12 μm). This other process is referred to as wave resonance or photon tunneling. In Mitchell (2000), the maximum tunneling contribution is shown to be directly proportional to n_r. In Fig. 1, the solid curves refer to ice and the ice n_r curve is seen to increase almost linearly between 11 and 13 μm, implying a quasi-linear absorption contribution from tunneling. Although previous literature has credited n_i for the cirrus cloud emissivity difference between ε(11 μm) and ε(12 μm), it is actually n_r that is responsible, with the emissivity difference due to differences in tunneling contributions to absorption.

The dashed curves in Fig. 1 refer to liquid water refractive indexes and $Q_{abs,ADT}$ for a cloud droplet having d_e = 10 μm. It is seen for water that tunneling does not contribute to the difference between ε(11 μm) and ε(12 μm) since n_r is almost constant over those wavelengths. The rapid change in $Q_{abs,ADT}$ between 11 and 12 μm shows that it is Beer's Law absorption based on n_i that is responsible for the emissivity differences in liquid water clouds.

We now show that small ice crystals can be evaluated using the properties of photon tunneling or wave resonance. Photon tunneling can be described as the process by which radiation beyond the physical cross-section of a particle is either absorbed or scattered outside

the forward diffraction peak. As shown in Mitchell (2000) and Mitchell et al. (2006a), tunneling is strongest when:

1) The wavelength and the effective size of the particle are comparable
2) The particle is spherical or quasi spherical
3) The real part of the refractive index is relatively large

Attribute (1) is illustrated in Fig. 2 for a wavelength of 12 μm, where it is seen that the absorption contribution from tunneling is significant for hexagonal columns less than 60 μm, and can account for 20% or more of the absorption efficiency. This tunneling contribution was calculated from Eq. 10 in Mitchell (2000). Since the shape of ice crystals becomes more spherical as their size decreases (Korolev and Isaac 2003), their tunneling contribution is enhanced via attribute (2). Finally, the wavelength dependence of tunneling in Fig. 1 suggests the difference in absorption between 12 and 11 μm, or the 12/11 μm absorption efficiency ratio defined as β, might be a useful signal for detecting small ice crystals.

The operating principle of this remote sensing method is further illustrated in Fig. 3. The solid curve shows $\overline{Q}_{abs}$ for a bimodal size distribution of quasi-spheres (droxtals) in the small mode and bullet rosettes in the large mode. The dashed curve is for the large mode, rosettes only. The $\overline{Q}_{abs}$ for wavelengths more than 11 μm are greater for the complete PSD due to tunneling. The reason $\overline{Q}_{abs}$ is greater between 11 μm and 13 μm when the full PSD is used is due to the first two factors listed above regarding small ice crystals, and $\overline{Q}_{abs}(12\ \mu m) > \overline{Q}_{abs}(11\ \mu m)$ due to the third factor [$n_r(12\ \mu m) > n_r(11\ \mu m)$]. Since tunneling is only a measure of the small mode, and the ratio $\overline{Q}_{abs}(12\ \mu m)/\ \overline{Q}_{abs}(11\ \mu m)$, or β, is determined from tunneling, this ratio serves as a measure of the small mode of the cirrus PSD. These calculations are based on the optical property database given in Yang et al. (2005), but the same result is given by MADA.

MADA is unique in that it is analytically formulated in terms of explicitly parameterized scattering/absorption processes. As described in Mitchell et al. (2006a), tunneling efficiencies (T_e) for various ice crystal shapes were determined by comparisons between MADA and finite-difference time-domain (FDTD) calculations, and were parameterized as a function of ice particle shape and large mode $\bar{D}$. Based on Cloud Particle Imager (CPI) ice crystal morphology measurements in synoptic cirrus, 53% of the small ice crystals were assumed to be quasi-spherical (T_e = 1.0), 31% compact-irregular (T_e = 0.70) and 16% budding bullet rosettes (T_e = 0.70). At these small sizes (D < 40 μm), most ice crystal shapes exhibit aspect ratios close to 1.0 and thus have relatively high tunneling efficiencies between 0.70 and 1.00. Tunneling contributions from the larger ice particles was negligible regardless of T_e due to the size dependence of tunneling (Fig. 2).

3. Estimating small ice crystal concentrations

a. Microphysical framework

Our challenge is to estimate the relative concentration of small-to-larger ice particles in a size distribution. A bimodal PSD framework is adopted here, where each mode of the PSD is described as a gamma function of the form:

$$N(D) = N_o D^{\nu} \exp(-\lambda D) , \quad (3)$$

where λ is the slope parameter, ν is the dispersion or width parameter and N_o relates the other two parameters to the PSD (or mode) number concentration N or IWC. While our objective is to estimate the complete PSD for a given IWC, each PSD mode is described by the three terms in (3). With six PSD terms, there are more unknowns than we can infer from two measured radiances. The PSD terms we cannot infer from satellite radiances are estimated from a

temperature-dependent PSD scheme (derived from in situ measurements) that provides a bimodal PSD estimate given a satellite retrieved cloud temperature and an assumed IWC. Since the measurement uncertainties associated with the larger ice particles are expected to be less than the small crystal uncertainties, we approximate the large mode mean size from temperature (e.g. Ryan 1996; Platt 1997; Ivanova et al. 2001; Donovan 2003; Field et al. 2007). For reasons given in Section 2, the relative contribution of the small ($D < 60$ μm) ice crystals can be estimated from satellite radiances. By combining the PSD scheme based on in situ measurements of the larger ice particles with radiance measurements that are sensitive to the small PSD mode, an estimate of the complete PSD (bimodal or monomodal) can be retrieved for a given IWC. The only restriction on the choice of IWC is that it should not yield an ice water path (IWP) that causes $\varepsilon(11\ \mu m) \rightarrow 1.0$ (i.e. a black body). We assumed IWC = 10 mg m^{-3} and IWP = 15 g m^{-3}.

A salient feature of this study is the ability to couch the derived cirrus PSDs in a "climatological context". Parameterizations of PSDs from six studies described in the literature are examined using satellite radiance measurements of cirrus (explained in Section 3*b*). The PSDs described in Lawson et al. (2006a) were parameterized as described in the Appendix. The other PSD schemes were extracted from Ivanova et al. (2001), Donovan (2003), Heymsfield (2003), Ivanova (2004) and Schmitt and Heymsfield (2009). The Donovan scheme is based on lidar-radar ground-based remote sensing.

The Heymsfield (2003) and Schmitt and Heymsfield (2009) PSD schemes are monomodal whereas the others are formulated as bimodal. The modified gamma functions in Donovan (2003) were reformulated as gamma functions. A given PSD scheme provides an initial estimate via cloud temperature for the large mode slope parameter or mean size. It also defines ν for the large and small mode, and λ for the small mode. The satellite-measured

radiances are used to estimate the small mode IWC (related to the parameter N_o) and sometimes to modify the large mode λ. For the monomodal PSD schemes, we use Ivanova et al. (2001) to define the small mode ν and λ in the retrieval algorithm.

b. Effective absorption optical depth ratio

To estimate the complete PSD we use the 12-to-11 μm effective absorption optical depth ratio, or β_{eff}, where β_{eff} is calculated from satellite measured effective emissivities (i.e. based on the zero-scattering approximation) of semi-transparent cirrus. The relative concentration of small ice crystals is then estimated from β_{eff}. To appraise these concentrations in a climatological context, the β_{eff} retrievals should be sufficiently extensive.

The absorption optical depth ratio is equivalent to the absorption efficiency ratio $\bar{Q}_{abs}(12\ \mu m)/\ \bar{Q}_{abs}(11\ \mu m)$ and is independent of IWC. To account for scattering effects, Parol et al. (1991) recommend using an effective absorption efficiency ratio that is equivalent to β_{eff}, where

$$\beta_{eff} = \bar{Q}_{abs,eff}(12\ \mu m)/\ \bar{Q}_{abs,eff}(11\ \mu m) \quad (4)$$

and

$$\bar{Q}_{abs,eff} = \bar{Q}_{abs}\,(1 - \omega_o\, g)/(1 - \omega_o)\,, \quad (5)$$

where g = asymmetry parameter and ω_o = single scattering albedo of the PSD. When all radiation is scattered in the forwards direction (approached in non-scattering conditions), g = 1 and $\bar{Q}_{abs,eff} = \bar{Q}_{abs}$. In the PSD retrieval algorithm, β_{eff} is calculated from (4) using the g parameterization given in Yang et al. (2005). In the effective emissivity satellite retrieval, β_{eff} is calculated as (Inoue 1985):

$$\varepsilon_{eff}(12\ \mu m) = 1 - [1 - \varepsilon_{eff}(11\ \mu m)]^{\beta_{eff}}. \quad (6)$$

1. SATELLITE RETRIEVAL OF β_{eff}

Using the AVHRR (Advanced Very High Resolution Radiometer) channels 4 (10.5-11.5 μm) and 5 (11.5-12.5 μm) aboard the polar orbiting satellite NOAA-7, Inoue (1985) found that $\beta_{eff} \approx 1.08$ based on (6) and 860 satellite measurements for eight cirrus clouds in a 550 km^2 region over the Pacific, centered at (25°N, 150°E). Parol et al. (1991) showed similar β_{eff} results for a small region of cirrus. Giraud et al. (1997) developed an automated split-window analysis using these AVHRR channels that estimates a maximum value for β_{eff}, using 21 AVHRR images of cirrus during fall over the northern Atlantic and Europe. For cirrus temperatures less than -40°C, the mean upper limit for β_{eff} was about 1.12. At warmer temperatures, β_{eff} was larger, but this is believed due to the presence of supercooled liquid water (Giraud et al. 2001) as shown by an analysis including POLDER satellite data where cloud thermodynamic phase was determined. Therefore, for the cirrus clouds in these studies, β_{eff} from AVHRR appears to have an average value of about 1.08 and a mean maximum value of about 1.12.

While these measurements are considerable in scope, they have two limitations: (1) the more extensive measurements of Giraud et al. (1997) do not yield mean values for β_{eff}, making a climatological estimate of average β_{eff} very uncertain, and (2) the retrieval equations involve three unknowns (cirrus emissivity ε for two satellite channels and cirrus temperature T) but the two radiance measurements allow only two unknowns to be solved for. Hence in these studies T was approximated as the brightness temperature of the nearest "black-body" cirrus ($\varepsilon \approx 1.0$).

To address these issues we developed a new retrieval method that solves for T independently of emissivity, using MODIS carbon dioxide channels. A more detailed description of this method can be found in Mitchell and d'Entremont (2008) and in a future paper. In brief, T is estimated using radiances measured in two CO_2 channels centered at 13.3

and 14.2 μm. The real refractive index here is 1.52 and 1.58 respectively, indicating the absorption contribution from tunneling is almost the same in these channels (Mitchell 2000). The imaginary index n_i is 0.355 and 0.246, respectively, yielding a PSD $\bar{Q}_{abs} \approx 1.0$ for each wavelength when tunneling is neglected. For these reasons the emissivity in each channel is essentially the same ($\varepsilon_{13.3} = \varepsilon_{14.2}$), allowing us to solve for T using radiance observations from these two channels. Considering their spectral response functions, the MODIS channels used to retrieve β_{eff} were centered at 11.00 and 12.01 μm. The corresponding response function weighted AVHRR channels are centered at 10.81 and 11.98 μm, making AVHRR β_{eff} slightly greater than MODIS β_{eff}. AVHRR and MODIS β_{eff} values are compared in Heidinger and Pavolonis (2009), although mean values of β_{eff} are not given.

To obtain more extensive sampling of β_{eff}, this method was applied to three case studies: the Tropical Western Pacific International Cirrus Experiment (TWP-ICE) on 2 February 2006, and the Tropical Composition, Cloud and Climate Coupling (TC4) campaign on 22 July and 5 August 2007. The cirrus sampled during these case studies covered approximately 10,428, 65,415 and 41,925 km^2, respectively, based on the approximation of 1 km^2 per MODIS pixel. Since these case studies contained both anvil and in situ cirrus, the mean β_{eff} values obtained should be fairly representative of tropical anvil and in situ cirrus (although it is unclear whether they are representative of cirrus at midlatitudes).

Only single-layer cirrus clouds over ocean were analyzed, making it more straightforward to estimate the clear-atmosphere contribution to the infrared upwelling radiances. These are influenced by two main physical processes: ocean-surface emissivity and atmospheric attenuation. We prescribe ocean-surface emissivity using the model of Nalli et al. (2008) which specifies emissivity as a function of sea surface temperature (SST), wavelength, ocean-surface

wind speed, and view angle. The SST analysis is obtained from the NCEP Global Forecast System (GFS) SSTs which, for our case studies, are valid within 45 minutes of the MODIS overpass times. Finally we use the Optimal Spectral Sampling (OSS) model of Moncet et al. (2008) to compute the clear-atmosphere transmittance profiles in the MODIS infrared channels using coincident GFS upper-air temperature and water-vapor analyses. With these inputs prescribed, the only unknown left to solve for in a given infrared band is the cirrus emissivity.

Since T was also retrieved, we filtered the retrievals such that 1) $T \leq -35\ ^{o}C$ (to insure we were not sampling mixed phase clouds) and 2) $\varepsilon(11\ \mu m) \leq 0.40$. The later was done for the following reasons: 1) to increase confidence that the satellite radiance observations, and hence the emissivity retrievals, are sensitive to ice particles throughout the entire vertical extent of the cloud, thereby strengthening the relationship between T and cirrus microphysics; 2) thermal radiances are affected strongly by the particle size and shape in thin cirrus but less so as the cirrus become optically thicker (Wendisch et al. 2007), with "black-body" cirrus radiances containing no microphysical information ($\beta_{eff} = 1.0$); 3) β_{eff} retrieval errors due to partial cloud coverage of a pixel are relatively low when $\varepsilon(11\ \mu m) < 0.5$ (Heidinger and Pavalonis 2009).

Results from this analysis are summarized in Fig. 4 and Fig. 5. Using all $\varepsilon(11\ \mu m)$ for $T \leq -35\ ^{o}C$, the retrievals were partitioned into nine $\varepsilon(11\ \mu m)$ intervals of width 0.10, with mean values of $\varepsilon(11\ \mu m)$ and β_{eff} calculated within each interval. These are shown in Fig. 4 for each case study, with one standard deviation (σ) from the mean β_{eff} given by the vertical bars. The curves are remarkably similar, suggesting little variance in β_{eff} as a function of $\varepsilon(11\ \mu m)$ as per location and cloud system. This relationship could be due to a relationship between PSD effective diameter D_e and the IWP where IWP is directly related to $\varepsilon(11\ \mu m)$, or it could result from reason (2) above, or perhaps both factors are responsible. For the three case studies, the

mean value of β_{eff} for $\varepsilon(11\ \mu m) \leq 0.4$ and $T \leq -35\ ^{o}C$ is 1.065 ± 0.046. This is the β_{eff} value that all the "retrievals" in this paper are based on, and since the PSD schemes are functions of T, a single β_{eff} value assumes that β_{eff} is independent of T. In Fig. 5, β_{eff} is related to T for the 22 July 2008 case study ($\varepsilon(11\ \mu m) \leq 0.4$, $T \leq -35\ ^{o}C$), where the retrievals were grouped into nine equally spaced temperature intervals to provide mean values and σ in β_{eff}. Figure 5 indicates that β_{eff} is independent of T for this case study. The same result was found for the 5 August TC4 case study, and the TWP-ICE case study did not have a sufficient range in T to draw any conclusions. The maximum β_{eff} values reported in Giraud et al. (1997) for $T < -35\ ^{o}C$ also indicate β_{eff} is independent of T. Thus it appears that β_{eff} for cirrus is generally independent of T.

c. Retrieval logic

The higher the small mode ice mass content (or small mode number concentration, N_{sm}), the larger β_{eff} becomes. This principle is used to determine N_{sm} by matching theory with observations, as described below:

1. The first step when retrieving cloud properties is to begin with a retrieved cloud temperature and a β_{eff} value. For the purposes of this paper, only β_{eff} is needed while temperature in systematically decreased from -20 to -60 ^{o}C.
2. From this temperature, the PSD scheme yields a rough estimate of the large mode mean size $\bar{D}$, the small and large mode dispersion parameters and the small mode mean size. A "first guess" of β_{eff} is calculated using only the large mode for an arbitrary IWC.
3. If the calculated $\beta_{eff} < 1.065$, the small mode contribution to the cirrus IWC is incremented until $\beta_{eff} = 1.065$. In this case the retrieved large mode $\bar{D}$ equals the original "first guess" large mode $\bar{D}$.

4. If the calculated $\beta_{eff} > 1.065$, then no small mode exists, and the large mode $\bar{D}$ is systematically increased until a match is obtained.
5. In this way the effective diameter D_e and the small-to-larger ice particle concentration ratio N_{sm}/N_{lg}, can be retrieved. For a given IWC, ice particle number concentration N and the complete PSD are retrieved.

This procedure requires a "most likely" value for α and β in the ice particle mass-dimension relationship: $m = \alpha D^{\beta}$. The same is true for the projected area-dimension relationship: $A = \gamma D^{\delta}$. Since we are using MADA to predict the optical properties, ice particle shape is expressed and quantified through these m-D and A-D relationships, with the m-D expression having the greater impact on the retrieval. New instrumentation and methods have provided improved estimates of α, β, γ, and δ, for both the small and larger ice particles as described in the Appendix, which provided the values used here. Since the m-D and A-D expressions change as a function of D, the incomplete gamma distribution is used when integrating microphysical and optical properties over the PSD, as described in Mitchell (2002). The sensitivity of the retrieval to these parameters is addressed in Section 4b.

4. Results and discussion

a. Size distributions

As shown in Figs. 4-6, the above retrieval was performed on the PSD schemes described in Ivanova et al. (2001), Donovan (2003) and the Appendix regarding mid-latitude synoptic cirrus, in Heymsfield (2003) and Ivanova (2004) regarding tropical anvil cirrus, and in Schmitt and Heymsfield (2009) regarding tropical tropopause cirrus. The Appendix describes a new PSD parameterization method, which has been developed using data from Lawson et al. (2006a)

collected from synoptic cirrus. This PSD scheme differs from others in that the large mode is parameterized by considering the entire measured PSD, possibly leading to a more realistic PSD shape. Henceforth this PSD scheme will be referred to as the Mitchell scheme. Ivanova (2004) is based on PSDs sampled during the Central Equatorial Pacific Experiment (CEPEX), and will henceforth be referred to as the CEPEX scheme. With the exception of the Donovan (2003), Heymsfield (2003) and Schmitt and Heymsfield (2009) studies, ice crystals less than 50 μm were sampled by an FSSP while larger ice particles were sampled by a 2D-C probe. A Cloud Particle Imager or CPI was used for the Lawson et al. (2006a) dataset for intermediate sizes (characterizing the transition between the FSSP and 2D-C). The novel Donovan PSD scheme is based on ground-based lidar and radar retrievals although some *a priori* microphysical information used in the retrieval is based on in situ measurements.

The above retrieval was applied to all of the PSD schemes using two values of β_{eff}; 1.065 to represent the average or climatological PSD for a given temperature, and 1.11 (mean $\beta_{eff} + \sigma$) to illustrate PSD behavior for 1 standard deviation σ above the mean β_{eff}. Using the methodology described in the previous section, the PSD was retrieved for each of these PSD schemes for three temperatures as shown in Fig. 6. The solid curves correspond to $\beta_{eff} = 1.065$ while the dashed curves correspond to $\beta_{eff} = 1.11$. The difference between the solid and dashed curves yields an estimate of uncertainty in small ice crystal concentration (only the mean + σ concentration is plotted for readability; the mean – σ PSD is always monomodal).

These results indicate that the following PSD configurations are consistent with satellite measured radiances at 11 and 12 μm: monomodal superexponential (Mitchell scheme), bimodal exponential (CEPEX scheme) and bimodal subexponential (Ivanova and Donovan schemes), where subexponential refers only to the large mode. There is a slight bimodality for the Mitchell

synoptic cirrus at -30 ^{o}C when β_{eff} = 1.11, but otherwise the PSD are superexponential monomodal spectra. The monomodal PSDs are consistent with the radiation since their superexponential attribute introduces many small ice crystals that increase β_{eff}. Non-superexponential PSDs require a separate small mode to satisfy β_{eff}. From these results it is difficult to say whether cirrus PSD tend to be monomodal or bimodal. It is possible that the distinction between monomodal and bimodal depends on the methodology employed in parameterizing the PSD. For example, parameterizing the particles measured by the FSSP and 2DC as two separate populations or modes (as done in the CEPEX anvil and Ivanova synoptic schemes) may artificially produce or enhance a bimodal structure. The Mitchell scheme avoids this practice by considering all the particles when parameterizing the large mode (see Appendix).

Figure 7 compares the retrieved climatological PSDs (solid curves) with their corresponding PSD generated by the original PSD scheme (dashed curves). For example, the retrieved PSD at -30 ^{o}C using *a priori* microphysics from the Ivanova synoptic scheme (solid red) is compared against the PSD at -30 ^{o}C predicted by the original Ivanova synoptic cirrus scheme (dashed red). It is seen that the differences between the dashed and solid curves for the Ivanova synoptic scheme are slightly less than the corresponding uncertainty differences reported in Fig. 6. This suggests that the small ice crystal concentrations predicted by the Ivanova scheme (2001) are well within the range of observed concentrations, based on the uncertainty in β_{eff}. For the other PSD schemes, the original scheme over-predicts the concentrations of small ice crystals (relative to the retrieval), often by an order of magnitude or more. A possible explanation is the ice particle shattering phenomena described in the Introduction. The Donovan scheme is not based on in situ aircraft measurements, so ice particle shattering was not a factor in this study. Over prediction by the Donovan scheme appears

greatest at T = -60 ^{o}C, but at T = -30 ^{o}C the Donovan PSD is within the concentration uncertainties shown in Fig. 6.

A possible explanation for the relative agreement between the Ivanova scheme and the Ivanova retrievals in Fig. 7 is that the FSSP-100 used in Ivanova et al. (2001) incorporated a 6 μs "deadtime", as suggested in that paper. That is, after a particle was detected and sized, the probe electronics were inactive for 6 μs before another particle could be sized. During this period (corresponding to 600 μm at an airspeed of 100 m s^{-1}), if the detected particle were the leading edge of a cluster of shattered artifacts, most of the trailing artifacts would be ignored as they pass through the sample volume. Other possible explanations may also exist and the cause of this agreement is speculative at this time.

The PSD schemes of Heymsfield (2003) and Schmitt and Heymsfield (2009) are evaluated in Fig. 8. The Heymsfield scheme applies to both mid-latitude and tropical anvil cirrus while the Schmitt and Heymsfield (henceforth SH) scheme applies only to tropopause cirrus between -56 and -86 ^{o}C. Since the small ice crystal measurements were not considered reliable in Heymsfield (2003), only ice particle sizes greater than 50 μm were considered. Using a β_{eff} of 1.065, the retrieved PSDs indicate the concentrations of small ice crystals are underestimated by the monomodal Heymsfield scheme (dashed curves). However, the Heymsfield scheme is consistent with a β_{eff} of ~ 1.035, which lies within one σ of β_{eff}. In general, these retrievals are highly uncertain when $\beta_{eff} < 1.03$ since a small change in β_{eff} produces a large change in large mode $\bar{D}$. The SH scheme (dashed) agrees fairly well with the retrieved PSD (right panel). The long-dashed curve shows the retrieved PSD when based on $\beta_{eff} = 1.11$ (mean β_{eff} + σ) while the solid curve is for mean β_{eff}. The unmodified SH PSD slope lies between those of the two retrieved PSDs, showing consistency with the retrieved PSDs. The SH scheme is based mostly

on VIPS measurements, which accurately measures down to 10 μm particle size. Shattering may be less of a problem for the VIPS since it is not having the inlet tube that characterizes the FSSP and other probes. Lastly, the SH comparison illustrates how the retrieval decreases the PSD slope when the initial PSD estimate yields a β_{eff} larger than 1.065 (see Section 3c, item 4).

The "radiance corrected" Mitchell scheme exhibits PSDs that appear the most similar to PSDs measured with the new two-dimensional stereo (2D-S) probe, where the shattering problem is much reduced. Examples of 2D-S PSDs are shown in Jensen et al. (2009).

b. Uncertainties

The retrieved PSDs in Figs. 4-6 depend on the ice particle mass-dimension (m-D) power law assumed. For example, if we use a single m-D expression for bullet rosettes (Eq. 22 in Heymsfield et al. 2002), the retrieved CEPEX PSDs are monomodal for temperatures -40 ^{o}C and colder. This is because the bullet rosette m-D expression yields lower ice particle masses for a given D than the m-D expressions in the Appendix, which translates to a lower effective size D_e. Each PSD ice particle has its own effective size d_e and the tunneling contribution to absorption increases with decreasing d_e. Thus, by decreasing d_e, fewer small ice crystals are required in the PSD retrieval to produce a β_{eff} of 1.065. Due to the dependence of our PSD results on the m-D expression, we have developed a new method to better characterize an m-D power law for cirrus, as described in the Appendix. Since our m-D expressions predict more mass per unit length than many of the m-D expressions in the literature (e.g. Mitchell 1996), our main findings will not be changed by using different m-D expressions. That is, the retrieved PSDs have lower concentrations of small ice crystals than the original PSD schemes predict. Naturally, if the PSD retrievals depend on the m-D expression, so also will the sedimentation velocity V_f, D_e and N

that are derived from the retrieved PSD. Since our m-D expression is supported by measurements from the Counterflow Virtual Impactor (CVI), we feel our estimates for V_f, D_e and N are realistic. In addition, since the same m-D expression is used for all the PSD schemes considered, relative differences between the retrieved PSDs and the PSD scheme predicted PSDs should be meaningful (as well as corresponding differences in V_f and D_e) .

Reasonable changes in the tunneling efficiency T_e had little effect on the retrieved PSD, V_f, D_e and N. This is because T_e for small ice crystals is relatively high (Mitchell et al. 2006) and the tunneling contribution for the larger ice particles is always relatively low (regardless of T_e). For example, regarding the CEPEX PSD, setting the value of T_e to 1.0 for all the small ice crystals changed V_f and D_e (calculated from retrieved PSD) by less than 1% and 2%, respectively. This change reduced N by up to 13%.

b. PSD sedimentation rates

As noted in the introduction, one of the two factors that most affect climate sensitivity in GCM simulations is the ice fallspeed (Sanderson et al. 2008; Mitchell et al. 2008). In this study, we use the ice particle mass- and area-dimensional relationships developed in the Appendix and the radiance-corrected PSD schemes developed in this study to estimate the ice fallspeed (that yields the cirrus ice mass sedimentation rate) as a function of temperature. For a given temperature and PSD scheme, the ice fallspeed will be calculated from both the original and the retrieved PSD.

The relationship between the PSD ice fall velocity and the PSD slope and mass-area dimension power laws will now be described. For a monomodal PSD described by (3), the fall velocity giving the mass flux removal rate from a cirrus layer, V_f, corresponds to the median

mass flux dimension or D_f (i.e. the size that divides the PSD mass flux into equal parts). From Ivanova et al. (2001), D_f is defined as

$$D_f = (\beta + B + \nu + 0.67)/\lambda \quad (7)$$

where B is the power on the fallspeed expression:

$$V = A\, D^B . \quad (8)$$

From Eq. (7) and (12) in Mitchell and Heymsfield (2005), B is given as a function of the Best number X and the mass- and area-dimensional power laws, where the mass and projected area A_p are given as

$$m = \alpha\, D^{\beta} , \quad (9)$$

$$A_p = \gamma\, D^{\sigma} , \quad (10)$$

and

$$X = \frac{2\, \alpha\, g\, \rho_a\, D^{\beta+2-\sigma}}{\gamma\ \eta^2} , \quad (11)$$

where g = gravitational constant, η = dynamic viscosity of air and ρ_a = density of air. The prefactor A in (8), given by (6) and (11) in Mitchell and Heymsfield (2005), is also a function of m-D and A_p-D power laws. To obtain V_f, D_f is substituted into (8), and the mass flux removal rate is simply V_f IWC. It can now be seen that accurate estimates of V_f rely on how accurately the PSD slope λ and the m-D and A_p-D relationships are estimated. It might be noteworthy that ice sedimentation rates are often related to the median mass dimension D_m [$D_m = (\beta + \nu + 0.67)/\lambda$], but it is more accurate to relate them to D_f. For a bimodal PSD, one applies this method to both modes as described in Ivanova et al. (2001):

$$V_f = (IWC_{sm}/IWC)\, V_{f,sm} + (IWC_{lg}/IWC)\, V_{f,lg} , \quad (12)$$

where subscript "sm" donotes the PSD small mode, "lg" denotes the large mode and IWC (in denominator) refers to the total IWC. In the retrieval of small mode information, the ratio IWC_{sm}/IWC is retrieved, which is used in (12).

The results of this analysis are shown in Fig. 9-10, where V_f was based on the m-D and A_p-D expressions given in the Appendix. Since the treatment of m-D/A_p-D expressions was identical across PSD schemes, differences in V_f can be attributed solely to differences in PSD formulations. Small discontinuities result from the fact that each 5 ^oC interval has a fixed, unique A_p-D expression that abruptly changes between intervals. An m-D expression specific to small ice crystals less than 240 μm ($\alpha = 0.08274$, $\beta = 2.8135$) and another for larger ice particles ($\alpha = 0.001902$, $\beta = 1.802$) was used for all temperatures (see Appendix). Atmospheric pressure p was estimated for a given temperature T assuming an upper troposphere lapse rate Γ of 7.5 $^oC/km$ with $T_o = -20\ ^oC$ at $p_o = 500$ hPa:

$$p = p_o (T/T_o)^{g/R\Gamma}, \qquad (13)$$

where R is the gas constant for dry air and g is the gravitational constant.

The V_f predicted for the original PSD schemes is shown in Fig. 9 as a function of temperature. The variability in V_f is tremendous, ranging from a few cm s^{-1} to ~ 80 cm s^{-1} at cold temperatures. The Heymsfield scheme has higher values due to the absence of small crystals and the PSD shape, resulting in a temperature dependence of λ and ν that causes D_f to increase slightly with decreasing temperature.

Figure 10 shows the same analysis except that V_f is now derived for the retrieved PSD schemes. While β_{eff} is assumed to be constant (1.065) over this entire temperature range, this has been demonstrated only for T < -35 ^oC for glaciated conditions (Fig. 5). For the 22 July case at warmer temperatures, β_{eff} slowly increases probably due to the increasing presence of a liquid phase (Giraud et al. 2001), but mean $\beta_{eff} \leq 1.10$ for T ≤ -26 ^oC. This appears consistent with a constant β_{eff} over the range of temperatures plotted here for all-ice conditions.

It is seen in Fig. 10 that by including the retrieved estimates of the small ice crystal concentrations, the variance in V_f is reduced considerably. However, considerable variance remains, showing the importance of large mode D_f for predicting V_f. The CEPEX, Ivanova and Donovan schemes generally yield similar V_f values, consistent with their similar large mode behavior described in Fig. 6 and Fig. 7. For T < -40 ^oC, the Donovan and CEPEX schemes exhibit higher V_f than before (sometimes a factor of 2 or more), while V_f for the Mitchell scheme is higher at all temperatures. The Lawson scheme V_f is roughly constant for T < -40 ^oC since the retrieval increases the original $\bar{D}$, producing a quasi-constant $\bar{D}$. In general, V_f is substantially higher in Fig. 10 when the IWC contribution of the small mode is substantially decreased. Since for the Heymsfield scheme the retrieved small mode IWC was only 4-5% of the total IWC, V_f for the Heymsfield scheme did not change much. Since the Ivanova small mode IWC did not change much, V_f did not change much.

In summary, satellite inferred small ice crystal concentrations may be helpful in reducing V_f uncertainties, but better instruments for in situ PSD measurements are also needed. Some uncertainty is expected due to natural variability between cloud systems sampled, and information on the type of cirrus (e.g. physical depth, optical depth, anvil, synoptic) may be useful in characterizing V_f. For example, the cirrus reported in Heymsfield (2003) were relatively thick while the Lawson et al. (2006a) cirrus were relatively thin.

c. Effective diameter, number concentration and mode concentration ratio

Another cloud property important to climate modeling is the effective diameter or D_e. Here we use the definition of D_e that is universal to both liquid and ice clouds (Mitchell 2002),

$$D_e = 3/2 \, (IWC/\rho_i \, P_t) \, , \qquad (14)$$

where ρ_i is the bulk density of ice (0.917 g cm^{-3}) and P_t is the PSD projected area. Figure 11 shows the temperature dependence of D_e based on the original five PSD schemes. The legend is the same as with Fig. 9 and 10. Since the m-D and A_p-D expressions are the same as used for V_t and apply to all PSD schemes, differences in D_e are due solely to the PSD differences. Since the Heymsfield scheme is based on D > 50 μm, D_e is larger there. But even if that scheme is not considered, D_e can still vary by a factor of 4 (from 15 to 60 μm). Figure 12 examines the temperature dependence of D_e when the 5 PSD schemes were modified for small crystals based on the retrieval. Although D_e differences for a given temperature are still substantial, the range in D_e values is greatly reduced due to the changes in small ice crystal concentration. These D_e values are larger than many previous estimates (e.g. Francis et al. 1999) due the m-D expression used, where for D < 240 μm, ice particle mass approaches that of a sphere (consistent with the observation of mostly quasi-spherical ice particle shapes). However, these D_e values are typical of those measured during the TC4 experiment where ice artifacts were either greatly reduced or removed from the measured PSD (Jensen et al. 2009).

Using an arbitrary IWC of 10 mg m^{-3}, we contrast the temperature dependence of the number concentration N predicted by the 5 original PSD schemes with that predicted by the radiance modified PSD schemes, shown in Fig. 13. The curve legend is the same as in Fig. 10. The N curves given by the modified PSD are colored blue and are clustered in the 40-100 $liter^{-1}$ range with virtually no temperature dependence. This concentration range corresponds to the

peak in the probability density function for cirrus cloud N sampled during the TC4 experiment (Jensen et al. 2009), where ice artifacts from shattering were minimized or removed. Those curves in Fig. 13 retrieved from the Ivanova and Donovan schemes are superimposed on one another, as is also true for the Heymsfield scheme at warmer temperatures. The N given by the original PSD schemes are in red and lie above these curves, excepting the Heymsfield scheme (corresponding to N ~ 5 liter^{-1}). The Ivanova scheme appears less sensitive to shattering (see also Fig. 7) and the Heymsfield scheme addressed only the larger ice crystals.

If the radiance modified N curves are representative of nature, this might imply that ice nucleation rates in cirrus clouds are not very dependent on temperature. As temperatures increase, some subset of the nucleated ice crystals might grow more rapidly, producing an ever broadening large mode and increasing bimodal (or superexponential) appearance (see Fig. 6). More research is needed to verify that the MODIS $\beta_{eff} \approx 1.065$ at cirrus temperatures, as N here is dominated by the small ice crystals that are largely determined by β_{eff}.

It is not clear why N as given by the original CEPEX, Donovan and Mitchell schemes increases at the coldest temperatures relative to the corresponding retrieved N. If the N difference (between the original and retrieved PSD) is due to shattering, then this implies that shattering contributions are higher at the colder temperatures where particle sizes are smaller. This finding appears at variance with other studies (Field et al. 2003; McFarquhar et al. 2007; Jensen et al. 2009) that show shattering contributions increase with increasing ice mass and particle size. It is hoped that this paradox will be resolved through future research. It may be noteworthy that the Schmitt and Heymsfield (2009) PSD scheme for thin tropopause cirrus and the Ivanova scheme are not suggestive of enhanced shattering at cold temperatures.

Regarding sampling statistics, the Heymsfield scheme was based on 13 aircraft spiral descents and 3 balloon-borne ascents and the Ivanova scheme was based on 17 flights, while the CEPEX scheme was based on 3 anvil case studies (1 leg-profile per anvil) and the Mitchell scheme was based on 22 flight missions reported in Lawson et al. (2006a) where the cirrus were relatively thin (mean depth = 1.5 km ± 1.0 km).

A study by Gultepe et al. (2000) evaluated the temperature dependence of N (0 to -45 ^{o}C) from many field campaigns, and characterized N based on the 2DC probe alone as well as the FSSP alone. Similar to the Heymsfield and Ivanova schemes in Fig. 13, they found no evidence for any N-temperature dependence, consistent with our retrieved N results.

5. Summary

Considerable uncertainty exists regarding the concentrations of small ice crystals (D < 60 μm) in cirrus clouds, and their contribution to the PSD may strongly affect GCM predictions of climate sensitivity through their impact on the ice fallspeed (Mitchell et al. 2008, Sanderson et al. 2008). The small ice crystals are difficult to measure in situ in part due to the shattering of natural ice particles impacting the inlet tube of the probe used to measure these crystals, thus producing artifacts. Based on a new understanding of the emissivity difference between the 11 and 12 μm channels aboard several satellites, this emissivity difference is used to infer the concentration of small ice crystals for several PSD schemes. This emissivity difference was represented by the 12-to-11 μm absorption optical depth ratio β_{eff}, which was found by several case studies to have a mean value of 1.065 for semi-transparent cirrus clouds [ε(11 μm) ≤ 0.4]. Based on this ratio (which appears independent of temperature), a retrieval algorithm was designed to retrieve the small particle mode of the PSD. An existing PSD scheme supplies *a*

priori information to the algorithm, enabling it to estimate the contribution of small ice crystals to the PSD. Combining this small ice crystal estimate with the PSD for larger particles (initially supplied to the retrieval by the original PSD scheme), the complete PSD is obtained. Comparing these retrieved PSD with the original PSD scheme used in the algorithm, the possible impact of ice particle shattering is evaluated for each PSD scheme. Moreover, the retrieved PSD provide new estimates of the temperature dependence of the PSD effective diameter D_e and fallspeed V_f for each of the five PSD schemes considered. For a given IWC, the temperature dependence of the ice particle number concentration N was evaluated for each original PSD scheme and its corresponding retrieved PSD.

This analysis revealed that the in situ measurements of small ice crystals do appear to be overestimated (presumably due to shattering), but more so at colder temperatures. However, N from two PSD schemes agreed within one standard deviation of their corresponding retrieved N (Figs. 6, 7, 8 & 13). This study suggests that elevated concentrations of small ice crystals may be real, but that their concentrations are generally not as high as some in situ measurements have indicated. However, the spread in our β_{eff} retrievals indicate that cirrus containing high concentrations of small ice crystals (~ 1 cm^{-3}) at moderate-to-low IWPs do sometimes occur. Whether or not the retrieved PSDs are monomodal depends on how the large mode of the PSD is parameterized in the original PSD scheme. If the large mode is parameterized as superexponential, the retrieved PSD tends to be monomodal and superexponential. Otherwise the retrieved PSD tends to be bimodal. The retrieved N was independent of temperature.

If the retrieved PSD are truly representative of natural cirrus, then the uncertainties associated with the temperature dependence of D_e and V_f (as predicted by the original PSD schemes) are reduced considerably for D_e but less so for V_f, based on D_e and V_f from the

retrieved PSD. This may be helpful in representing cirrus clouds in GCMs but also underscores the need for improving the treatment of V_f in GCMs. Cirrus radiative properties and climate feedbacks are largely determined through these properties.

Recently there have been instrumentation improvements regarding PSD measurements (e.g. Lawson et al. 2006b, Jensen et al. 2009), and the findings of this study are in general accord with those in Jensen et al. (2009). In order to have confidence in representing the cirrus PSD in climate models, consistency between in situ and remote PSD measurements is desirable. While Donovan (2003) may have been the first to evaluate the cirrus PSD using ground-based remote sensing, this research effort may be the first to attempt to characterize the cirrus PSD using a satellite remote sensing approach. In this approach, the retrieval infrastructure was derived from in situ measurements of the larger ice particles, and in this way this research can be viewed as a hybrid between remote sensing and in situ measurements. It should be noted that this work did not address Arctic cirrus.

Acknowledgment: This research was sponsored by the Office of Science (BER), U.S. Dept. of Energy, Grant No. DE-FG02-06ER64201. We also gratefully acknowledge the contributions of John Eylander at the U.S. Air Force Weather Agency for supporting the development of the satellite-based cirrus emissivity retrievals. Comments from the three reviewers of this paper have improved it and are much appreciated. The microphysics retrieval computer codes used in this research are freely available to the scientific community.

Appendix: Parameterization of ice particle mass, area and size distributions using in situ data

This appendix describes the methodology used to develop the Mitchell PSD scheme used in this study. In addition, the ice particle mass-dimension and projected area-dimension power laws used in this study are developed here. Separate power laws apply to the small and larger ice crystals, and these are an important component of the retrieval algorithm.

The aircraft data used to develop this methodology and PSD scheme are described in Lawson et al. (2006a) and consist of 22 flight missions in mid-latitude cirrus of non-convective origin, 104 horizontal flight legs (one PSD per leg), and 15,000 km of in-cloud sampling. The PSDs were measured by the FSSP, CPI and 2D-C probes over the approximate size range of 2-30 μm, 31-200 μm, and 201-2000 μm, respectively. These settings varied somewhat between flight missions depending on particle concentrations. Due to the continuous nature of these PSD, it was possible to develop this methodology. Although shattering is likely to have produced many small artifact crystals in this data set (Jensen et al. 2009), it is nonetheless useful for demonstrating and evaluating a new methodology for parameterizing PSD.

The PSD in the Lawson et al. (2006a) mid-latitude cirrus dataset can be described as two populations of ice particles. The first population is likely to often be contaminated with shattering artifacts and can be described as a single mode exhibiting a mean maximum dimension $\overline{D}$ between about 10 and 20 μm and extending to sizes of about 60 μm. The second population of ice particles is often observed as a broadened shoulder of the first mode for maximum dimension D > 60 μm for temperatures greater than –50 ^{o}C. Due to ice particle morphology changes that occurred around a N(D) inflection point near 60 μm, 60 μm was selected as the size dividing the two populations for this particular dataset.

a. Analytically describing the PSD

The two populations are parameterized using two gamma functions as defined by (3). The methodology for parameterizing the PSD is similar to that described in Ivanova et al. (2001) but with some improvements. While some PSDs may not require the parameterization of two modes, sometimes PSD are bimodal and this possibility should be allowed for in a parameterization scheme. The two-gamma approach effectively defaults to a single-gamma PSD if there is only one size mode.

The formulae for calculating the gamma distribution parameters when PSD are monomodal (or for the small mode when PSD are bimodal) are as follows:

$$\nu = [(\beta + 0.67)\ \bar{D} - D_m] / (D_m - \bar{D}) , \qquad \text{(A1)}$$

where β is defined in (9), $\bar{D}$ is the mean maximum dimension and D_m is the median mass dimension of a given mode. The slope parameter is defined as

$$\lambda = (\nu + 1)/\ \bar{D} \qquad \text{(A2)}$$

and the N_o parameter can be defined in terms of N or IWC:

$$N_o = \frac{N\,\lambda^{\nu+1}}{\Gamma(\nu+1)} , \qquad \text{(A3)}$$

or

$$N_o = \frac{\lambda^{\beta+\nu+1}\,IWC}{\alpha\,\Gamma(\beta+\nu+1)} . \qquad \text{(A4)}$$

To obtain these parameters, ν is first determined from the measured PSD. This requires knowledge of $\bar{D}$, D_m and β. While the calculation of $\bar{D}$ is straightforward via numerical integration over the measured PSD, the calculation of D_m involves integrating the PSD mass until it matches half of the IWC:

$$IWC/2 = \sum_{i=1}^{n(Dm)} m(D_i)\, N(D_i) \Delta D_i \,, \qquad (A5)$$

where i refers to PSD bin number, D_i is midpoint of ith bin, ΔD_i is the bin width, and $N(D_i)$ is the ice particle concentration in the ith bin. The IWC is given by the right side of (A5) when the upper limit is the maximum size of the PSD. The calculation of D_m is not sensitive to the choice of α (Mitchell 1991), allowing ν to be determined from (A1). Once ν is determined, λ is calculated from (A2) and N_o can be calculated from (A3) using the measured number concentration N. Alternatively, (A4) can be used if the IWC is measured.

If the PSD are bimodal, the calculation of the large mode gamma parameters is more involved because the concentrations of the smallest particles in the large mode gamma distribution are "masked" by the small particle mode. Thus the behavior of the large mode is only partially revealed by the measured PSD. However, ν can be estimated for the large mode by using the entire measured PSD and solving for ν via (A1). But since (A1) is based on $\bar{D}$ and D_m, the largest ice particles in the PSD are not always well represented by the gamma fit. To remedy this, ν can also be expressed in terms of D_Z which is the D that divides the entire PSD into equal parts of radar reflectivity Z:

$$\nu = [(2\beta + 0.67)\ \bar{D} - D_Z] \,/\, (D_Z - \bar{D}) \,, \qquad (A6)$$

where D_Z is determined from

$$Z/2 = \sum_{i=1}^{n(Dz)} [m(D_i)]^2\, N(D_i) \Delta D_i \qquad (A7)$$

and Z is given by (A7) with maximum size as the summation upper limit (Mitchell et al. 2006b). For a given gamma function, (A6) yields the same value of ν as (A1) does. However, for measured PSD, (A6) yields a gamma fit having a lower (or more negative) value for ν than does

(A1) while better representing the largest ice particle concentrations. Equation (A6) can be derived analogous to (A1) as described in Mitchell (1991).

Once the large mode ν is determined, the large mode λ is given by (A2) where $\bar{D}$ and ν correspond to the entire PSD. Equation (A3) or (A4) cannot be used to calculate N_o since the number concentration N or the IWC for the large mode is not known (i.e. the contribution of smaller particles to the large mode gamma distribution fit). However, the large mode N_o can be determined by solving (3) for N_o:

$$N_o = N(D)/ [D^{\nu} \exp(-\lambda D)]. \quad \text{(A8)}$$

Using the measured PSD, a point corresponding to the large mode is selected to fix D and N(D) so that N_o can be calculated. In practice, to avoid unrepresentative behavior at a given point, D and N(D) can be averaged over a 5 or 10 micron interval. We now have equations describing all six parameters for the small and large mode gamma distributions based on the measured PSD. In Section c we will describe methods of obtaining α and β, thus closing this system of equations and yielding analytical fits to the observed PSD.

b. Parameterizing the PSD

In the approach taken here, the key to parameterizing the PSD in mid-latitude cirrus is to first analytically describe the PSD, as described above. Once the various PSD terms are known for each temperature level, the PSD can be diagnosed as a function of temperature and IWC by relating some terms to temperature using polynomial curve fitting. The terms related only to temperature are ν and $\bar{D}$ (for both modes). From these, λ is calculated using (A2). The polynomial best-fit equations are not shown here due to space limitations.

For bimodal PSD, the two N_o terms can be determined for a given IWC if one knows the ratio of small mode IWC to total IWC. This ratio can be calculated from the fitted PSD modes using corresponding values for α and β. Then this IWC ratio can be related to temperature using curve-fitting methods. So for a given temperature and IWC, one knows the IWC in each mode. For example, if the total IWC = IWC_t , the small mode IWC (IWC_{sm}) is estimated by multiplying the IWC ratio (IWC_{sm}/IWC_t) by IWC_t. Similarly, the large mode IWC is given by the difference $IWC_t - IWC_{sm}$. Knowing the IWC for each mode, N_o for each mode can be estimated by (A4). However, since the small mode includes some particles having D > 60 μm and the large mode includes many particles having D < 60 μm, and the mass-dimension relationships change across the PSD modes, N_o is most accurately calculated using the incomplete gamma function. This equation for N_o is described in Mitchell (2002; Eq. A11).

The PSD predicted from this parameterization scheme (dashed curves) are compared with the sampling time-weighted mean PSD (solid curves) for each 5 ^oC temperature interval in Fig. A1. The parameterized PSD at the two warmest temperatures are based on an extrapolation scheme using results from Ivanova et al. (2001). Since there are no measured PSD to compare with in these two cases, only the predicted curves are shown. For each temperature interval the mid-point temperature (at which the PSD scheme was evaluated) is indicated, along with the D_e based on the measured and predicted PSD. The measurement derived IWC was used as input for the PSD scheme.

c. Estimating m-D power laws for cirrus clouds

Little is known about the m-D relationships for cirrus particles as it is difficult to measure in situ the masses of individual ice crystals and to gather meaningful statistics on crystal mass and

dimension. However, Baker and Lawson (2006) have developed a method that relates an ice particle's projected area to its mass. Using field measurements of photographed ice crystals and their corresponding melted hemispherical droplet images from which their mass was estimated (described in Mitchell et al. 1990), Baker and Lawson related the projected area of these crystals to their masses. This resulted in m-A_p relationships for calculating the IWC since the A_p directly measured by the optical probes can be translated into particle mass and integrated over the PSD to provide IWC. Figure A2 shows IWCs obtained by applying this technique to 2D-S probe (Lawson et al. 2006b) PSD measurements during the NASA TC4 campaign. As demonstrated in Jensen et al. (2009), the 2D-S measures ice particles from 10 to 1280 μm at jet aircraft speed and electronically process these measurements using inter-arrival times to remove shattered particles. These 2D-S IWCs are compared with IWCs measured simultaneously by the co-located Counterflow Virtual Impactor (CVI) aboard the DC-8. Given that these are two very different methods for estimating the IWC, the agreement is quite good (within ~20% usually). The CVI uncertainty in IWC is estimated to be 13% at water contents of 0.05 to 1.0 g m^{-3}, and increases to 16% at 0.01 g m^{-3} and to 40% at 0.0025 g m^{-3} (Heymsfield et al. 2007b; Twohy et al. 1997, 2003). The data in Fig. A2b are from all flights in anvil and aged anvil cirrus during the TC4 campaign (covering ~2600 km). Regions of CVI data where the CVI saturates have been eliminated. The CVI saturated between 0.5 and 1.0 g m^{-3}, depending on how the operator set the flow rate. Also, regions where the CVI shows non-zero IWC after exiting cloud (due to residual moisture in the CVI chamber) have been set to zero in Fig. A2b. Figure A2a shows such regions where the blue 2D-S curve is at zero (no cloud) while the red CVI curve is non-zero. This agreement between the CVI and 2D-S IWC provides some level of confidence that the 2D-S IWCs are realistic. It should be noted that Heymsfield et al. (2002) also found that ice particle area was a better predictor of mass than ice particle maximum dimension.

The 2D-S measurements combined with the m-A_p relationships provides estimates of differential mass concentration in each size bin of the 2D-S, and integrating over the PSD yields the IWC. Dividing the bin mass concentration by the bin number concentration yields the average ice particle mass for that bin. Figure A3 plots for a given PSD the bin average ice particle mass against the bin size midpoint (i.e. approximate average ice particle length in bin), generating m-D relationships for the various PSD. The red curve represents an average of all the PSDs sampled in aged anvils that were generally characterized by dense quasi-spherical particles (classified as spheres or irregulars). The blue curve corresponds to PSD sampled at the top of an aged anvil at -58 ^{o}C comprised almost entirely of quasi-spherical particles. As expected, it conforms closely to the dashed black line that gives the m-D relationship for ice spheres. The purple curve is from PSD measured in non-anvil (in situ) cirrus having relatively high bullet rosette concentrations (~ 20% of total and 50-60% of the larger ice particles). Surprisingly the purple curve is not too different from the other curves characterized by dense, blocky or quasi-spherical ice particles. The black lines are the best-fit lines for the averaged PSD (red curve). The two black lines meet at a size D of 240 μm that seems to divide the PSD into two ice particle shape regimes.

The above illustrates how 2D-S estimates of size-resolved mass and number concentration can be used to produce m-D expressions that yield IWCs similar to those measured by the CVI. This consistency provides added confidence that these m-D expressions are realistic. From the 2D-S PSD data, two m-D expressions are estimated for aged anvil cirrus (red curve); one for D < 240 μm:

$$m = 0.08274\ D^{2.814}, \qquad \text{(A9)}$$

and one for D > 240 μm:

$$m = 0.001902\ D^{1.802}, \qquad \text{(A10)}$$

where all units are cgs. These expressions were used exclusively in this study. Previous studies (e.g. Heymsfield et al. 2007) have also related m-D expressions to CVI measurements but only a single m-D expression was used to characterize the PSD. As a result of this, ice particles having $D < \sim 100$ μm generally have predicted masses greater than those of an ice sphere of the same length, which is non-physical. While one can prevent the particle mass from exceeding that of an ice sphere in numerical integrations, it is more practical and accurate to use the incomplete gamma function to perform the integration analytically using two m-D expressions. Near cloud top, maximum particle size is often around 100-300 μm, making a two m-D approach a must.

In the future we intend to develop temperature-dependent m-D expressions for other types of cirrus, but (A9) and (A10) are sufficient for the purpose of this study.

d. Estimating A_p-D power laws for cirrus clouds

Ice particle projected area-dimension (A-D) power law relationships were developed for this dataset that are representative for each PSD mode at each temperature interval. The CPI renders accurate measurements of ice particle projected area that have been used to determine A_p-D relationships for each PSD mode at each temperature interval. When the PSD projected area for each mode was determined directly from the CPI measurements, the difference between this measured projected area and the projected area calculated by integrating the A_p-D relationships over the PSD was no more than about 3%. The pre-factors and exponents for these A_p-D relationships are given in Table A1 as a function of PSD mode and temperature interval, and these relationships were used in this study. Analogous to N_o, the incomplete gamma function can be used for obtaining the highest accuracy when calculating P_t in (14).

REFERENCES

Baker, B. and R.P. Lawson, 2006: Improvement in determination of ice water content from two-dimensional particle imagery. Part I: Image-to-mass relationships. *J. Appl. Meteorol. Clim.*, **45**, 1282-1290.

Baumgardner, D., H. Jonsson, W. Dawson, D. O'Connor and R. Newton, 2001: The cloud, aerosol and recipitation spectrometer: a new instrument for cloud investigations. *Atmos. Res.*, **59-60**, 251-264.

Donovan, D.P., 2003: Ice-cloud effective particle size parameterization based on combined lidar, radar reflectivity, and mean Doppler velocity measurements. *J. Geophys. Res.*, **108**, D18, 4573, doi:10.1029/2003JD003469, 2003.

Downing, H.D., and D. Williams, 1975: Optical constants of water in the infrared. *J. Geophys. Res.*, **80**, 1656-1661.

Field, P.R., R. Wood, P.R.A. Brown, P.H. Kaye, E. Hirst, R. Greenaway, and J.A. Smith, 2003: Ice particle interarrival times measured with a fast FSSP. *J. Atmos. Ocean. Tech.*, **20**, 249-261.

Field, P.R., A.J. Heymsfield and A. Bansemer, 2007: Snow size distribution parameterization for midlatitude and tropical ice clouds. *J. Atmos. Sci.*, **64**, 4346-4365.

Francis, P.N., J.S. Foot and A.J. Baran, 1999: Aircraft measurements of solar and infrared radiative properties of cirrus and their dependence on ice crystal shape. *J. Geophys. Res.*, **104**, 31,685-31,695.

Garrett, T. J., B.C. Navarro, C. H. Twohy, E. J. Jensen, D. G. Baumgardner, P. T. Bui, H. Gerber, R. L. Herman, A. J. Heymsfield, P. Lawson, P. Minnis, L. Nguyen, M. Poellot, S. K. Pope, F. P. J. Valero, and E. M. Weinstock, 2005: Evolution of a Florida cirrus anvil. *J. Atmos. Sci*., **62**, 2352-2372.

Gayet, J-F., V. Shcherbakov, H. Mannstein, A. Minikin, U. Schumann, J. Strom, A. Petzold, J. Ovarlez and F. Immler, 2006: Microphysical and optical properties of midlatitude cirrus clouds observed in the southern hemisphere during INCA. *Q.J.R. Meteorol. Soc*., **132**, 2719-2748.

Giraud, V., J.C. Buriez, Y. Fouquart, and F. Parol, 1997: Large-Scale Analysis of Cirrus Clouds from AVHRR Data: Assessment of Both a Microphysical Index and the Cloud-Top Temperature. *J. Appl. Met.*, **36**, 664-674.

Giraud, V., O. Thouron, J. Reidi and P. Goloub, 2001: Analysis of direct comparison of cloud top temperature and infrared split window signature against independent retrievals of cloud thermodynamic phase. *Geophys. Res. Lett*., **28**, 983-986.

Gultepe, I., G.A. Isaac and S.G. Cober, 2001: Ice crystal number concentration versus temperature for climate studies. *Int. J. Climatol*., **21**, 1281-1302.

Hallett, J., 1976: Measurements of size, concentration and structure of atmospheric particulates by the airborne continuous particle replicator. Air Force Geophysics Laboratory, Air Force Systems Command, United States Air Force, Report AFGL-TR-76-0149, Hanscom AFB, MA. 92 pp.

Heidinger, A., and M.J. Pavolonis, 2009: Gazing at cirrus clouds for 25 years through a split window. Part I: Methodology. *J. Appl. Meteor. Climatol*., **48**, 1100-1116.

Heymsfield, A.J., S. Lewis, A. Bansemer, J. Iaquinta and L.M. Miloshevich, 2002: A general approach for deriving the properties of cirrus and stratiform ice cloud properties. *J. Atmos. Sci*., **59**, 3-29.

Heymsfield, A.J., 2003: Properties of tropical and mid-latitude ice cloud ensembles. Part II: Applications for mesoscale and climate models. *J. Atmos. Sci*., **60**, 2592-2611.

Heymsfield, A. J., 2007a: On the measurement of small ice crystals in clouds. Geophys. Res. Lett., 34, L23812, doi:1029/2007GL03051.

Heymsfield, A.J., A. Bansemer, and C. Twohy, 2007b: Refinements to ice particle mass dimensional and terminal velocity relationships for ice clouds. Part I: Temperature dependence. *J. Atmos. Sci.*, **64**, 1047-1067.

Inoue, T., 1985: On the temperature and emissivity determination of semitransparent cirrus clouds by bispectral measurements in the 10 μm window region. *J. Meteorol. Soc. Jpn.*, **63**, 88-98.

Ivanova, D., D.L. Mitchell, W.P. Arnott and M. Poellot, 2001: A GCM parameterization for bimodal size spectra and ice mass removal rates in mid-latitude cirrus clouds. Atmos. Res., **59**, 89-113.

Ivanova, D., 2004: Cirrus clouds parameterization for global climate models (GCMs) and North American (Mexican) monsoon modeling study. Ph.D. dissertation, University of Nevada, Reno, 181 pp.

Jensen, E. J., P. Lawson, B. Pilson, B. Baker, Q. Mo, A. J. Heymsfield, A. Bansemer, T.P. Bui, M. McGill, D. Hlavka, G. Heymsfield, S. Platnick, G. T. Arnold, and S. Tanelli, 2008: On the importance of small ice crystals in tropical cirrus. *Atmos. Chem. Phys. Discuss.*, **9**, 5321-5370.

Knollenberg, R.G., 1981: Techniques for probing cloud microstructure. *Clouds Their Formation, Optical Properties, and Effects,* P.V. Hobbs and A. Deepak, Eds., Academic Press, New York, NY. 15-91.

Korolev, A., and G.A. Isaac, 2003: Roundness and aspect ratios of particles in ice clouds. *J. Atmos. Sci*., **60**, 1795-1808.

Korolev, A., and G.A. Isaac, 2006: Relative humidity in liquid, mixed phase and ice clouds. *J. Atmos. Sci*., **63**, 2865-2880.

Lawson, R.P., B. Baker, B. Pilson and Q. Mo, 2006a: In situ observations of the microphysical properties of wave, cirrus and anvil clouds. Part 2: Cirrus clouds. *J. Atmos. Sci*., **63**, 3186-3203.

Lawson, R.P., D. O'Conner, P. Zmarzly, K. Weaver, B. Baker, Q. Mo, F. Jonnson, 2006b: The 2D-S (stereo) probe: Design and preliminary tests of a new airborne, high-speed, high-resolution particle imaging probe. *J. Atmos. Ocean. Tech*., **23**, 1462-1477.

McFarquhar, G.M., and A.J. Heymsfield, 1997: Parameterization of tropical cirrus ice crystal size distributions and implications for radiation transfer: Results from CEPEX. *J. Atmos. Sci*., **54**, 2187-2200.

McFarquhar, G.M., J. Um, M. Freer, D. Baumgardner, G. Kok and G. Mace, 2007: The importance of small ice crystals to cirrus properties: Observations from the Tropical Warm Pool International Cloud Experiment (TWP-ICE). Geophys. Res. Lett., 34, L13803,doi:10.1029/2007GL02986, 2007.

McFarquhar, G.M., and A.J. Heymsfield, 1996: Microphysical characteristics of three anvils sampled during the Central Equatorial Pacific Experiment. *J. Atmos. Sci*., **53**, 2401-2422.

Mitchell, D.L., R. Zhang and R.L. Pitter, 1990: Mass-dimensional relationships for ice particles and the influence of riming on snowfall rates. *J. Appl. Meteor*., **29**, 153-163.

Mitchell, D.L., 1991: Evolution of snow-size spectra in cyclonic storms. II: Deviations from the exponential form. *J. Atmos. Sci.*, **48**, 1885-1899.

Mitchell, D.L., and W.P. Arnott, 1994: A model predicting the evolution of ice particle size spectra and radiative properties of cirrus clouds. Part II: Dependence of absorption and extinction on ice crystal morphology. *J. Atmos. Sci*., **51**, 817-832.

Mitchell, D.L., 1996: Use of mass- and area-dimensional power laws for determining precipitation particle terminal velocities. *J. Atmos. Sci*., **53**, 2967-2988.

Mitchell, D.L., A. Macke, and Y. Liu, 1996: Modeling cirrus clouds. Part II: Treatment of radiative properties. *J. Atmos. Sci*., **53**, 2967-2988.

Mitchell, D.L., 2000: Parameterization of the Mie extinction and absorption coefficients for water clouds. *J. Atmos. Sci*., **57**, 1311-1326.

Mitchell, D.L., 2002: Effective diameter in radiation transfer: General definition, applications and limitations. *J. Atmos. Sci*., **59**, 2330-2346.

Mitchell, D.L., and A.J. Heymsfield, 2005: Refinements in the treatment of ice particle terminal velocities, highlighting aggregates. *J. Atmos. Sci*., **62**, 1637-1644.

Mitchell, D.L., A.J. Baran, W.P. Arnott and C. Schmitt, 2006a: Testing and comparing the modified anomalous diffraction approximation. *J. Atmos. Sci*., **63**, 2948-2962.

Mitchell, D.L., A. Huggins, V. Grubisic, 2006b: A new snow growth model with application to radar precipitation estimates. *Atmos. Research*., **82**, 2-18.

Mitchell, D.L., P.J. Rasch, D. Ivanova, G.M. McFarquhar and T. Nousiainen, 2008: Impact of small ice crystal assumptions on ice sedimentation rates in cirrus clouds and GCM simulations. Geophys. Res. Lett., **35**, L09806, doi:10.1029/2008GL033552, 2008.

Mitchell, D.L., and R.P. d'Entremont, 2008: Satellite remote sensing of small ice crystal concentrations in cirrus clouds. International Conference on Clouds and Precipitation, Cancun, Mexico, 7-11 July 2008. Available on CD.

Moncet, J-L., G. Uymin, A. E. Lipton, and H. E. Snell, 2008: Infrared Radiance Modeling by Optimal Spectral Sampling. *J. Atmos. Sci*., **65**, 3917–3934.

Nalli, N. R., P. J. Minnett and P. van Delst, 2008: Emissivity and reflection model for calculating unpolarized isotropic water surface-leaving radiance in the infrared. I: Theoretical development and calculations. *Applied Optics,* **47**, 3701-3721, doi:10.1364/AO.47.003701.

Parol, F., J.C. Buriez, G. Brogniez and Y. Fouquart, 1991: Information content of AVHRR channels 4 and 5 with respect to the effective radius of cirrus cloud particles. *J. Appl. Meteorol.*, **30**, 973-984.

Platt, C.M.R., 1997: A parameterization of the visible extinction coefficient of ice clouds in terms of the ice/water content. *J. Atmos. Sci*., **54**, 2083-2098.

Ryan, B., 1996: On the global variation of precipitating layer clouds. *Bull. Am. Meteorol. Soc*., **77**, 53-70.

Sanderson, B.M., C. Piani, W.J. Ingram, D.A. Stone, M.R. Allen, 2008: Towards constraining climate sensitivity by linear analysis of feedback patterns in thousands of perturbed physics GCM simulations. Clim. Dyn., 30, 175-190.

Schmitt, C.G., and A.J. Heymsfield, 2009: The size distribution and mass weighted terminal velocity of low-latitude tropopause cirrus crystal populations. *J. Atmos. Sci*., in press.

Stubenrauch, C., F. Eddounia and G. Rädel, 2004: Correlations between microphysical properties of large-scale semi-transparent cirrus and the state of the atmosphere. *Atmos. Res.*, **72**, 403-423.

Twohy, C.H., A.J. Schanot, and W.A. Cooper, 1997: Measurement of condensed water content in liquid and ice clouds using an airborne counterflow virtual impactor. *J. Atmos. Oceanic Technol.*, **14**, 197–202.

Twohy, C.H., J.W. Strapp, and M. Wendisch, 2003: Performance of a counterflow virtual impactor in the NASA icing research tunnel. *J. Atmos. Oceanic Technol*., **20**, 781-790.

Warren, S. G., and R. E. Brandt, 2008: Optical constants of ice from the ultraviolet to the microwave: A revised compilation. *J. Geophys. Res*., **113**, D14220, doi:10.1029/2007JD009744, 2008.

Wendisch, M., P. Yang and P. Pilewskie, 2007: Effects of ice crystal habit on thermal infrared radiative properties and forcing of cirrus. J. Geophys. Res., 112, D08201, doi:10.1029/2006JD007899.

Yang, P., H. Wei, H-L. Huang, B.A. Baum, Y.X. Hu, G.W. Kattawar, M.I. Mishchenko, and Q. Fu, 2005: Scattering and absorption property database for nonspherical ice particles in the near- through far-infrared spectral region. *Appl. Opt*., **44**, 5512–5523.

FIGURE CAPTIONS

Figure 1. Solid curves correspond to ice while dashed curves are for liquid water, showing the real refractive index (top) and imaginary refractive index (bottom). The two middle curves show the ADT absorption efficiency for an ice crystal having an effective size of 25 μm and a 10 μm cloud droplet, where absorption occurs only over the particle cross-section. See text for details.

Figure 2. Size dependence of the photon tunneling contribution (i.e. wave resonance) to the absorption efficiency of a hexagonal column for a wavelength of 12 μm.

Figure 3. Absorption efficiencies for a bimodal size distribution (solid) and the same PSD but without the small crystal mode (dashed). The difference in the curves between 11 and 13 μm is due only to tunneling.

Figure 4. The mean values of the retrieved effective absorption optical depth ratio (β_{eff}) related to retrieved mean emissivity for the three case studies, where retrieved cirrus temperature < -35 ^{o}C to insure the clouds are only ice phase. Vertical bars indicate standard deviations and the β_{eff} = 1.0 line is given for ease of reference.

Figure 5. The retrieved effective absorption optical depth ratio (β_{eff}) related to cirrus cloud temperature for ε(11 μm) ≤ 0.4 and T < -35 ^{o}C, using the 22 July 2008 TC4 case study. Mean β_{eff} are given by the pink curve and vertical bars indicate standard deviations.

Figure 6. Retrieved PSD from the indicated PSD schemes based on the mean β_{eff} of 1.065 (solid) and the mean + σ β_{eff} of 1.11 (dashed) for the indicated IWC.

Figure 7. Retrieved PSD (solid) based on $\beta_{eff} = 1.065$ compared with the corresponding PSD from the original PSD scheme (dashed).

Figure 8. Similar to Fig. 7 but for the PSD schemes of Heymsfield (left panel) and Schmitt and Heymsfield (right panel). The long-dashed curve in the right panel is the PSD corresponding to $\beta_{eff} = 1.11$, which is one standard deviation above the mean β_{eff} (corresponding to solid curve). See text for details.

Figure 9. Temperature dependence of the PSD median mass flux fall velocity for the 5 applicable PSD schemes that share the same ice particle mass and projected area relationships and standard atmosphere conditions.

Figure 10. Same as Fig. 9 but fall velocities are now based on the retrieved PSD for each PSD scheme.

Figure 11. Temperature dependence of D_e for each of the PSD schemes where all schemes share the same ice particle mass and area assumptions. Legend is the same as in Fig. 10.

Figure 12. Same as Fig. 11 except now D_e is based on the retrieved PSD from each PSD scheme. Legend is the same as in Fig. 10.

Figure 13. Temperature dependence of the total number concentration for the original PSD schemes (in red) at the indicated IWC, and the same for the corresponding retrieved PSD (in blue). For T > -35 ^{o}C, the curves for the retrieved Ivanova, Donovan and Heymsfield schemes are superimposed, with the Ivanova curve only visible around T = -50 ^{o}C. Legend is the same as in Fig. 10.

Figure A1: Comparisons of PSD predicted by the parameterization scheme (dashed) with the time weighted mean PSD from Lawson et al. (2006a) midlatitude cirrus measurements (solid) for each temperature interval. Note that there are no measurements to compare with the -27°C and -22°C parameterizations. Measurement derived and predicted D_e are compared to evaluate the accuracy of the analytical fits and parameterization procedure.

Figure A2: A: Time series of the 2D-S and CVI IWC for a TC4 case study. CVI response time lagged 6 seconds behind 2D-S measurements, producing a slight offset. B: 2D-S IWCs compared with CVI IWCs for 12,000 1-Hz measurements (averaged over 10-s) in TC4 anvils cirrus.

Figure A3: m-D relationships derived from 2D-S PSD measurements as described in Appendix.

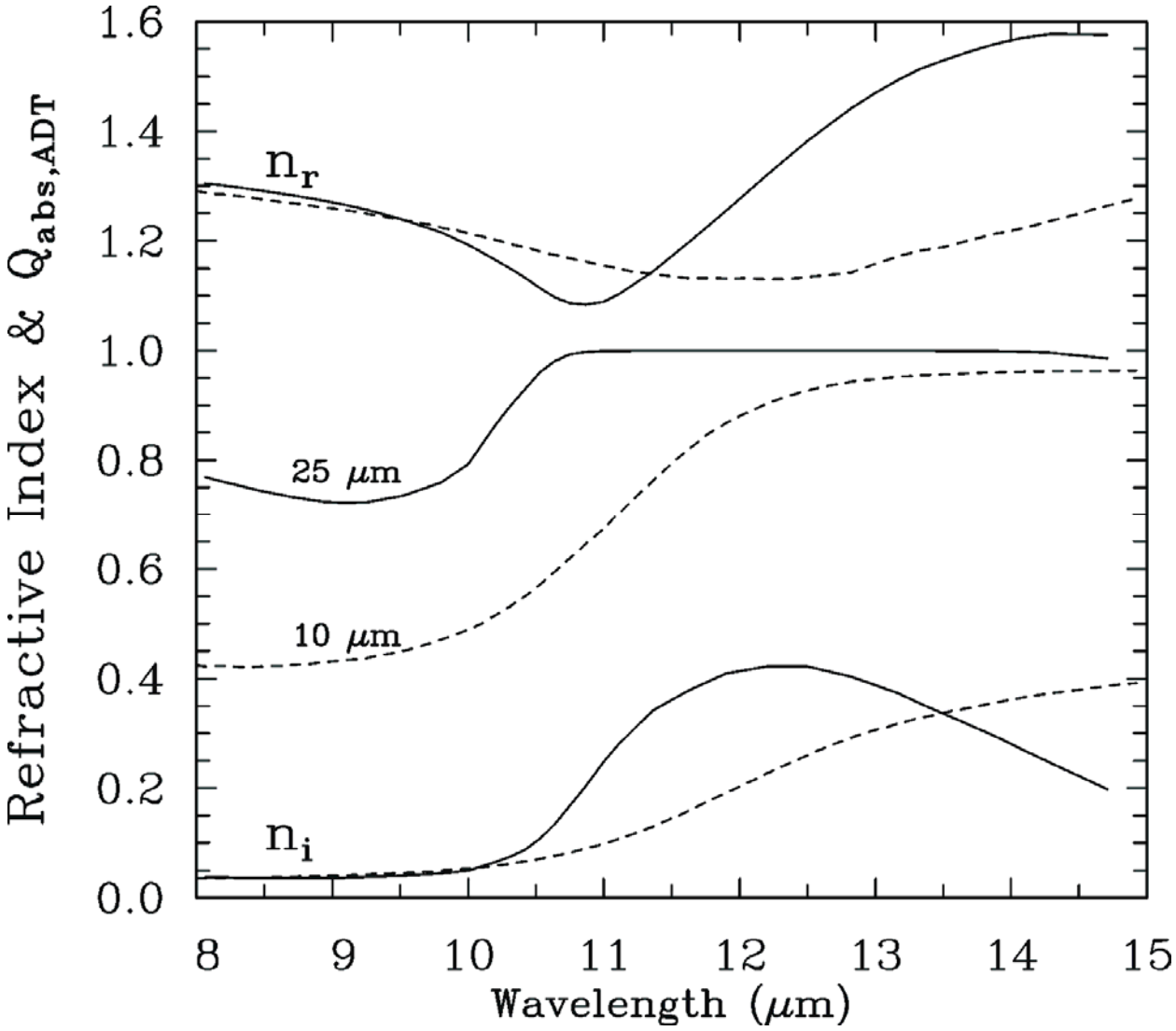

Figure 1. Solid curves correspond to ice while dashed curves are for liquid water, showing the real part (top) and imaginary part (bottom) of the refractive index. The two middle curves show the ADT absorption efficiency for an ice crystal having an effective size of 25 μm and a 10 μm cloud droplet, where absorption occurs only over the particle cross-section. See text for details.

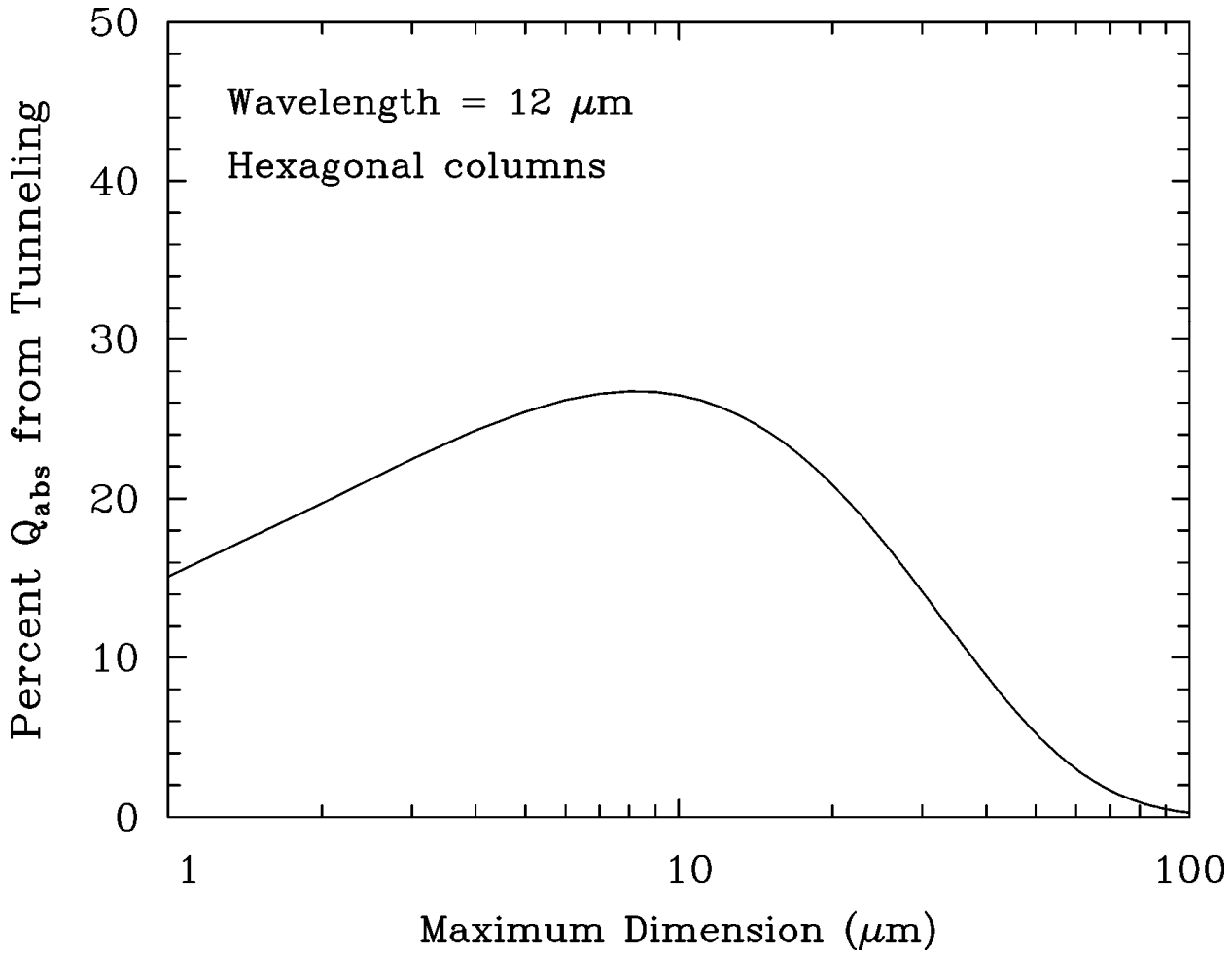

Figure 2. Size dependence of the photon tunneling contribution (i.e. wave resonance) to the absorption efficiency of a hexagonal column for a wavelength of 12 μm.

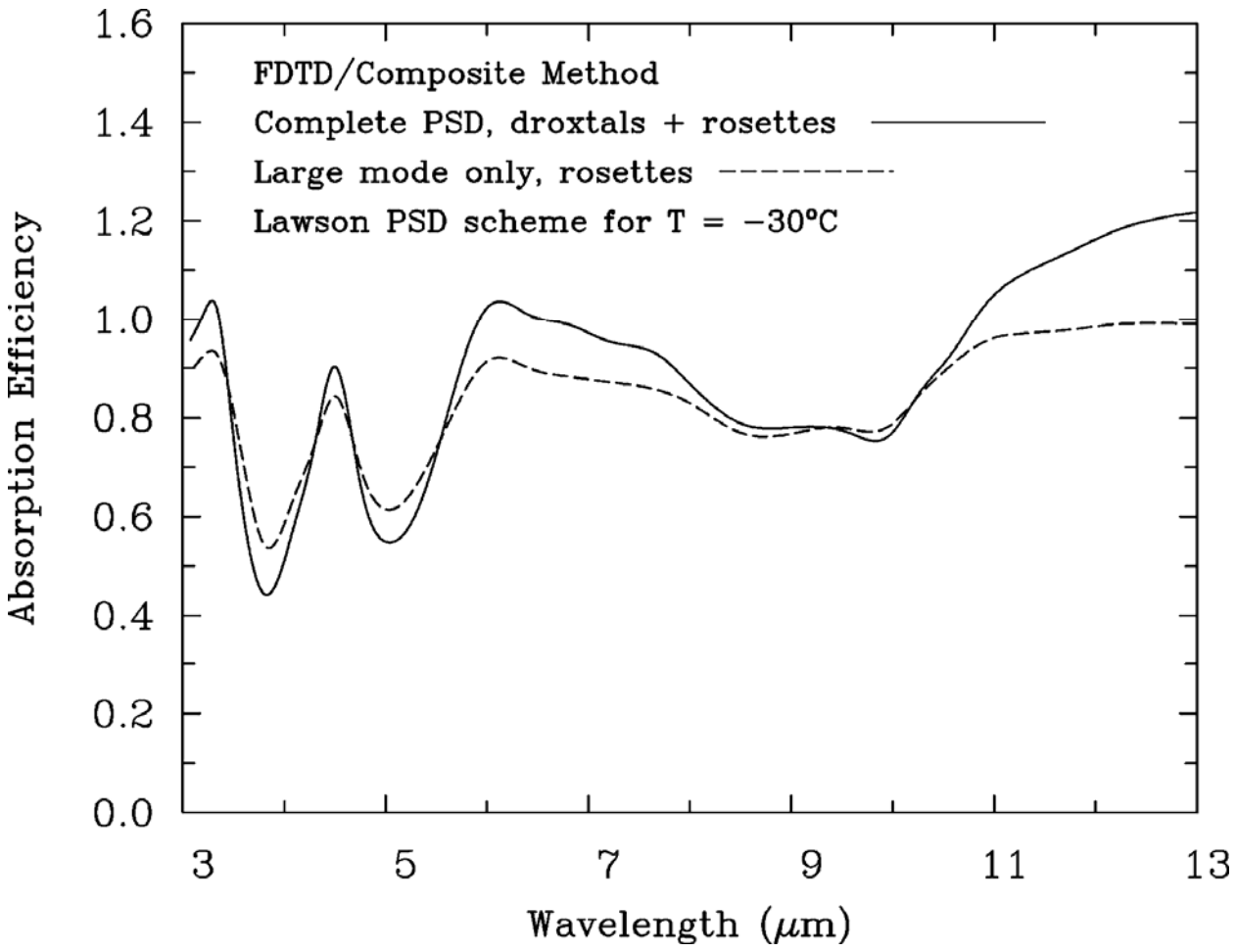

Figure 3. Absorption efficiencies for a bimodal size distribution (solid) and the same PSD but without the small crystal mode (dashed). The difference in the curves between 11 and 13 μm is due only to tunneling.

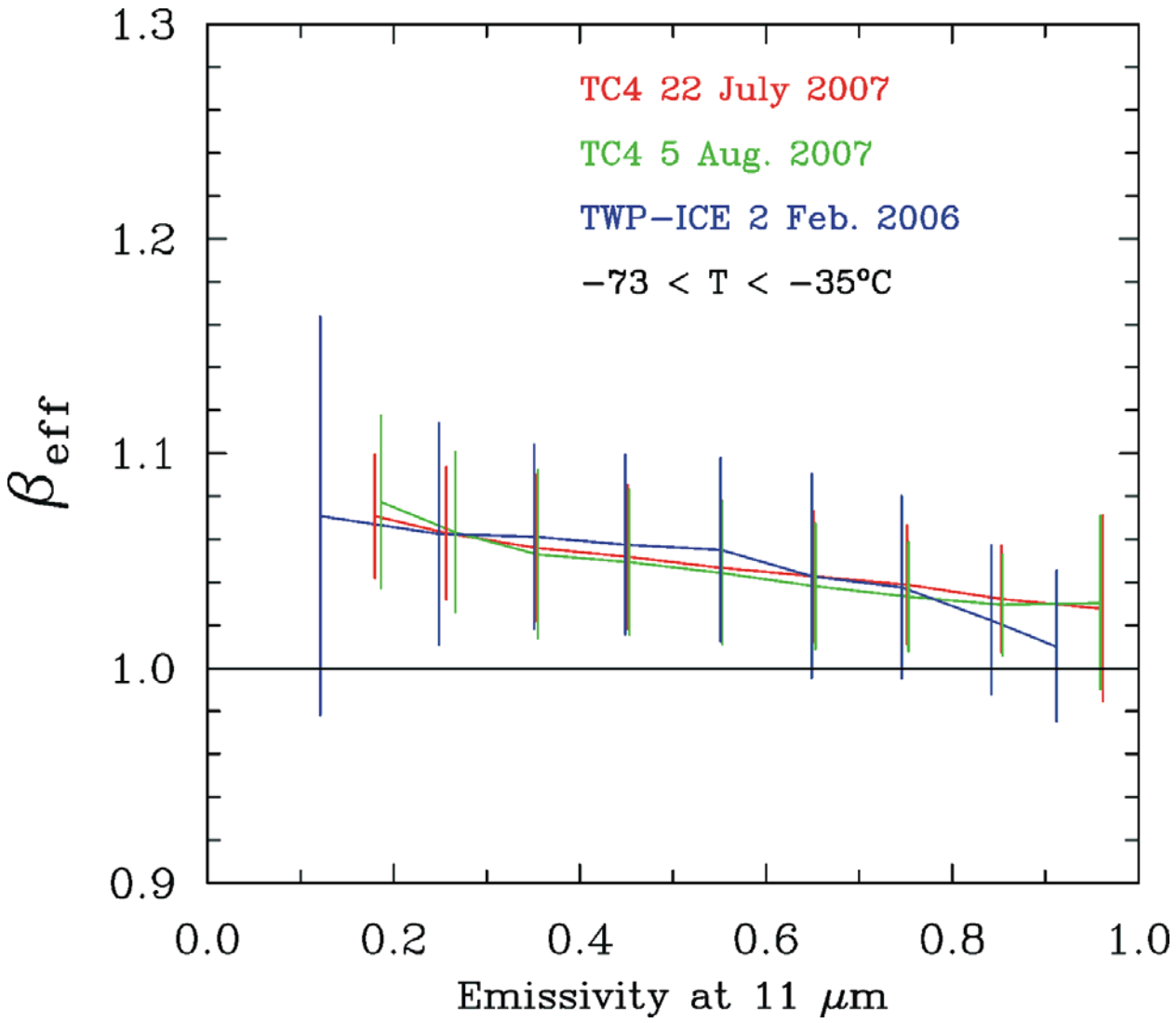

Figure 4. The mean values of the retrieved effective absorption optical depth ratio (β_{eff}) related to retrieved mean emissivity for the three case studies, where retrieved cirrus temperature < -35 ^{o}C to insure the clouds are only ice phase. Vertical bars indicate standard deviations and the β_{eff} = 1.0 line is given for easy reference.

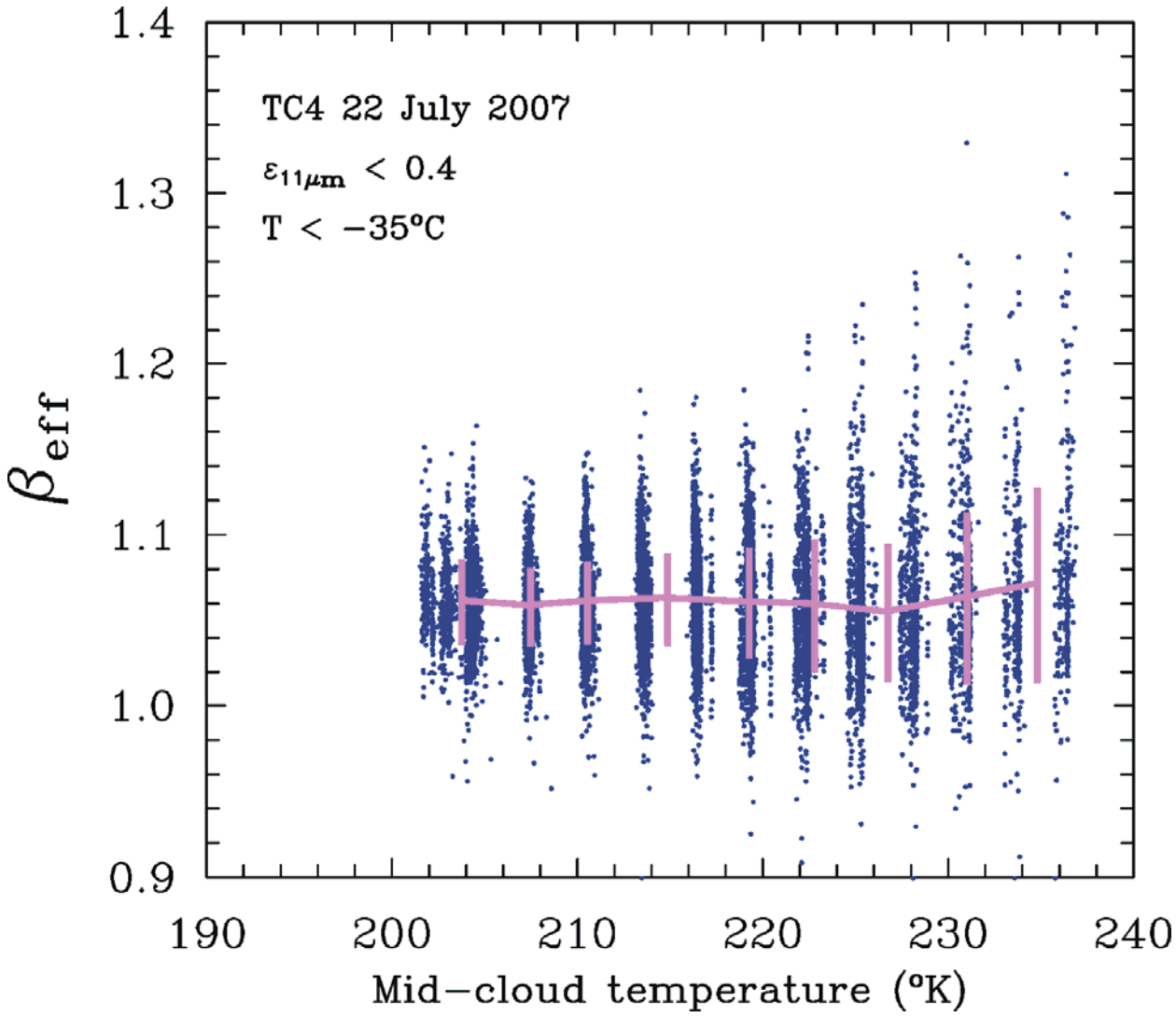

Figure 5. The retrieved effective absorption optical depth ratio (β_{eff}) related to cirrus cloud temperature for $\varepsilon(11\ \mu m) \leq 0.4$ and $T < 35\ ^{o}C$, using the 22 July 2008 TC4 case study. Mean β_{eff} are given by the pink curve and vertical bars indicate standard deviations.

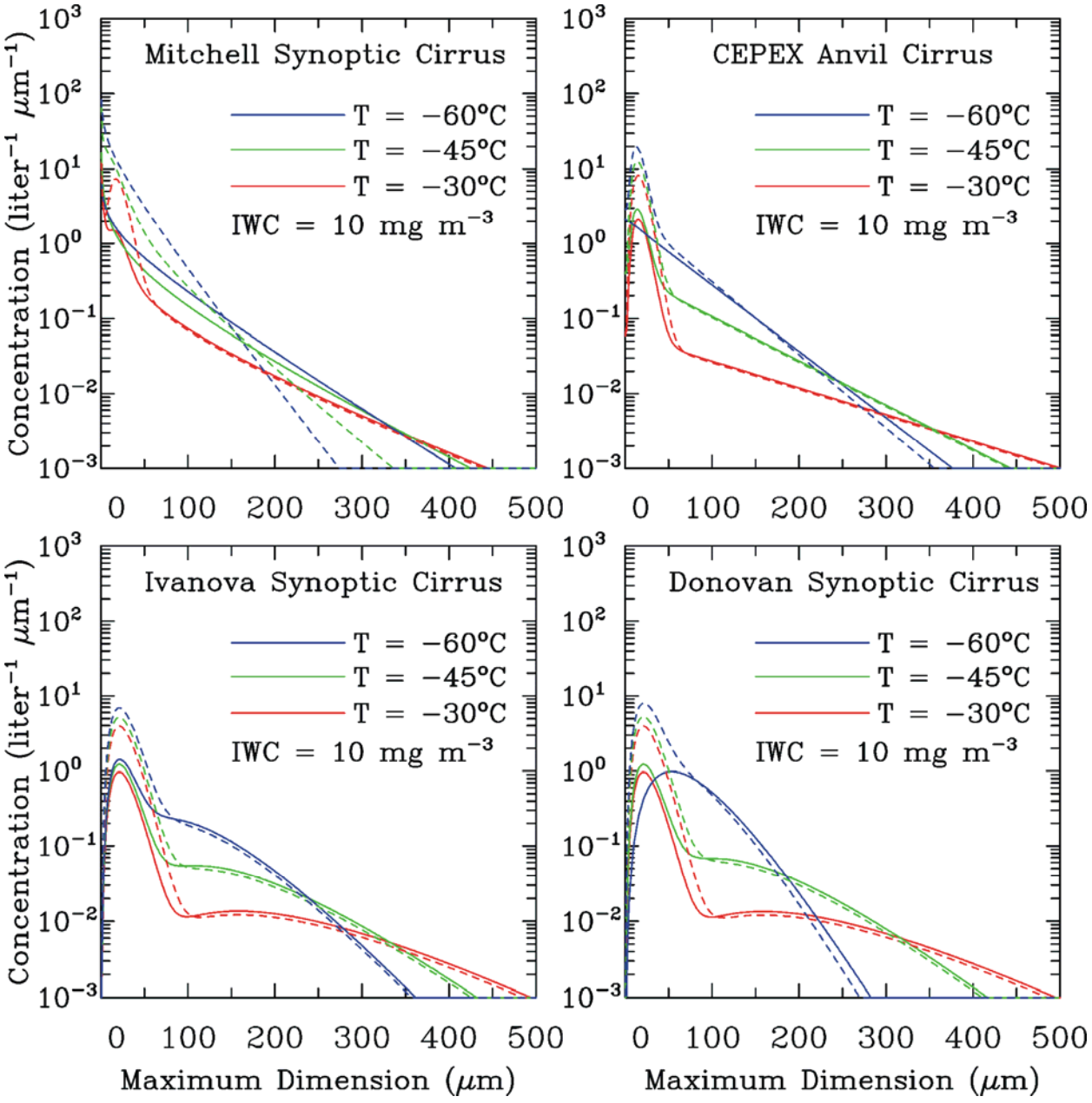

Figure 6. Retrieved PSD from the indicated PSD schemes based on the mean β_{eff} of 1.065 (solid) and the mean + σ β_{eff} of 1.11 (dashed) for the indicated IWC.

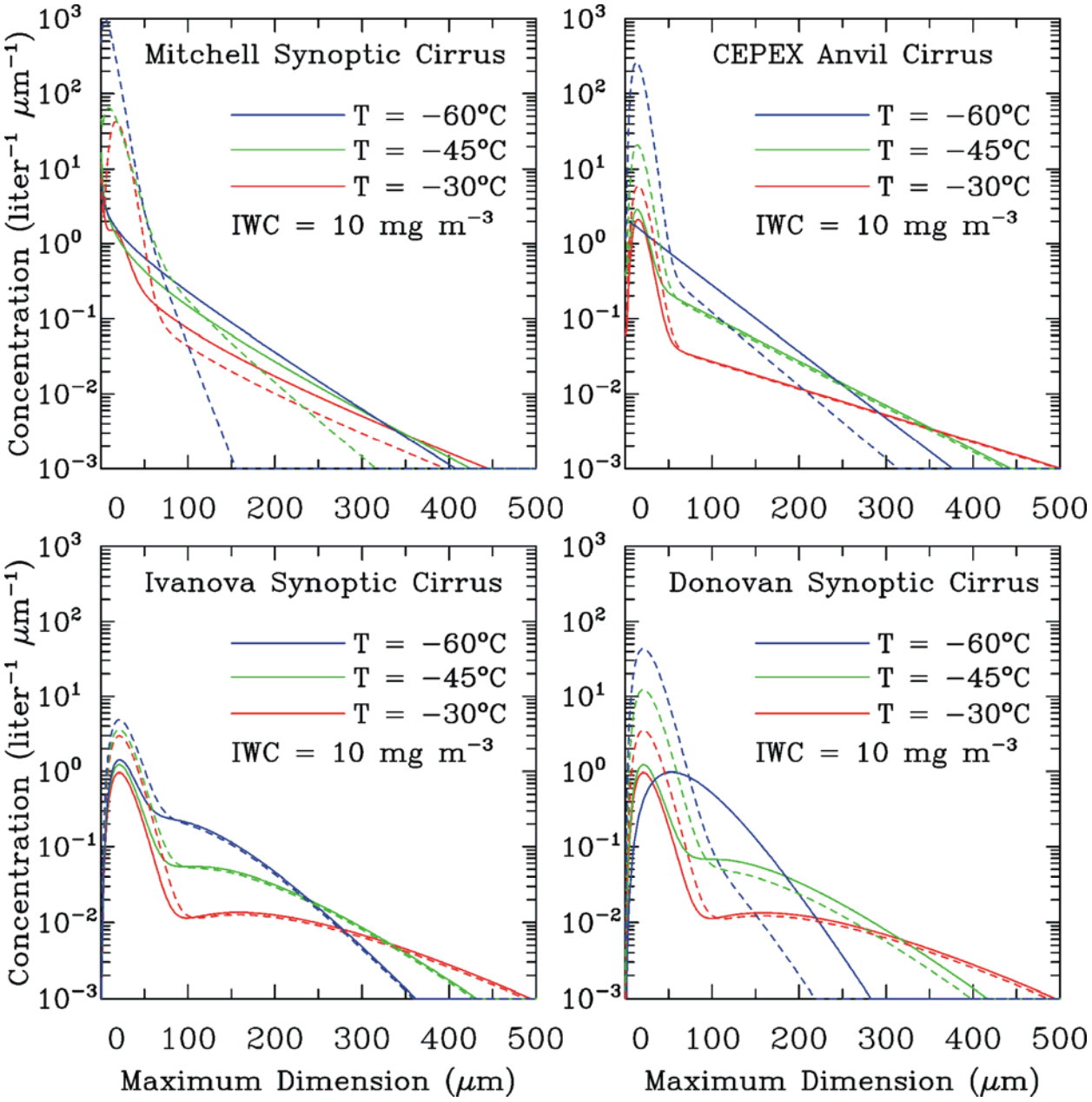

Figure 7. Retrieved PSD (solid) based on $\beta_{eff} = 1.065$ compared with the corresponding PSD from the original PSD scheme (dashed).

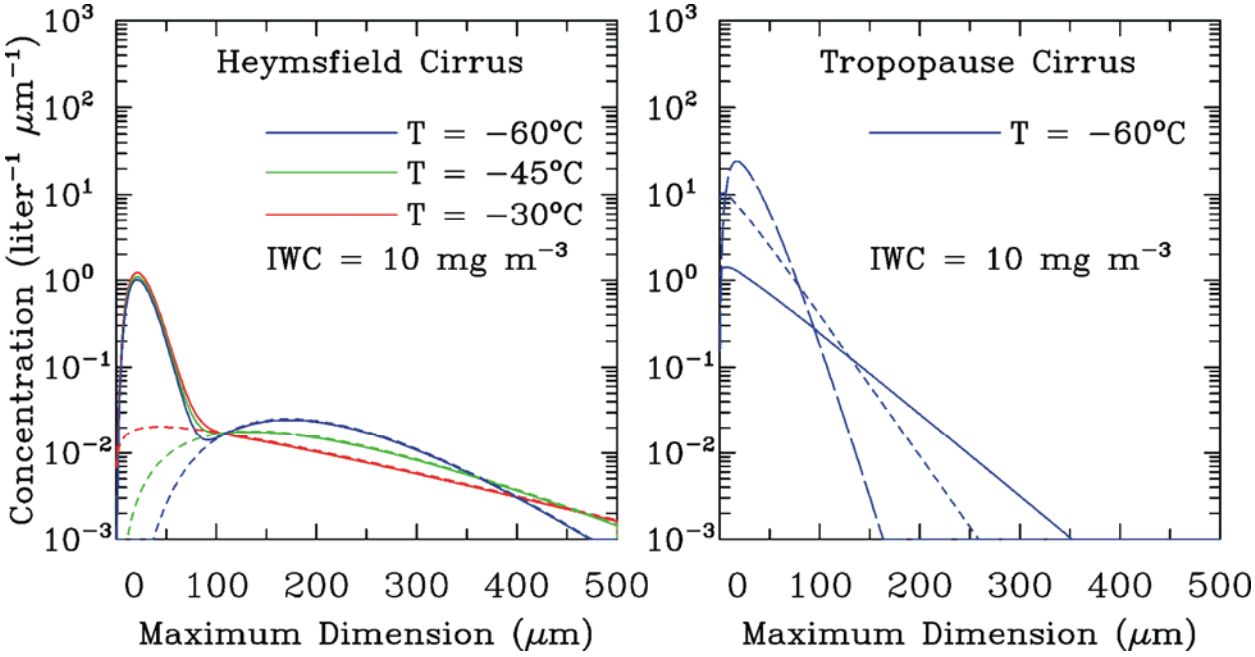

Figure 8. Similar to Fig. 7 but for the PSD schemes of Heymsfield (left panel) and Schmitt and Heymsfield (right panel). The long-dashed curve in the right panel is the PSD corresponding to $\beta_{eff} = 1.11$, which is one standard deviation above the mean β_{eff} (corresponding to solid curve). See text for details.

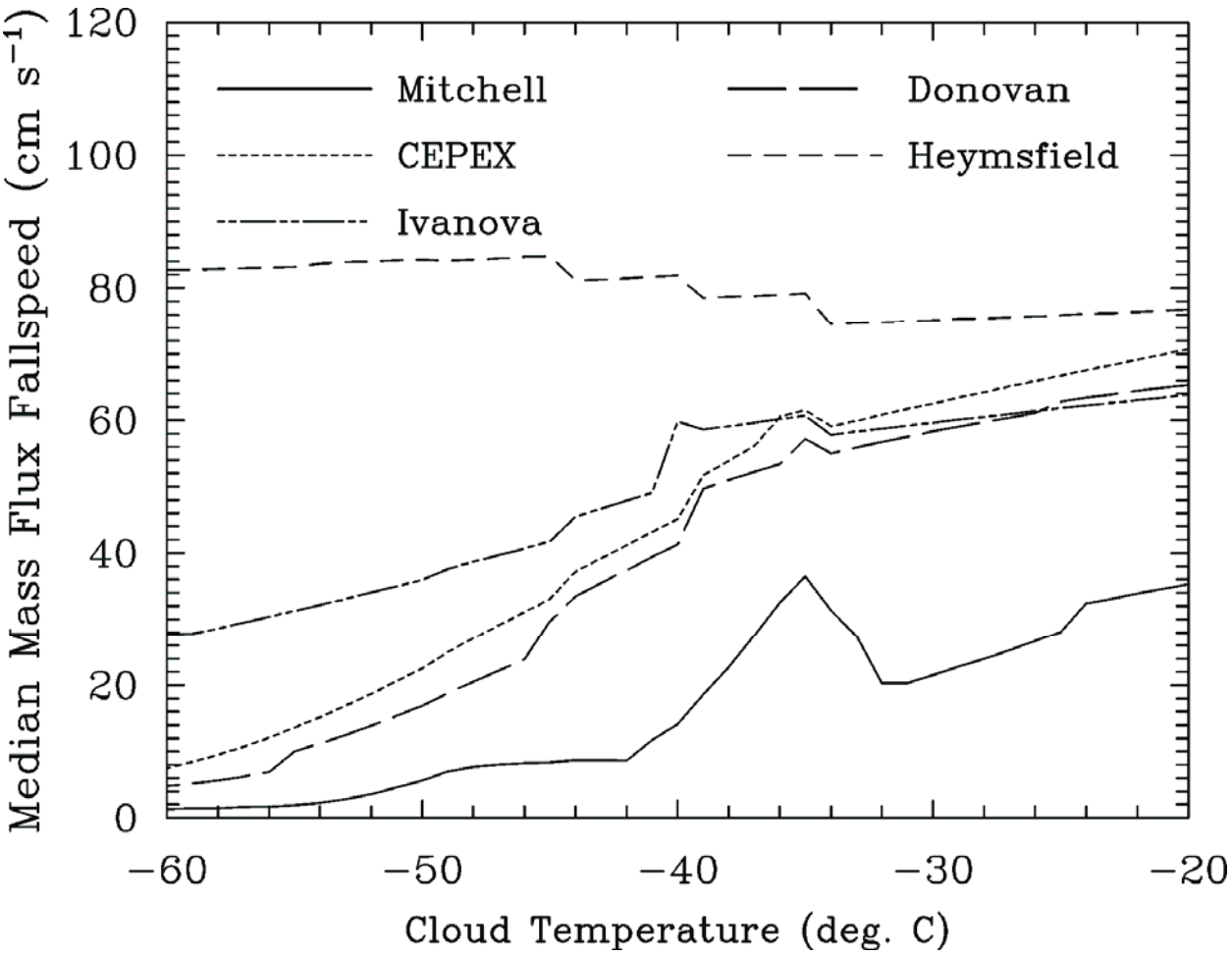

Figure 9. Temperature dependence of the PSD median mass flux fall velocity for the 5 applicable PSD schemes that share the same ice particle mass and projected area relationships and standard atmosphere conditions.

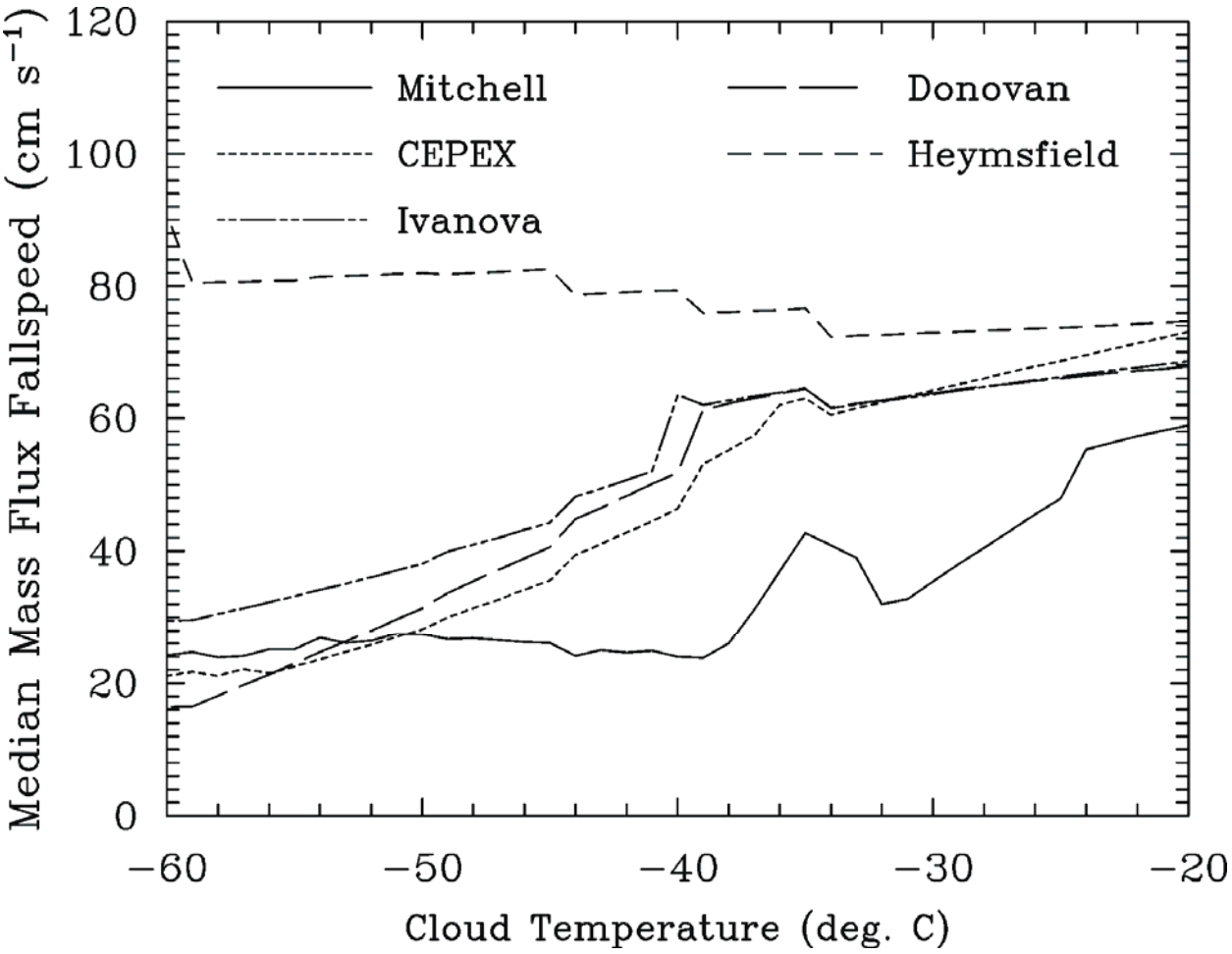

Figure 10. Same as Fig. 9 but fall velocities are now based on the retrieved PSD for each PSD scheme.

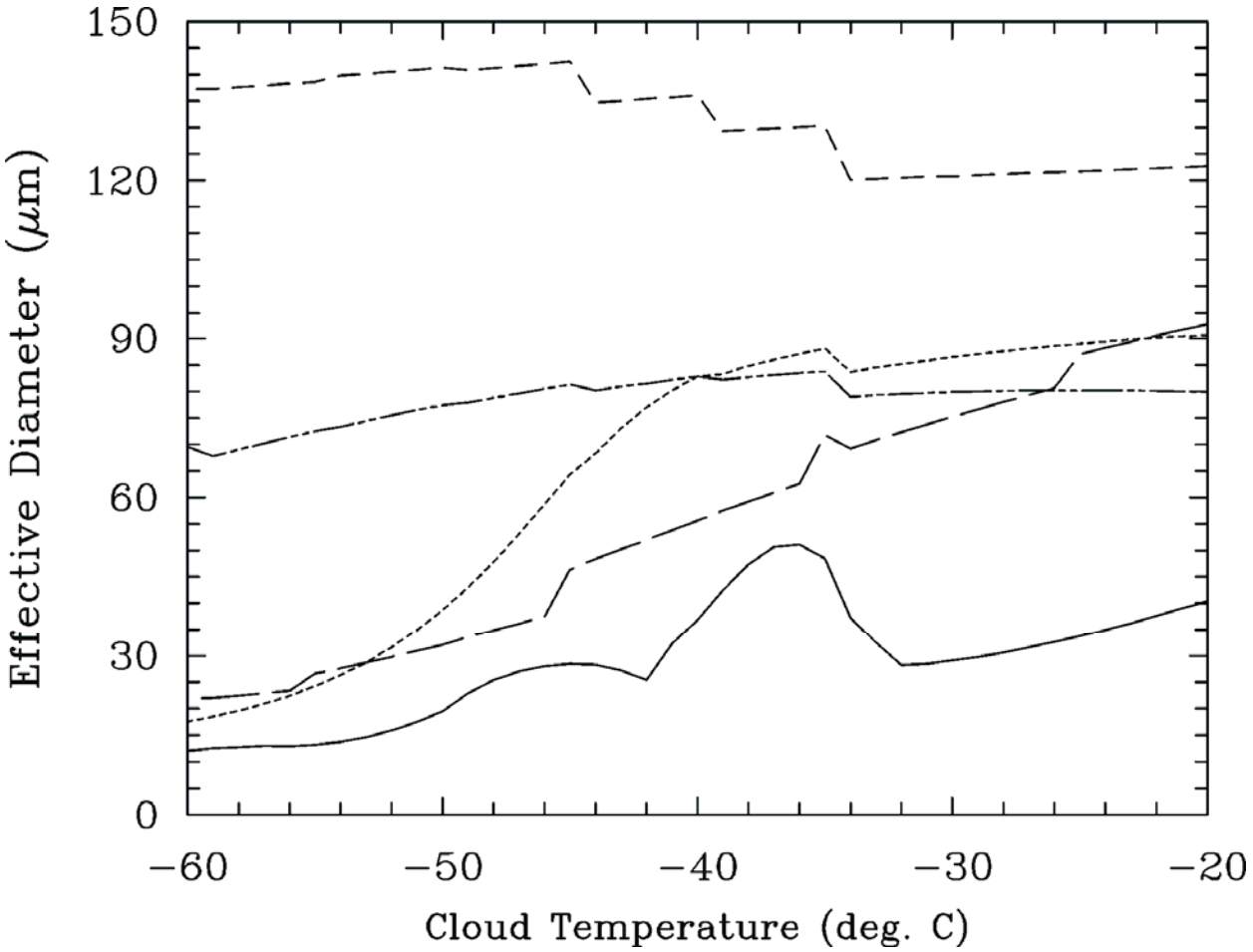

Figure 11. Temperature dependence of D_e for each of the PSD schemes where all schemes share the same ice particle mass and area assumptions. Legend is same as in Fig. 10.

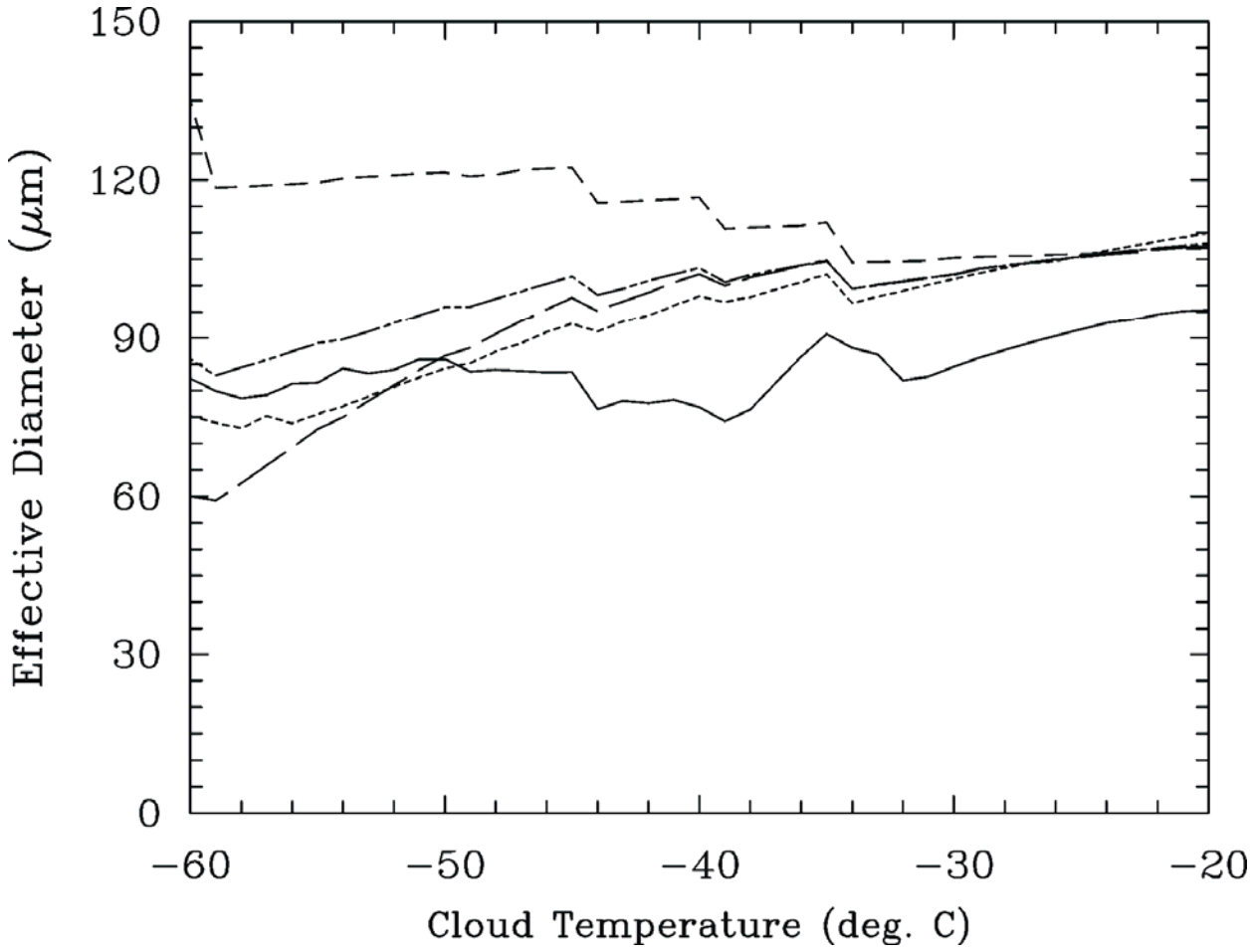

Figure 12. Same as Fig. 11 except now D_e is based on the retrieved PSD from each PSD scheme. Legend is same as in Fig. 10.

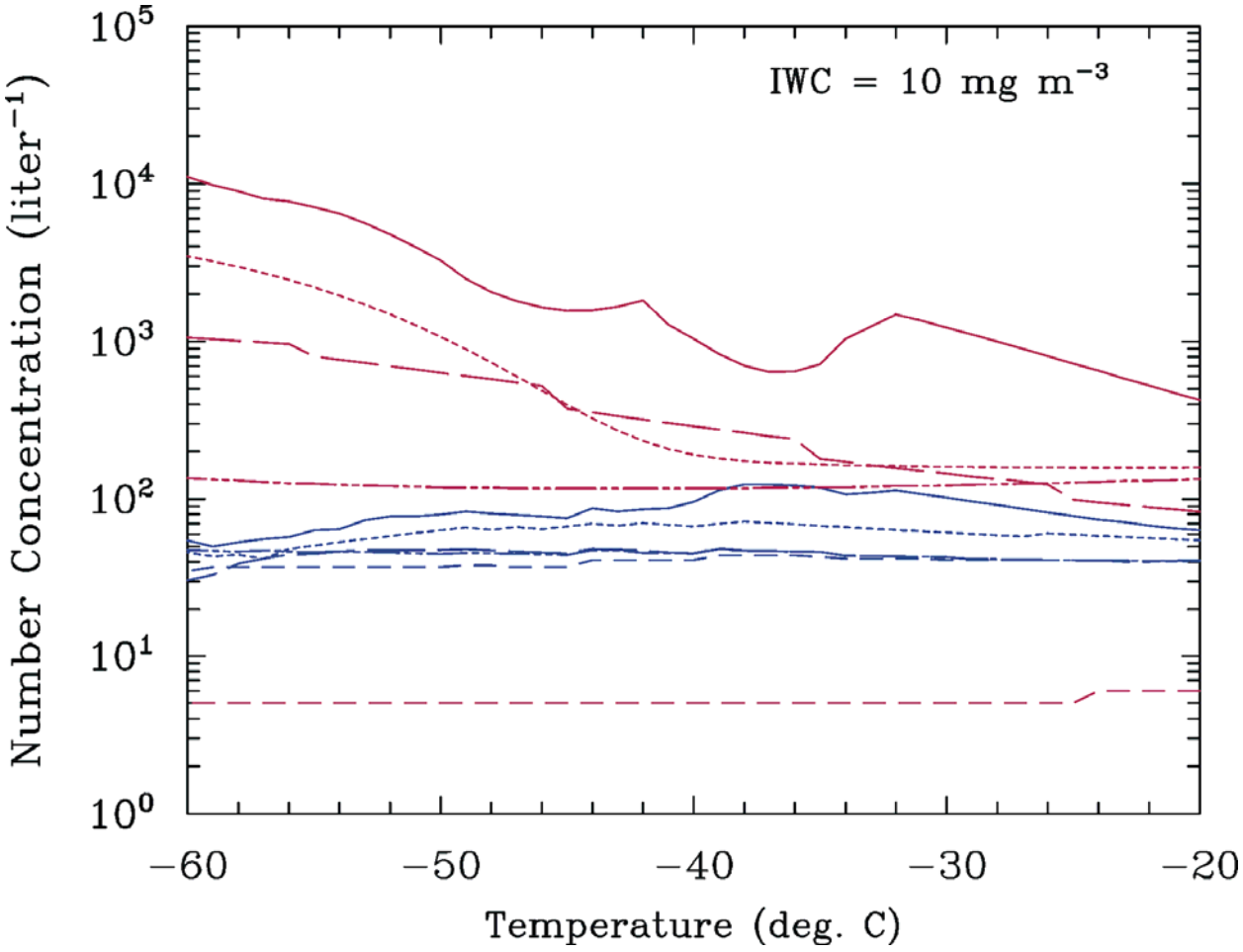

Figure 13. Temperature dependence of the total number concentration for the original PSD schemes (in red) at the indicated IWC, and the same for the corresponding retrieved PSD (in blue). The curves for the retrieved Ivanova and Donovan schemes are generally superimposed, as well as the Heymsfield scheme at warmer temperatures. Legend is same as in Fig. 10.

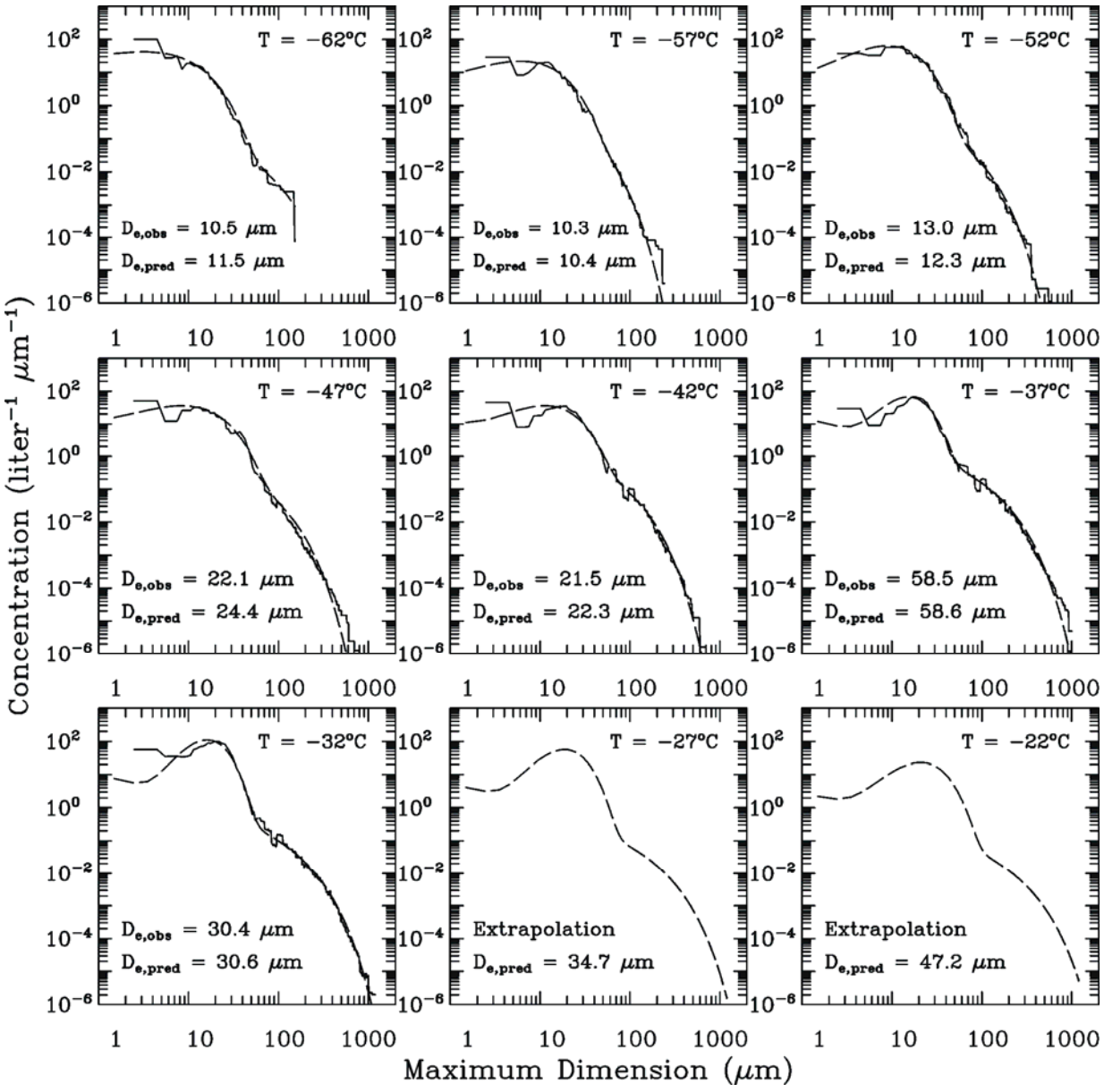

Figure A1. Comparisons of PSD predicted by the parameterization scheme (dashed) with the time weighted mean PSD from Lawson et al. (2006a) midlatitude cirrus measurements (solid) for each temperature interval. Note that there are no measurements to compare with the -27°C and -22°C parameterizations. Measurement derived and predicted D_e are compared to evaluate the accuracy of the analytical fits and parameterization procedure.

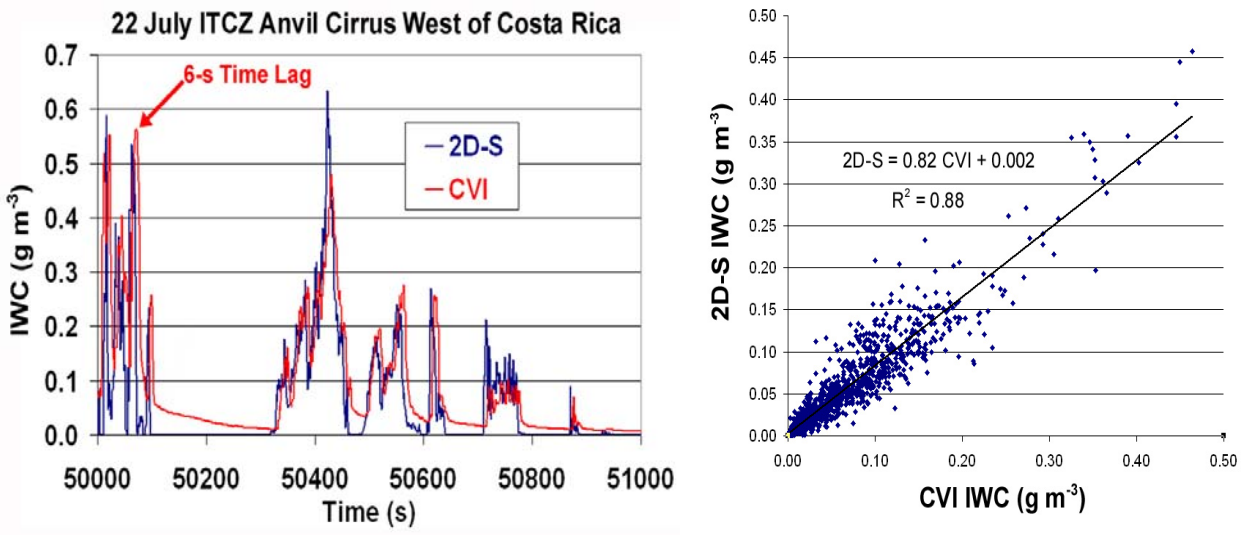

(A) (B)

Figure A2. A: Time series of the 2D-S and CVI IWC for a TC4 case study. CVI response time lagged 6 seconds behind 2D-S measurements, producing a slight offset. B: 2D-S IWCs compared with CVI IWCs for 12,000 1-Hz measurements (averaged over 10-s) in TC4 anvils cirrus.

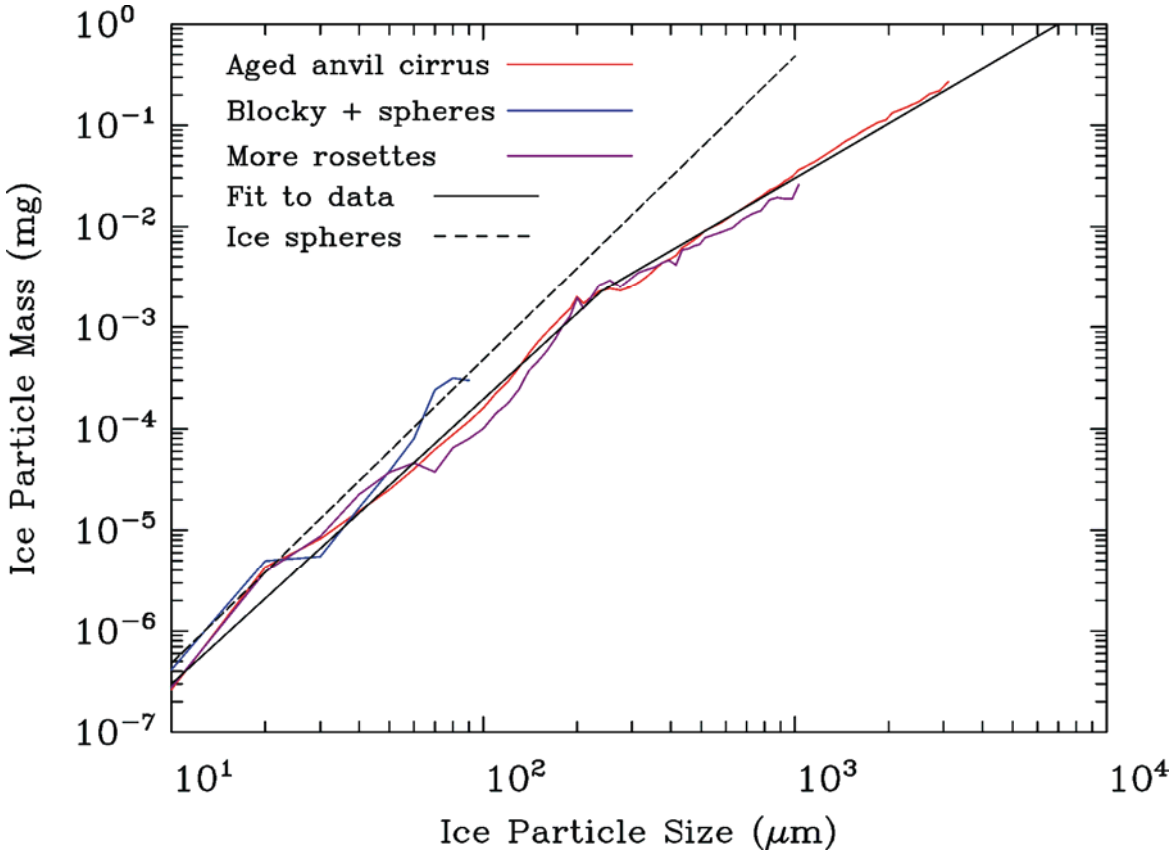

Figure A3. m-D relationships derived from 2D-S PSD measurements as described in Appendix.

Table A1. Ice particle projected area-dimension power law relationships for each PSD mode and temperature interval.

Temperature	Small particle mode		Large particle mode	
Interval	Prefactor	Power	Prefactor	Power
-30 to -35 ^{o}C	0.4205	1.902	0.1774	1.712
-35 to -40 ^{o}C	0.2890	1.843	0.1447	1.676
-40 to -45 ^{o}C	0.3991	1.896	0.1118	1.617
-45 to -50 ^{o}C	0.4791	1.924	0.09907	1.600
-50 to -55 ^{o}C	0.5081	1.933	0.1087	1.628
-55 to -60 ^{o}C	0.5068	1.932	0.1248	1.665
-60 to -65 ^{o}C	0.4565	1.914	0.05869	1.499

Appendix B

Satellite Remote Sensing of Small Ice Crystal Concentrations in Cirrus Clouds

David L. Mitchell* and Robert P. d'Entremont†

*Desert Research Institute, 2215 Raggio Pkwy, Reno, NV 89512, USA
†Atmospheric and Environmental Research, Inc., 131 Hartwell Ave., Lexington, MA 02421, USA

Abstract. Cirrus cloud ice crystal concentrations corresponding to maximum dimensions less than 60 microns have been difficult to measure, with some instruments reporting their concentrations up to 3 orders of magnitude higher relative to the larger (60-100 μm) ice crystals. Whether these are really found in nature or are artifacts caused by shattering at the instrument inlet needs to be determined since the climatology predicted by global climate models (GCMs) depends strongly on how they are represented. This paper addresses this question by applying new insights into the light absorption process to satellite remote sensing. The number concentration ratio of small (D < 60 μm) to larger ice particles is retrieved, as well as the ice water path (IWP), effective diameter (D_e), and cirrus optical depth, using split-window channels to address the small ice crystals.

INTRODUCTION

Measurement of small ice crystals (D < 60 μm) remains an unsolved and controversial issue in the atmospheric sciences community. Concentrations of small ice crystals are hard to measure due to shattering of crystals at probe inlets. However, depending on the in situ measurements one uses, these small ice crystals may affect cirrus cloud optical depth by a factor of two [1]. Through their impact on ice fall speeds, they also strongly affect the cirrus cloud feedback and climate sensitivity in global climate models [2].

To facilitate better estimation of small ice crystal concentrations in cirrus clouds, a new satellite remote sensing technique has been used in combination with in situ aircraft measurements. That is, in situ measurements of ice particle size distributions (PSD) are parameterized by temperature and ice water content (IWC), and these PSD schemes in combination with radiances measured from satellite and a treatment of ice cloud optical properties serve as the framework of the retrieval algorithm. The latter is the modified anomalous diffraction approximation [3], or MADA, where the extinction and absorption coefficients are expressed in terms of the size distribution parameters and the measured mass- and projected area-dimension power law relationships for various ice crystal shapes or shape recipes.

THEORY

Small ice crystals are evaluated using the properties of photon tunneling or wave resonance. Photon tunneling can be described as the process by which radiation beyond the physical cross-section of a particle is either absorbed or scattered outside the forward diffraction peak. As shown in [4] and [3], tunneling is strongest when:

- The effective size of the particles and the wavelength of radiation are comparable.
- The particle is spherical or quasi spherical (an attribute of many small ice crystals)
- The real index of refraction is relatively large

Tunneling contributions to the absorption efficiency in the window region can exceed 20% when particle size is less than 60 μm (Fig. 1a). Tunneling depends on the real refractive index, which increases substantially for ice between 11 and 12 μm wavelengths. The corresponding emissivity difference at these wavelengths is almost all due to tunneling, making the tunneling signal ideal for inferring the concentrations of small ice crystals. Historically this emissivity difference was attributed to differences in the imaginary refractive index, but for ice clouds, it is the real refractive index that accounts for this difference in emissivity.

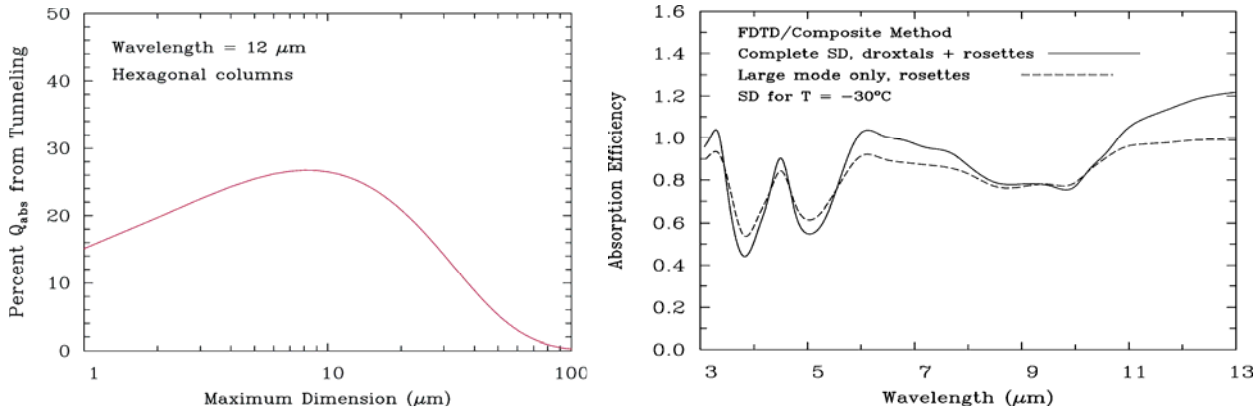

(a) (b)

FIGURE 1. (a) Size dependence of tunneling contributions to the absorption efficiency for hexagonal columns at 12 μm wavelength based on MADA. (b) Absorption efficiencies (Q_{abs}) for a bimodal size distribution (solid) and the same PSD but without the small ice crystal mode (dashed). The difference in the curves between 11 and 13 μm is due to tunneling.

The wavelength dependence of this remote sensing/tunneling technique is shown in Fig. 1b. The solid curve shows absorption efficiencies (Q_{abs}) for a bimodal size distribution (e.g. Fig. 2a) of quasi-spheres (droxtals) in the small mode and bullet rosettes in the large mode. The dashed curve is for the large mode, rosettes only. Note that $Q_{abs} = \beta_{abs}/P_t$, where β_{abs} = absorption coefficient and P_t = PSD projected area. Q_{abs} for wavelengths > 11 μm are greater for the complete PSD due to tunneling. Tunneling depends strongly on the real index of refraction, n_r. The reason Q_{abs} is greater at 12 μm than 11 μm when the full PSD is used is because n_r has a minimum near 11 μm but is substantial at 12 μm. Since tunneling is a measure of the small mode, and the 12 – 11 μm Q_{abs} difference is only from tunneling, this difference serves as a measure of the small mode of the cirrus PSD. These calculations are based on the optical property database given in [5], but the same result is given by MADA.

ESTIMATING SMALL ICE CRYSTAL CONCENTRATIONS

A typical example of a bimodal PSD from anvil cirrus sampled during the Central Equatorial Pacific Experiment (CEPEX) is shown in Fig. 2a. The ice crystals associated with the small mode (D < 50 μm) were sampled by the Forward Scattering Spectrometer Probe (FSSP), with the larger particles sampled by the 2DC probe.

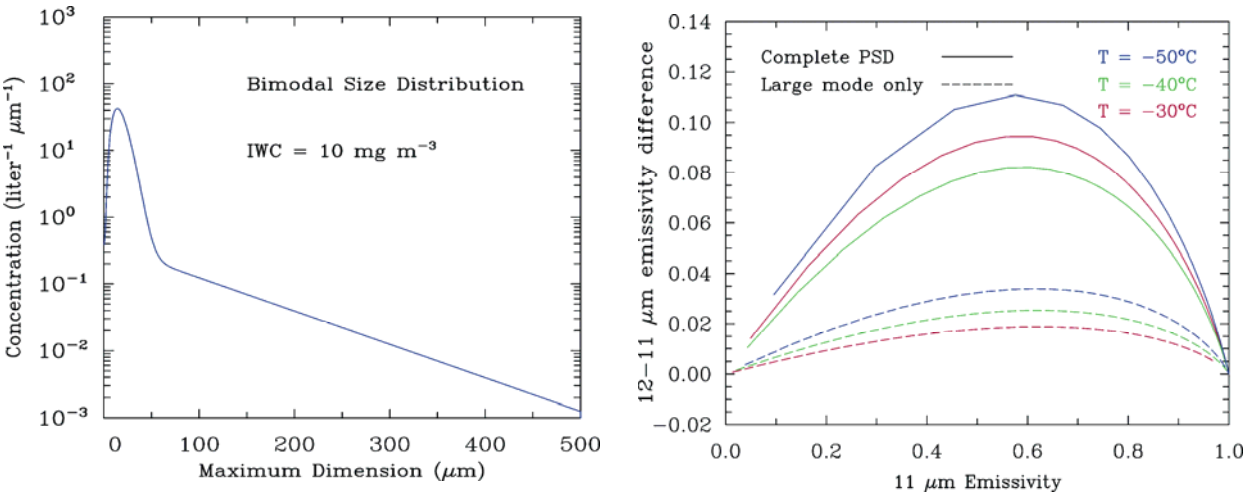

(a) (b)

FIGURE 2. (a) Example of a bimodal size distribution based on FSSP and 2DC measurements from anvil cirrus clouds during CEPEX. (b) Theoretical curves denoting the large mode (dashed) and the complete PSD (solid) corresponding to 3 temperature-dependent PSD.

The key question is whether the small mode is real or an artifact of crystal shattering at the probe inlet (or a little of both). To help answer this, we use satellite radiances at 11 and 12 μm to estimate the number concentration in the small mode. The large mode is first estimated from a temperature-dependent PSD parameterization but can be modified based on the satellite-measured radiances. The small mode ice mass content can be estimated by the "arches" in Fig. 2b and also from the absorption optical depth ratio based on 12 and 11 μm, referred to as β. The higher the small mode ice mass content (or small mode number concentration, N_{sm}), the higher the arches are. This principle is used to determine N_{sm} by matching theory with observations, as described now.

1. Step one is to begin with satellite retrievals of cloud temperature and cloud emissivity (ε) at the 11 and 12 μm wavelength channels.
2. The cloud temperature can then be used to estimate PSD mean size $\bar{D}$ and dispersion for the large and small mode. The difference between the solid and dashed curves above results primarily from differences in the contribution of the small mode to the IWC. This also determines the effective diameter (D_e). The PSD dispersion parameter has little influence on the emissivities or emissivity differences.
3. Locate retrieved Δε (Fig. 2b y-axis) and the 11 μm ε by (1) incrementing the modeled ice water path (IWP) to increase ε(11 μm) and (2) incrementing the small mode contribution to the arbitrary IWC, which elevates the curve.
4. If retrieved point lies below the "large mode only" curve (e.g. a dashed curve in Fig. 2b), then systematically increase $\bar{D}$ for the large mode until a match is obtained.
5. This method retrieves IWP, $\bar{D}$, D_e, and the small-to-large mode ice crystal concentration ratio. For a given IWC, it also estimates ice particle number concentration and the complete PSD, even when it is bimodal.

Regarding (1), the cirrus temperature was retrieved using MODIS CO_2 channels between 13.3 and 14.2 μm. Since the real refractive index in these channels is approximately the same (i.e. tunneling contributions to absorption are the same), and since the imaginary index of refraction is sufficiently large to insure an absorption efficiency of 1.0 in the absence of tunneling for cirrus crystal sizes, then cirrus emissivity in these channels will be the same. This reduces the number of unknowns in the radiation transfer equations, allowing us to solve for cloud temperature unambiguously. Once cloud temperature is known, cirrus emissivity for the 11 and 12 μm channels is easily solved for using traditional methods [6].

The modified anomalous diffraction approximation (MADA) was used to calculate ice cloud optical properties in this retrieval algorithm since it couples explicitly with the cloud microphysics and its analytical formulation makes it computationally efficient [3, 4]. A temperature dependent ice crystal shape recipe was used based on the observations in [7], and the mass- and area-dimension relationships were derived from this recipe. As described in [3], tunneling efficiencies for various ice crystal shapes were determined by comparisons between MADA and finite-difference time-domain (FDTD) calculations, and were parameterized as a function of ice particle shape and large mode $\bar{D}$.

TESTING THE RETRIEVAL WITH IN SITU MEASUREMENTS

Satellite retrievals of cirrus PSD (for a given IWC) were compared with aircraft in situ measurements for the same cloud scene during the TWP-ICE and TC4 field campaigns. During TWP-ICE, PSD were measured with the Cloud Droplet Probe (CDP) and the Cloud Imaging Probe (CIP), both having an open path design (i.e. no inlet tube) to minimize the contribution of shattered particles to the sample volume. During TC4 (conducted in 2007 near Costa Rica), the new 2DS probe was used for PSD sampling that avoids the shattering problem. Comparisons between these measured PSD and PSD retrieved via satellite (for an assumed IWC) at comparable times and locations shared strong similarities in that both lacked a distinct small particle mode beginning around 60 μm (a feature that tended to characterize earlier PSD measurements). The TWP-ICE comparison on 2 February 2006 was especially fortuitous since a MODIS satellite overpass occurred during the aircraft in situ sampling and retrieved cirrus pixels were matched with in situ measurements spatially and within 4 minutes temporally. The comparison of the retrieved PSD from MODIS with PSD measurements from the Proteus aircraft are shown in Fig. 3 (left panel). Since the CDP exhibited peculiar behavior during this period (i.e. several bins were not registering any counts over several minutes in cirrus) we trust the CIP measurements (25-1550 μm size range) better, but acknowledge that CIP measurements at the observed sizes have substantial uncertainties. The PSD were retrieved using two methods. The first uses a temperature-dependent PSD scheme to estimate the distribution of larger ice particles, but this method has the advantage of estimating the degree of PSD bimodality provided the PSD scheme provides a reasonable estimate of larger ice particle behavior (long-dashed line). Neither the probe measurements nor this retrieved PSD

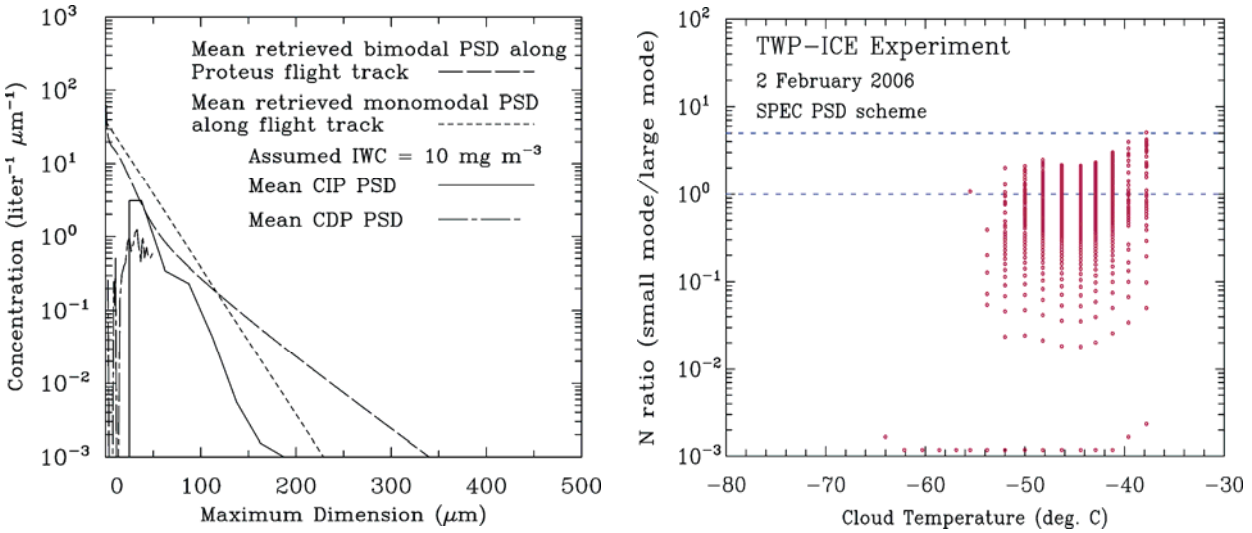

FIGURE 3. Left: PSD measurements (CIP & CDP) compared with PSD retrieved from MODIS radiances using two methods: (1) algorithm that allows for bimodal PSD using a PSD scheme to describe the larger particles (long-dashed) and (2) algorithm that constrains PSD to be monomodal but does not involve any PSD scheme (short-dashed). Right: Small-to-larger ice particle number concentration ratio retrieved for the MODIS scene. See text for details.

indicate that the actual PSD were strongly bimodal. The number concentration ratio of small (D < 60 μm) to larger ice particles is shown in Fig. 3 (right panel) for all clouds identified as cirrus in the MODIS scene. All retrieved cloud pixels (circles) below the lower dashed line are monomodal, while those between the two dashed lines could be either monomodal or moderately bimodal, depending on PSD slope. If slopes are relatively steep, as indicated by the in situ PSD, these PSD should be monomodal. If we assume all PSD are monomodal/exponential, the retrieval algorithm can be reconfigured with this assumption, doing away with the need for a PSD scheme to estimate the distribution of larger ice particles based on cloud temperature. This second method is shown by the retrieved short-dashed PSD (left panel), where the emissivity difference allows us to solve for the monomodal PSD slope. The PSD retrieved in this way (short-dashed) agrees well with the CIP PSD. By retrieving the PSD slope (which is done here), ice sedimentation rates can be more accurately estimated [8].

In summary, these retrievals and others (see http://www.dri.edu/Projects/Mitchell/) do not support the existence of anomalously high concentrations of small ice crystals as frequently reported by earlier in situ measurements of these small crystals. This case study suggests that it may be valid to approximate the PSD as monomodal and use this monomodal assumption in satellite retrievals. This would greatly simplify the retrieval by reducing the number of unknowns that radiance information must solve for.

ACKNOWLEDGMENT

This research was sponsored by the Office of Science (BER), U.S. Dept. of Energy, Grant No. DE-FG02-06ER64201. The DOE ARM program is greatly appreciated for its support of this research.

REFERENCES

1. G. M. McFarquhar, J. Um, M. Freer, D. Baumgardner, G. Kok and G. Mace, *Geophys. Res. Lett.* **34**, L13803, doi:10.1029/2007GL02986 (2007).
2. D. L. Mitchell, P.J. Rasch, D. Ivanova, G.M. McFarquhar and T. Nousiainen, *Geophys. Res. Lett.* **35**, L09806, doi:10.1029/2008GL033552 (2008).
3. D. L. Mitchell, A. J. Baran, W. P. Arnott and C. Schmitt, *J. Atmos. Sci.* **63**, 2948-2962 (2006).
4. D. L. Mitchell, *J. Atmos. Sci.* **57**, 1311-1326 (2000).
5. P. Yang, H. Wei, H-L. Huang, B. A. Baum, Y. X. Hu, G. W. Kattawar, M. I. Mishchenko and Q. Fu, *Appl. Opt.* **44**, 5512–5523 (2005).
6. T. Inoue, *J. Meteorol. Soc. Jpn.* **63**, 88-98 (1985).
7. R. P. Lawson, R.P., B. Baker, B. Pilson and Q. Mo, *J. Atmos. Sci.* **63**, 3186-3203 (2006).
8. D. Ivanova, D. L. Mitchell, W. P. Arnott and M. Poellot, *Atmos. Res.* **59**, 89-113 (2001).

Appendix C

International Conference on Clouds and Precipitation, Cancun, Mexico, 7-11 July 2008

GROUND BASED REMOTE SENSING OF SMALL ICE CRYSTAL CONCENTRATIONS IN ARCTIC CIRRUS CLOUDS

Subhashree Mishra[1], David L. Mitchell[1], Daniel DeSlover[2] and Greg McFarquhar[3]

1. Desert Research Institute, Reno, NV
2. University of Wisconsin, Madison, WI
3. University of Illinois, Urbana, IL

1. INTRODUCTION

Measurement of small ice crystals (D < 60 μm) remains an unsolved and controversial issue in the cloud physics community. Concentrations of small ice crystals are hard to measure due to shattering of crystals at probe inlets. However, these small ice crystals alter cirrus cloud radiative properties and may affect the cirrus cloud feedback in global climate models. To facilitate better estimation of small ice crystal concentrations in cirrus clouds, a new ground-based remote sensing technique has been used in combination with in situ aircraft measurements. That is, data from the Mixed-Phase Arctic Cloud Experiment (M-PACE) conducted at Barrow on the north slope of Alaska (Fall 2004) is being used to develop an Arctic ice particle size distribution (PSD) scheme, that in combination with the anomalous diffraction approximation (for ice cloud optical properties), serves as the framework of the retrieval algorithm.

2. THEORY

Small ice crystals are evaluated using the properties of photon tunneling or wave resonance. Photon tunneling can be described as the process by which radiation beyond the physical cross-section of a particle is either absorbed or scattered outside the forward diffraction peak (Fig. 1). Tunneling is strongest when:

1) The effective size of the particles and the wavelength of radiation are comparable.
2) The particle is spherical or quasi spherical (an attribute of many small crystals)
3) The real index of refraction is relatively large

Tunneling contributions to the absorption efficiency in the window region can reach 20% when particle size is less than 60 μm. Tunneling depends on the real refractive index, which changes abruptly for ice between 12 and 11 μm wavelengths. The corresponding emissivity difference at these wavelengths is only due to tunneling, which makes the tunneling signal an ideal signal for inferring the concentrations of small ice crystals. Historically this emissivity difference was attributed to differences in the imaginary refractive index, but in essence, it is the real refractive index that accounts for this difference in emissivity in ice clouds.

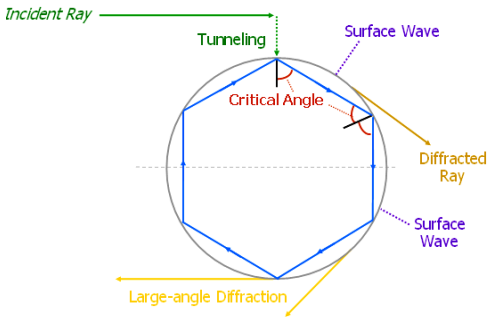

Figure1: Depiction of possible trajectories of an incident grazing ray after tunnelling to the drop surface.

Better understanding of remote sensing of small crystals by applying the tunneling technique is shown in Fig. 2. The solid curve shows absorption efficiencies (Q_{abs}) for a bimodal size distribution of quasi-spheres (droxtals) in the small mode and bullet rosettes in the large mode. Dashed curve is for the large mode, rosettes only. Bimodal PSD are shown in Fig. 3. Q_{abs} for wavelengths > 11 μm are greater for the complete PSD due to tunneling. Tunneling depends strongly on the real index of refraction, n_r. The reason Q_{abs} is greater at 12 μm than 11 μm when the full PSD is used is because n_r has a minimum near 11 μm but is substantial at 12 μm. Since tunneling is a measure of the small mode, and the 12 – 11 μm Q_{abs} difference is only from tunneling, this difference serves as a measure of the small mode of the cirrus PSD. These calculations are based on the optical property database given in Yang et al. (2005).

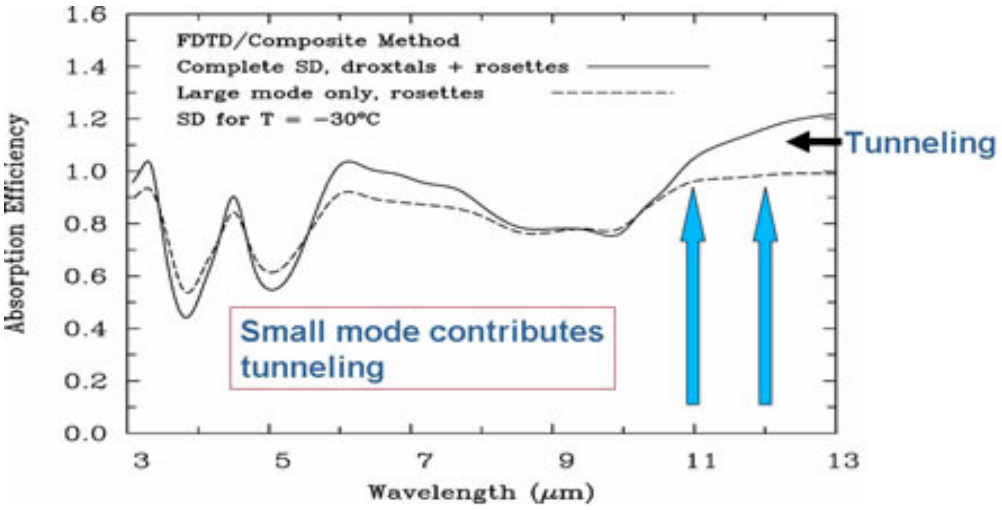

Figure 2: Absorption efficiencies (Q_{abs}) for a bimodal size distribution.

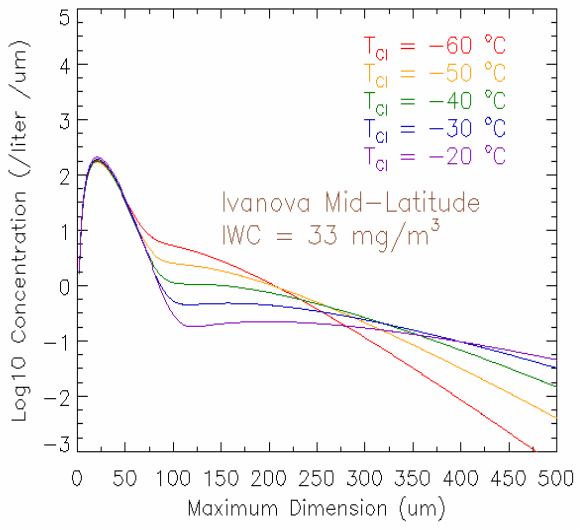

Figure 3. Examples of bimodal size distributions based on measurements from mid-latitude cirrus clouds (Ivanova et al. 2001).

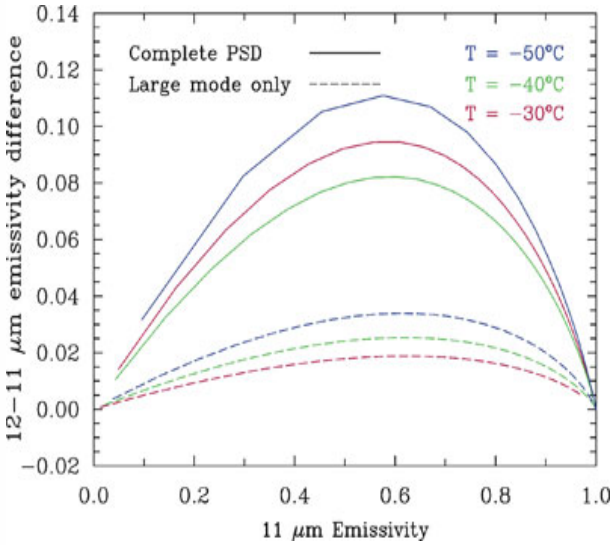

Figure 4. Theoretical curves denoting the large mode (dashed) and the complete PSD (solid) corresponding to 3 different temperatures.

3. ESTIMATING SMALL CRYSTAL CONCENTRATIONS

The small mode ice mass content can be estimated by the "arches" in Fig. 4 and also from the absorption optical depth ratio at 12 and 11 μm, referred to as β. Several studies have shown that β ≈ 1.08 for synoptic and anvil cirrus. The higher the small mode ice mass content (or ice crystal number concentration, N_{sm}), the higher the arches are. This principle is used to determine N_{sm} by matching theory with observations, as described below.

1. The first step is to begin with retrievals of cloud temperature and cloud emissivity (ε) at 11 and 12 μm wavelength channels from the ground based Atmospheric Emitted Radiance Interferometer (AERI), and from a corresponding sounding and cloud radar profile.
2. The cloud temperature can then be used to estimate PSD mean size (D) and dispersion for large and small mode. The difference between the solid and dashed curves results primarily from differences in the contribution of the small PSD mode to the ice water content (IWC). This also determines the effective diameter (D_{eff}). The dispersion parameter has little influence on the emissivities or emissivity differences.
3. Locate retrieved Δε (y-axis) and the 11 μm ε by (1) incrementing the modeled ice water path (IWP) to increase ε(11 μm) and (2) incrementing the small mode contribution to the cloud IWC, which elevates the curve.
4. If all IWC is in small mode and retrieved Δε and ε (11 μm) are still not located, then decrease small mode D to locate them.
5. If retrieved point lies below the "large mode only" curve (e.g. a dashed curve), then systematically increase D for large mode until a match is obtained. Negative Δε values correspond to maximum allowed D values.
6. This method retrieves IWP, $D_{eff,}$ and the small-to-large mode ice crystal concentration ratio. For a given IWC, it also estimates ice particle number concentration and the complete PSD, even when it is bimodal.

The modified anomalous diffraction approximation (MADA) was used to calculate ice and water cloud optical properties in this AERI retrieval algorithm since it couples explicitly with the cloud microphysics and its analytical formulation makes it computationally efficient (Mitchell et al. 2006; Mitchell 2000).

4. CASE STUDY ANALYSIS

The Ivanova et al. (2001) PSD scheme for mid-latitude synoptic cirrus was used in our retrieval algorithm, but soon we will replace this with a PSD scheme developed from M-PACE PSD data for ice clouds, based on ice water content (IWC) and temperature. Measurements made by the ground-based AERI are used to indicate the concentration of small ice crystals (D < 60 μm) relative to the larger ice particles.

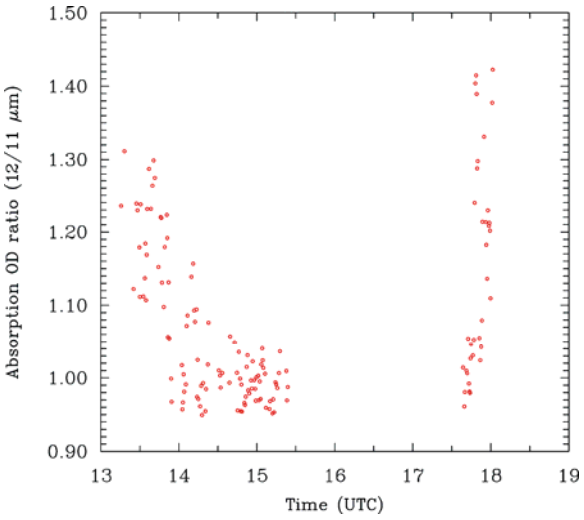

Figure 5: Ratio of the absorption optical depth between 12 μm and 11 μm as a function of hour of the day (UTC).

The absorption optical depth (AOD) of these clouds for three wavelengths (12.19 μm, 11.09 μm and 8.73 μm) are obtained from the AERI and the 12-to-11 μm AOD ratios are plotted in Fig. 5 above. Visible optical depth (OD) is less than 4.5 (to prevent emissivity saturation) and greater than 0.5. An AOD ratio above 1.1 suggests the presence of liquid water in the cloud (Giraud et al. 1997, 2001).

Figure 6 shows that the cloud temperature ranges between -27 °C and -39 °C. According to the homogeneous nucleation theory, super cooled water may be present along with ice in clouds at temperatures above -36 °C. This is supported by AERI AOD values that are higher than 1.1 (Fig. 5).

Combining the small crystal information (from AERI radiances) with the PSD scheme describing the larger particle concentrations yields the retrieved PSD. The products from this AERI retrieval scheme are the PSD and ice particle number concentration for a given IWC, as well as the ice water path, effective diameter and the ratio of the small mode-to-large mode number concentration. However this presumes that the cloud does not contain significant amounts of liquid water.

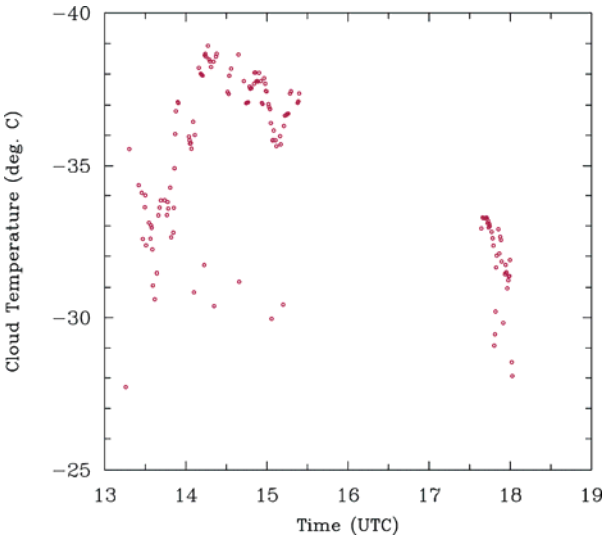

Figure 6: Plot of the cloud temperature in (deg. C) versus the hour of the day in UTC.

As noted, the AOD ratios in Fig. 5 and the radiance-weighted cloud temperatures in Fig. 6 suggest the presence of liquid water in the cirrus. In addition, recent findings shown on our website, http://www.dri.edu/Projects/Mitchell/ , indicate that the cirrus PSD is either monomodal or weakly bimodal (based on applying our retrieval algorithm to several published remote sensing studies, as well as a case study we recently analyzed). Therefore we have modified our retrieval algorithm to interpret all condensate in the small mode as liquid water. The small mode mean diameter, D_{sm}, and the dispersion parameter were assumed to be 7 μm and 9, respectively, which may be representative of droplet spectra in mixed phase conditions. Unfortunately, the cloud retrievals are sensitive to what one assumes for D_{sm}, and this is the major limitation of this retrieval method. For example, increasing D_{sm} from 7 to 10 μm

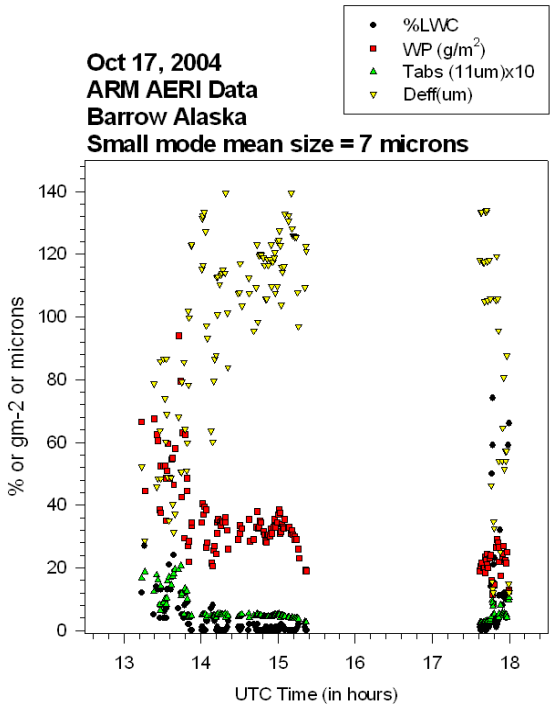

Figure 7: Retrieval results for M-PACE case study of 17 Oct. 2004.

can increase the retrieved percent liquid water content (LWC) by a factor of 3 and decrease the retrieved water path (WP) and D_{eff} by 40% and 32%, respectively.

Results from this analysis are shown in Fig. 7 for the M-PACE cirrus case study of 17 Oct. 2004. T_{abs} in Fig. 7 is the absorption optical depth at 11 μm multiplied by a factor of 10. Consistent with Figs. 5 and 6, the percentage of liquid condensate is significant from 13 to 14.2 UTC and from 17.6 to 18 UTC. If the mean cloud droplet size was assumed to be 5 μm instead of 7 μm, the %LWC would not exceed 26%. The effective diameter, D_{eff}, is for both liquid and ice fractions combined. Therefore D_{eff} is largest between 14.2 and 15.4 UTC when the cloud is glaciated (LWC is negligible), and these D_{eff} values are typical of the ice phase in general for this case study. At least over this time period, AERI radiances indicate the PSD is generally monomodal with ice particle concentrations of about 4 – 7 liter^{-1} when the IWC = 10 mg m^{-3} (see Fig. 8). For other time periods having significant liquid water, the cloud droplet number

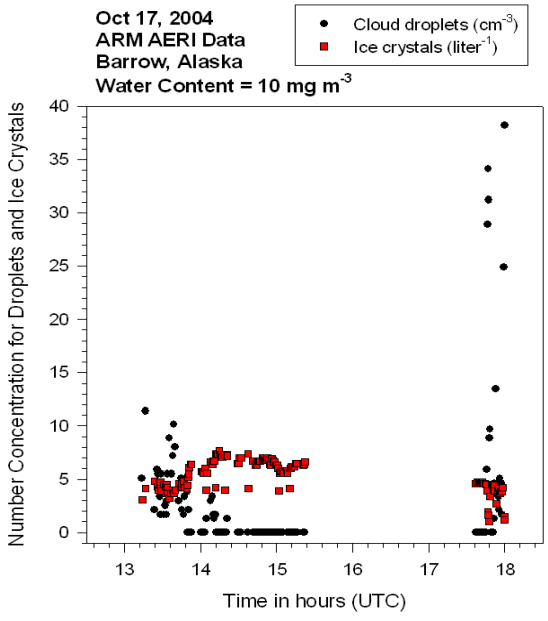

Figure 8. Retrieved cloud droplet and ice crystal number concentrations assuming a total water content (ice + liquid) of 10 mg m^{-3}.

concentration N_d can exceed 30 cm^{-3}. When we changed the algorithm to assume the small mode is comprised of ice crystals (based on Ivanova et al. 2001) instead of cloud droplets, N_{ice} ranged from about 1 to 10 cm^{-3} in the regions where the AOD ratio exceeds 1.08. It seems unlikely that N_{ice} would change so abruptly, making the mixed phase explanation most reasonable. T_{abs} in Fig. 7 is minimum between 14.2 and 15.4 UTC, which corresponds to glaciated cloud conditions, lower N and larger D_{eff}.

Finally, Fig. 9 shows lidar depolarization ratios and Millimeter Cloud Radar (MMCR) backscatter for this case study. The high depolarization ratios indicate the dominance of the ice phase, and the MMCR backscatter provides more detail on cloud structure and position. Since we only used AERI data having visible OD between 0.5 and 4.5, the cirrus between 15.4 and 17.6 UTC was not included in this analysis. Note that the low patch of cloud near 18 UTC could be responsible for the higher percent LWC in Fig. 7.

The physics responsible for the differences in AOD at 12 and 11 μm are different for liquid water than for ice. Whereas tunneling produces the AOD differences in small mode ice crystals, the role of tunneling is relatively minor in water droplets since the real refractive index is similar for water at these wavelengths. For

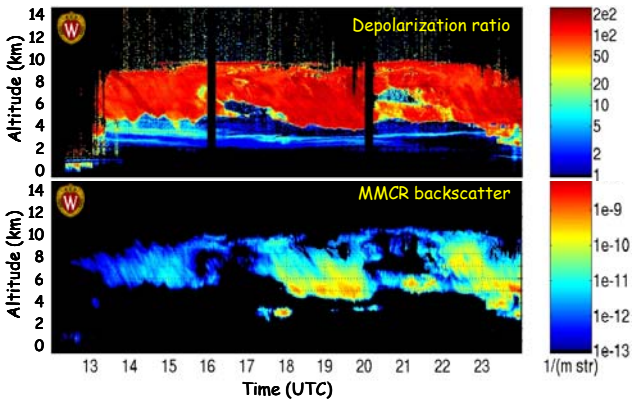

Figure 9. Lidar depolarization ratios and MMCR backscatter for the M-PACE 17 October case study at Barrow, Alaska, courtesy of Ed Eloranta (Univ. of Madison, WI).

cloud droplets, it is the transition from area dependent absorption to mass dependent absorption (as droplet size decreases for D < 10 μm) that causes the sudden changes in AOD ratio (see Mitchell and Arnott 1994 for a discussion of area and mass dependent absorption). This is why the retrieval algorithm is so sensitive to D_{sm}.

5. CONCLUDING REMARKS

By applying the principle of photon tunneling or wave resonance to radiances at 11 and 12 μm, we have found in previous work that the cirrus PSD tends to be monomodal or weakly bimodal, allowing us to infer that the small mode of the retrieved PSD, when present, is mainly comprised of liquid water. When the LWC was negligible, the retrieved ice particle concentrations appear consistent with known ice nucleation processes.

Acknowledgment: This research was sponsored by the Office of Science (BER), U.S. Dept. of Energy, Grant No. DE-FG02-06ER64201.

BIBLIOGRAPHY

- Giraud, V., O. Thouron, J. Riedi, and P. Goloub, 2001: Analysis of direct comparison of cloud top temperature and infrared split window signature against independant retrievals of cloud thermodynamic phase. *Geophys. Res. Let.*, **28**, 983-986.

- Giraud, V., J.C. Buriez, Y. Fouquart, and F. Parol, 1997: Large-Scale Analysis of Cirrus Clouds from AVHRR Date: Assessment of Both a Microphysical Index and the Cloud-Top Temperature. *J. Appl. Met.*, **36**, 664-674.

- Ivanova, D., D.L. Mitchell, W.P. Arnott and M. Poellot, 2001: A GCM parameterization for bimodal size spectra and ice mass removal rates in mid-latitude cirrus clouds. Atmos. Res., **59**, 89-113.

- Mitchell, D.L., and W.P. Arnott, 1994: A model predicting the evolution of ice particle size spectra and radiative properties of cirrus clouds. Part II: Dependence of absorption and extinction on ice crystal morphology. J. Atmos. Sci., **51**, 817-832.

- Mitchell, D.L., 2000: Parameterization of the Mie extinction and absorption coefficients for water clouds. J. Atmos. Sci., **57**, 1311-1326.

- Mitchell, D.L., A.J. Baran, W.P. Arnott and C. Schmitt, 2006: Testing and comparing the modified anomalous diffraction approximation. *J. Atmos. Sci*., **63**, 2948-2962.

- Yang, P., H. Wei, H-L. Huang, B.A. Baum, Y.X. Hu, G.W. Kattawar, M.I. Mishchenko, and Q. Fu, 2005: Scattering and absorption property database for nonspherical ice particles in the near- through far-infrared spectral region. *Appl. Opt*., **44**, 5512–5523.

Appendix D

GROUND BASED RETRIEVALS OF SMALL ICE CRYSTALS AND WATER PHASE IN ARCTIC CIRRUS

Subhashree Mishra*, David L. Mitchell* and Daniel DeSlover€

**Dept. of Atmospheric Sci., Desert Research Institute, 2215 Raggio Pkwy, Reno, NV 89512, USA*
€Dept. of Atmospheric & Oceanic Sci., University of Wisconsin, 1225 W. Dayton St., Madison, WI 53706, USA

Abstract. The microphysical properties of cirrus clouds are uncertain due to the problem of ice particles shattering at the probe inlet upon sampling. To facilitate better estimation of small ice crystal concentrations in cirrus clouds, a new ground-based remote sensing technique has been used in combination with in situ aircraft measurements. Data from the Mixed-Phase Arctic Cloud Experiment (M-PACE), conducted at the north slope of Alaska (winter 2004), have been used to test a new method for retrieving the liquid water path (LWP) and ice water path (IWP) in mixed phase clouds. The framework of the retrieval algorithm consists of the modified anomalous diffraction approximation or MADA (for mixed phase cloud optical properties), a radar reflectivity-ice microphysics relationship and a temperature-dependent ice particle size distribution (PSD) scheme. Cloud thermal emission measurements made by the ground-based Atmospheric Emitted Radiance Interferometer (AERI) yield information on the total water path (TWP) while reflectivity measurements from the Millimeter Cloud Radar (MMCR) are used to derive the IWP. The AERI is also used to indicate the concentration of small ice crystals (D < 50 μm) relative to the larger ice particles. Combining this small crystal information with the PSD scheme describing the larger particle concentrations yields the retrieved PSD. Small ice crystals are evaluated using the absorption properties of photon tunneling or wave resonance while the liquid water fraction is evaluated using classical Beer's law absorption. While this is still a work in progress, the anticipated products from this AERI-radar retrieval scheme are the IWP, LWP, small-to-large ice crystal number concentration ratio and effective diameter for cirrus, as well as the ice particle number concentration for a given ice water content (IWC).

THEORY

Small ice crystals are evaluated using the properties of photon tunneling or wave resonance. Photon tunneling can be described as the process by which radiation beyond the physical cross-section of a particle is either absorbed or scattered outside the forward diffraction peak (Fig. 1(a); see [1] for details). Tunneling is strongest when:

- The effective size of the particles and the wavelength of radiation are comparable.
- The particle is spherical or quasi spherical (an attribute of many small crystals)
- The real index of refraction is relatively large

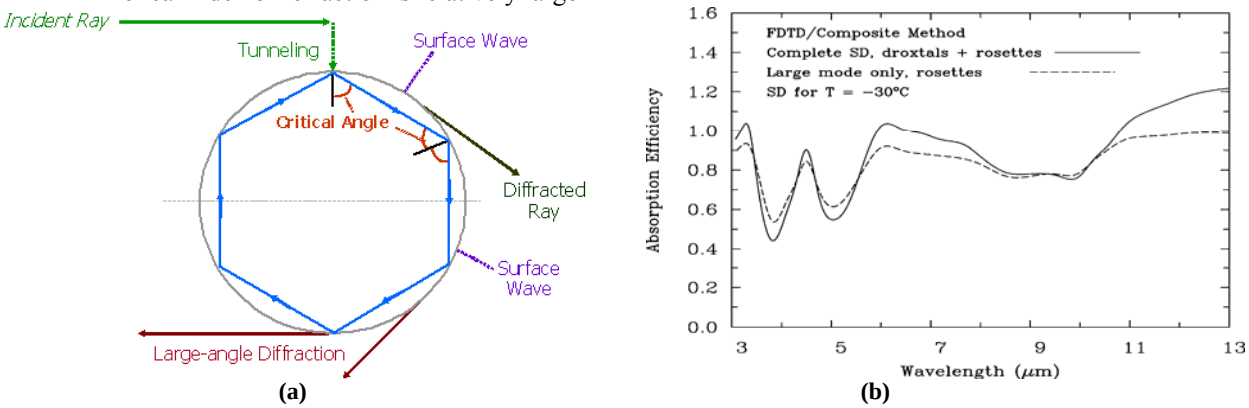

Figure 1. (a) Depiction of possible trajectories of an incident grazing ray after tunnelling to the drop surface. **(b)** Absorption efficiencies (Q_{abs}) for a bimodal size distribution (solid) and the same PSD but without the small ice crystal mode (dashed). The difference between the curves for wavelengths greater than 10.5 μm is due only to tunneling.

Tunneling contributions to the absorption efficiency in the window region can reach 20% when particle size is less than 60 μm. Tunneling depends on the real refractive index (n_r) [1], which changes abruptly for ice between 11 and 12 μm wavelengths. The corresponding emissivity difference at these wavelengths is only due to tunneling. Moreover, the tunneling contribution to absorption is negligible at 12 μm for ice crystal lengths > 60 μm, making tunneling an ideal signal for inferring the concentrations of small ice crystals. Historically this emissivity difference was attributed to differences in the imaginary refractive index, but in essence, it is the real refractive index that accounts for this difference in emissivity in ice clouds [1].

Better understanding of remote sensing of small crystals by applying the tunneling technique is shown in Fig. 1(b). The solid curve shows absorption efficiencies (Q_{abs}) for a bimodal size distribution of quasi-spheres (droxtals) in the small mode and bullet rosettes in the large mode. Dashed curve is for the large mode, rosettes only. An example of a bimodal PSD is shown in Fig. 2(a). Q_{abs} for wavelengths > 10.5 μm are greater for the complete PSD due to tunneling. Tunneling depends strongly on the real index of refraction, n_r. The reason Q_{abs} is greater at 12 μm than 11 μm when the full PSD is used is because n_r has a minimum near 11 μm but is substantial at 12 μm. Since tunneling is a measure of the small mode, and the 12 – 11 μm Q_{abs} difference is only from tunneling, this difference serves as a measure of the small mode of the cirrus PSD. While these calculations are based on the optical property database given in Yang et al. [2], the same results are obtained with MADA [3].

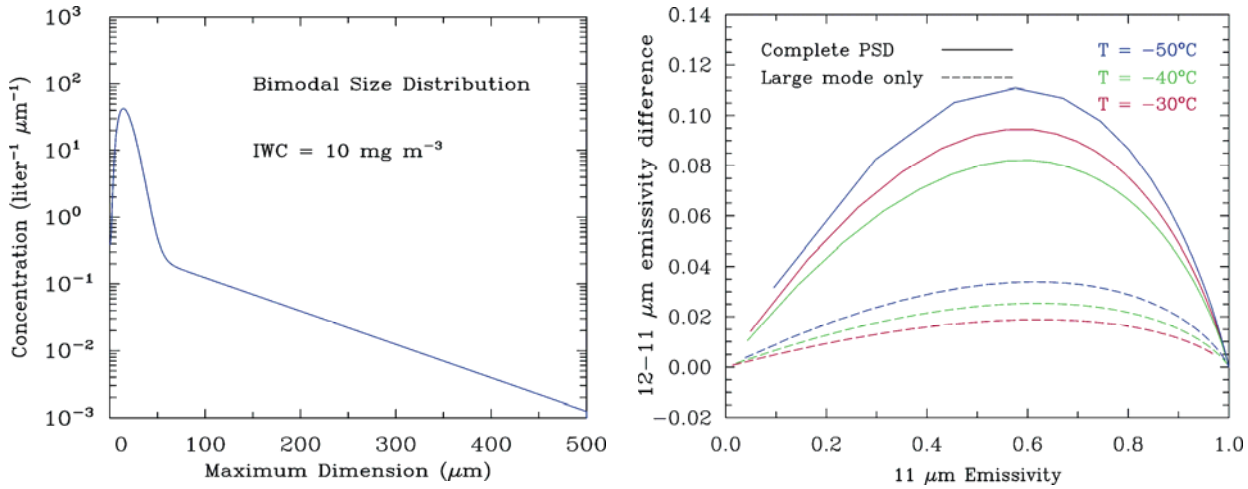

(a) **(b)**

Figure 2. (a) An example of a bimodal size distribution based on measurements from mid-latitude cirrus clouds (Ivanova et al. 2001). **(b)** Theoretical curves denoting the large mode (dashed) and the complete PSD (solid) corresponding to 3 different PSD measured by an FSSP (small mode) and 2DC probe (large mode) in mid-latitude cirrus.

ESTIMATING SMALL CRYSTAL CONCENTRATIONS

The small mode ice water content can be estimated by the "arches" in Fig. 2(b) and also from the absorption optical depth ratio at 12 and 11 μm, referred to as β. The higher the small mode ice water content (or ice crystal number concentration, N_{sm}), the higher the arches are. This principle is used to determine N_{sm} by matching theory with observations, as described below.

1. The first step is to begin with retrievals of cloud temperature and cloud emissivity (ε) at 11 and 12 μm wavelength channels from AERI and from a corresponding sounding.
2. Using a synoptic cirrus PSD scheme [4], the cloud temperature can then be used to estimate PSD mean size (D) and dispersion for large and small mode. The difference between the solid and dashed curves results primarily from differences in the contribution of the small PSD mode to the IWC. This also determines the effective diameter (D_e). The dispersion parameter has little influence on the emissivities or emissivity differences.
3. Locate retrieved Δε (y-axis) and the 11 μm ε by (1) incrementing the modeled IWP to increase ε(11 μm) and (2) incrementing the small mode contribution to the cloud IWC, which elevates the curve.
4. If retrieved point lies below the "large mode only" curve (e.g. a dashed curve), then systematically increase D for large mode until a match is obtained. Negative Δε values correspond to maximum allowed D values.

5. This method retrieves IWP, D_{eff}, and the small-to-large mode ice crystal concentration ratio. For a given IWC, it also estimates ice particle number concentration and the complete PSD, even when it is bimodal.

ESTIMATING ICE AND LIQUID WATER PATH FROM AERI AND MMCR DATA

Our experience with the above method regarding synoptic and anvil cirrus generally indicates that the small crystal mode is diminished or even absent relative to most PSD measurements (see http://www.dri.edu/Projects/Mitchell/ and [5]). This same result holds when the technique is applied using the β retrieved from satellites found in several published studies [e.g. 6, 7, 8], where β ~ 1.08. These studies show that when β > 1.1, it is probably due to the presence of liquid water. In this study it was found that for relatively long time periods, β was < 1.1 and then abruptly increased to higher values. Interpreting the cloud as ice only, this implies ice crystal concentrations suddenly increase from order of 10 per liter to order of 1000 per liter or higher. Since we know of no physical mechanism capable of rendering such behavior, we interpret such β jumps as transitions to mixed-phase conditions (or, conversely, mixed-phase to ice only conditions). Also note that β should be less for ground-based IR remote sensing since radiances are weighted towards larger ice crystals in the lower cloud (i.e. satellite retrievals of β are weighted towards smaller crystal sizes dominating the upper cloud, biasing β towards larger values). This assumption forms the basis of our retrieval method for mixed phase clouds. When β is significantly larger than the β predicted by the temperature-dependent PSD scheme, the small mode is increased by assigning some portion of the total water content (TWC) as liquid cloud water until the predicted and observed β match. Moreover, both liquid and ice phases contribute to the thermal radiances measured by the AERI, so the AERI should measure the total water path (TWP). The millimeter cloud radar (MMCR) is sensitive only to large (i.e. ice) particles, so the MMCR measures the IWP. The LWP is simply TWP – IWP. The modified anomalous diffraction approximation (MADA) was used to calculate ice and liquid water cloud optical properties in this AERI retrieval algorithm since it couples explicitly with the cloud microphysics and its analytical formulation makes it computationally efficient [1, 2].

The IWC is estimated from the MMCR effective radar reflectivity Z_e at individual height levels and integrated over height intervals to produce the IWP using an equation that relates Z_e to the cirrus particle shape and PSD slope λ (large particle mode). The derivation of this equation is given in [9]. The PSD scheme [4] relates λ to cloud temperature where in this case the radiance weighted temperature based on lidar/radar and corresponding sonde data was used. For the case study below, the average cloud temperature was about -35 ^{o}C, and this temperature was used for estimating λ in the radar-IWC equation. In this way the MMCR IWP was compared to the AERI TWP.

M-PACE CASE STUDY OF 17 OCTOBER 2004

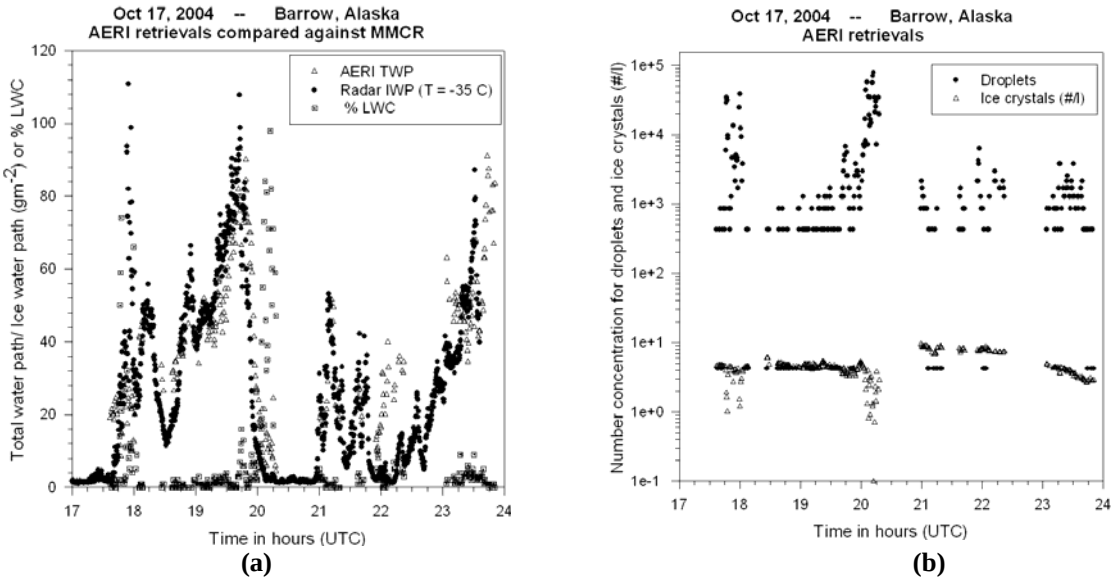

Figure 3. (a) Retrieved TWP and IWP for M-PACE case study of 17 Oct. 2004. **(b)** Retrieved cloud droplet and ice crystal number concentrations (per liter) assuming a total water content (ice + liquid) of 10 mg m^{-3}.

Measurements made by the ground-based AERI identified the glaciated regions of cloud as regions where PSD were not bimodal. The absorption optical depths (AOD) of these clouds for two wavelengths (12.19 μm and 11.09 μm) were obtained from the AERI. Visible optical depth (OD) was less than 4.5 (to prevent emissivity saturation) and greater than 0.5 (for good signal/noise ratio). The cloud temperature ranges between -27 °C and -39 ^{o}C. According to the homogeneous nucleation theory, super cooled water may be present along with ice in clouds at temperatures above -36 ^{o}C. AERI AOD ratios (β) higher than 1.1 were associated with such temperatures.

During mixed phase conditions, the small mode information (from AERI radiances) was combined with the PSD scheme describing the larger ice particle concentrations to yield the mixed phase PSD. The mean cloud droplet diameter D_c was fixed at 7 μm. Unfortunately, these cloud retrievals are sensitive to what one assumes for D_c, and this is a limitation of this retrieval method. In the future we hope to calculate D_c by integrating MMCR data more intimately with the AERI retrieval. The PSD scheme as described in [4] for mid-latitude synoptic cirrus was used in our retrieval algorithm, but soon we will replace this with a PSD scheme developed from M-PACE PSD data for ice clouds, based on IWC and temperature.

Results from this analysis are shown in Fig. 3 for the M-PACE cirrus case study of 17 Oct. 2004. The AERI and MMCR were collocated at the North Slope Alaska ARM site, although the field of view (FOV) for the AERI is 1.3 degrees compared to 0.2 degrees for the MMCR. Nonetheless, Fig. 3(a) shows reasonable agreement between the AERI TWP and the MMCR IWP, indicating glaciated conditions. Lidar depolarization ratios (not shown) also indicate this cloud was almost all ice. The percent LWC and TWP were estimated from the AERI retrieval independent of the MMCR data. The more that β exceeds the ice PSD predicted β, the greater the %LWC. The %LWC is consistent with TWP and IWP near 20 UTC and in glaciated regions where TWP and IWP coincide. However near 22 UTC, TWP and IWP indicate %LWC should be approaching unity but this is not realized. This could have something to do with differing FOVs between instruments. Figure 3b shows number concentrations for ice particles and cloud droplets. Ice particle concentrations are consistent with those expected from monomodal PSD at the assumed IWC.

CONCLUDING REMARKS

By applying the principle of photon tunneling or wave resonance to recent [5] and previous [e.g. 6, 7] split-window measurements, we have found that a 12/11 μm absorption optical depth ratio exceeding 1.1 generally indicates mixed phase conditions with a PSD small mode comprised of liquid water. The fact that (1) the radar retrieved IWP was generally consistent with the AERI TWP in glaciated regions (as evidenced by β), and that (2) these retrievals were independent based on very different physics, bodes well for using this general approach to characterize the IWP and LWP in mixed phase clouds. We plan to further develop this retrieval package by integrating the AERI and radar retrieval equations for greater accuracy.

This technique appears particularly useful for characterizing liquid and mixed phase clouds having TWP < 100 g m^{-2}, where the microwave radiometer (MWR) is not sufficiently accurate. It has been estimated that roughly 80% of Arctic mixed phase or liquid water clouds have TWP < 100 g m^{-2}.

ACKNOWLEDGMENTS

This research was sponsored by the Office of Science (BER), U.S. Dept. of Energy, Grant No. DE-FG02-06ER64201. The DOE ARM program is greatly appreciated for its support of this research.

REFERENCES

1. D. L. Mitchell, *J. Atmos. Sci*. **57**, 1311-1326 (2000).
2. P. Yang, H. Wei, H-L. Huang, B.A. Baum, Y.X. Hu, G.W. Kattawar, M.I. Mishchenko, and Q. Fu, *Appl. Opt*. **44**, 5512–5523 (2005).
3. D. L. Mitchell, A.J. Baran, W. P. Arnott and C. Schmitt, *J. Atmos. Sci*. **63**, 2948-2962 (2006).
4. D. Ivanova, D. L. Mitchell, W. P. Arnott and M. Poellot, *Atmos. Res*. **59**, 89-113 (2001).
5. D. L. Mitchell and R. P. d'Entremont, these proceedings (2008).
6. V. Giraud, O. Thouron, J. Riedi, and P. Goloub, *Geophys. Res. Let.* **28**, 983-986 (2001).
7. V. Giraud, J.C. Buriez, Y. Fouquart, and F. Parol, *J. Appl. Met*. **36**, 664-674 (1997).
8. F. Parol, J.C. Buriez, G. Brogniez and Y. Fouquart, *J. Appl. Meteorol*. **30**, 973-984 (1991).
9. D.L. Mitchell, A. Huggins, V. Grubisic, *Atmos. Res*. **82**, 2-18 (2006).